CREATION AND MODIFICATION OF ACOUSTIC SIGNALS BY DISCHARGE PLASMA

Richard Willis Tripp

United States
Naval Postgraduate School

THESIS

CREATION AND MODIFICATION OF
ACOUSTIC SIGNALS BY DISCHARGE PLASMA

by

Richard Willis Tripp, Jr.

Thesis Advisor: A.W. Cooper

June 1971

Approved for public release; distribution unlimited.

Creation and Modification of

Acoustic Signals by Discharge Plasma

by

Richard Willis Tripp, Jr.
Lieutenant Commander, United States Navy
B.S., United States Naval Academy, 1962

Submitted in partial fulfillment of the
requirements for the degree of

DOCTOR OF PHILOSOPHY

from the
NAVAL POSTGRADUATE SCHOOL
June 1971

ABSTRACT

Sound production and modification in an Argon discharge plasma was investigated theoretically and experimentally. Sound production by ions in the cathode region was shown to be feasible and consistent with earlier experimental results. A numerical analysis of the theoretical dispersion relation of Ingard and Schulz showed that plasma amplification effects will not compensate for acoustic losses. The theory of the mobility-limited thermionic diode operated as a microphone was expanded. Such microphones were used in an experimental investigation of sound production and modification by a discharge plasma. Possible plasma effects on sound propagation were observed. The characteristics of sound production by the plasma were found to be in reasonable agreement with theory. A departure from theory at low frequencies was interpreted as arising from the effects of particle diffusion, an effect not previously observed in acoustics.

TABLE OF CONTENTS

LIST OF FIGURES

ACKNOWLEDGEMENTS

This work was partially supported by the Office of Naval Research under the Foundation Research Program.

Many people have given me support and assistance in a variety of ways. I would like to acknowledge the contributions of and express my appreciation to:

Mr. Robert C. Schiele for his craftsmanship and professionalism in constructing several complex discharge tubes.

The staff of the W.R. Church Computer Facility for programming assistance and services provided in conjunction with the numerous computations made.

Mr. Robert L. Limes of the Electrical Engineering Computer Laboratory for his valuable assistance in the analog to digital conversion of data.

Professor A.W. Cooper, my advisor, for many fruitful discussions and guidance during the work. In particular I would like to thank him for his critical reading of this work.

The members of my committee for their assistance during the work and their critical evaluation of the results.

My wife, Karen, for her support and encouragement and for relieving me of much of the responsibilities at home.

I. INTRODUCTION

Plasma acoustics deals with the interactions between charged particles and sound fields. The problems encountered are different from those of ordinary acoustics since charged particles experience bulk forces from external fields whereas neutral particles do not. When neutral particles are present, they are indirectly influenced by the external fields through their interactions with the charged particles. The complete mechanism of interaction is very complex, involving ionization and recombination as well as elastic and non-ionizing inelastic collisions.

This paper focuses on the problem by studying the effect of the interactions on the neutral particles. Two aspects are treated. One is the creation of sound by the current modulation of a discharge. The other is the modification of the sound[1] when it propagates through a discharge. The two aspects are closely related.

The creation of sound in a gas requires a localized time-dependent pressure variation. In a weakly ionized gas, the partial pressures of the ion and electron fluid components are negligibly small with respect to the partial pressure of the neutral gas. For this reason, the acoustic wave made in a discharge plasma is concerned only with the neutral component except when the effect of

---

[1] "Sound" and "acoustic signal" or "acoustic wave" are used synonomously and are defined to mean any fluctuation in the pressure of the neutral particles.

ions and electrons on the neutral component is of interest. The pressure, expressed as $p = kNT$, can be changed by either a change in temperature, T, or particle density, N.

In the positive column of a glow discharge, energy is continually fed into the plasma from the electric field, which draws its energy from an external power supply. The energy is received by the electrons and ions in the plasma as kinetic energy. Since, in the aggregate, these particles are traveling at their terminal velocity, referred to as drift velocity, the increased kinetic energy of the individual electrons and ions is dissapated through collisions with the neutral particles. The average rate of energy drawn from the field, per unit volume, can be written

$$H = H_e + H_i = eN_e\mu_e E^2 + eN_i\mu_i E^2$$

where μ_e and μ_i are the electron and ion mobilities. Since the electron mobility is much larger than the ion mobility and the other terms are equal, the ion term is negligible. Thus only the electrons need to be considered in the energy transfer process.

In the equilibrium situation, the energy received by the electrons must be balanced by losses. The energy distribution of the electrons closely approximates a Maxwell Boltzman distribution. The difference is due to the effect of the electric field and the energy-dependent cross sections of the neutral particles with which the electrons interact. The electrons transfer energy to the neutrals through elastic and inelastic collisions. The energy transferred in inelastic collisions is usually transferred out of

the system of neutral particles through radiation. The energy received by the neutral particles in elastic collisions is thermal energy which, at equilibrium is balanced by thermal losses to the container and neutral gas outside of the ionized region. This energy transfer between the hot electrons and cold neutrals is comparable to mixing two gases at different temperatures except that the hot gaseous component stays hot. The elastic collision losses are normally much larger than the inelastic losses which can be neglected for this analysis.

Thus the processes discussed suggest a mixture of two fluids of different temperature which retain their identity in the mixture. The hot fluid receives energy from an external source to balance the energy transferred within the mixture to the colder fluid. The cold fluid is hotter than its surroundings, to which it loses energy.

The characteristic times for the three different processes; energy gain by the electrons, transfer to the neutrals and dissapation to the surroundings, are different. The latter process is very slow. The characteristic time for energy transfer to the neutrals is of the order of the electron-neutral collision time, typically $\approx 10^{-8}$ seconds. Thus, if the energy transfer to the electrons is caused to vary at acoustic frequencies, by varying N_e or E, the time delay can be neglected and the energy transfer to the neutrals can be considered in phase with the energy transfer to the electrons. Since the time for energy transfer to the surroundings is much greater, the temperature change, and therefore

the pressure, of the neutrals will be essentially in phase with the energy transferred in. This means that a change in either E, the electric field or N_e, the electron density, can generate a time dependent pressure component in the neutral gas which can act as an acoustic source.

Amplification of a wave occurs when the wave causes a change in the medium which leads to a change in the wave in phase with itself, i.e. "positive feedback" occurs. This can occur in a discharge plasma through the interaction of the pressure wave in the neutral gas with the electron energy source term H_e. The neutral gas density changes in phase with the acoustic pressure. Since both the mobility and electron density depend on the neutral density, the feedback can be introduced through them even with no change in the electric field.

In the simplest analysis, the electron density varies in phase with the neutral density. If n_e and n_n are the perturbations in the electron and neutral gas densities N_e and N_n, then

$$n_e \simeq \frac{n_n}{N_n} N_e.$$

This indicates that the energy transfer to the neutral gas varies in phase with the acoustic pressure variation. Since this would produce a pressure variation in phase with the original pressure variation, it constitutes an amplification mechanism. For net growth to occur, the acoustic losses due to thermal conductivity and viscosity must be less than the acoustic source gain.

A more sophisticated analysis indicates that phase differences occur between the electron, ion and neutral density variations with resultant generation of a space charge electric field. The phases of all of these quantities influence the phase of the feedback and determine whether the plasma effects increase or decrease the net attenuation of the acoustic wave.

A. CHRONOLOGY OF THE EXPERIMENT

Interest in plasma acoustics here at the Naval Postgraduate School arose out of the study of moving striations. Earlier work performed here was that of Partlow [1], Carreta and Moore [2], Wilson [3], Crandall [4] and Melville [5]. Melville's work represented a shift away from the study of moving striations. This was prompted by a theoretical paper by Ingard in 1966 [6], which predicted amplification of an acoustic wave in a discharge plasma. A more comprehensive theory by Ingard and Schulz followed in 1967 [7].

The experimental investigation described in this work began in 1968 as a natural continuation of the earlier work performed here. The earlier work here and elsewhere had demonstrated that sound could be generated by a plasma. This coupled with the prediction of effects on the sound as it passed through a discharge led the author to the consideration of a combined experiment. In the proposed experiment, a discharge would be used to create sound, and it would be observed before and after it propagated through the discharge. With the proper techniques, the experiment could provide information about both the creation of sound and its modification in the discharge.

A numerical analysis of the Ingard-Schulz dispersion relation contained in [7] was performed as part of this investigation in which the variables were neutral density, neutral temperature, electron density, electron temperature and angular frequency of the acoustic signal. The attenuation was minimized with no constraints placed on the values of the variables except for upper and lower limits. The results showed that the minimum attenuation occurred at high neutral densities, high electron densities and temperatures, low neutral temperatures and low frequencies. The maximum relative amplification[2] was also investigated. The conclusion drawn from a study of the behavior of these two quantties was that the experiment should test the theory in the medium pressure, high current region. The directionally dependent effects observed by Yatsui, et.al. [8,9] indicated the need to design the experiment so that the polarity of the discharge could be reversed. Also, it was felt that thermocouples were needed to determine the neutral gas temperature in and out of the discharge.

---

[2] "Relative amplification"(A_R) is the change in attenuation due to the plasma amplification referred to the classical attenuation. It is defined as

$$\frac{\beta_I - \beta_u}{\beta_u} = A_R$$

where β is the attenuation coefficient, I Signifies ionized and u signifies unionized. A negative value means that an amplification is operative in the plasma case.

The experiment was designed to use two mobility-limited thermionic diodes as microphones to observe the signal at two points with the signal being produced by a remote source discharge. Such an arrangement would permit a direct determination of the attenuation. The theory of the diode microphones was developed beyond the earlier elementary form so that an extensive calibration was not needed to use it as an analytical tool. Technical problems were solved so that the tube could be constructed with a smooth surface, free from side arms, bumps and bubbles which affect an acoustic signal, in spite of the numerous tube elements contained. A circuit was designed to control the discharge current to produce the sound in the desired form.

Pulsed currents were used to produce the sound with the source discharge. The current and sound waveforms were Fourier transformed to determine their spectra. By a process of comparison, extrapolation and comparison, the frequency dependence of the acoustic attenuation and the source transfer function were obtained. The measured values of the experimental parameters were used to determine the predicted values of attenuation from the Ingard-Schulz equations. These equations predicted that the plasma would not affect the attenuation under the conditions used. The experimental value for the attenuation co-efficient agreed with the predicted value within experimental accuracy although the results indicated the possibility of a plasma effect.

The results of Yatsui et.al. [8,9] were then reevaluated. It was noted that while the relative change in the attenuation coefficient was small, since the attenuation was very large, the amplification effect was large. In view of these results, it was recognized that the quantity to optimize is the difference in attenuation co-efficients between the ionized and un-ionized cases.

Earlier a theoretical study of the frequency characteristics of a discharge sound source was undertaken by Schulz [10]. He concluded that the energy transfer from the electrons was the dominant source mechanism. The predicted frequency dependence is $\sin(\nu\pi a/c)/(\nu\pi a/c)$. When the source transfer function was experimentally determined, it was found to be consistent with theory at high frequencies but not at low frequencies. The low frequency effect was attributed to diffusion effects.

In the following two sections of this chapter, earlier experiments relating to the creation and modification of sound are discussed. Following, Chapter III discusses the theoretical treatment of sound creation and modification. This order of presentation was chosen because it was felt to offer a better insight into the aspects which the theory should treat.

B. PREVIOUS EXPERIMENTAL WORK ON ACOUSTIC INTERACTIONS

Before considering specific papers of direct interest to this experiment, a quick general review of previous experimental investigations of the acoustic interaction is in order. Interest in the

interaction between charged particles and neutral acoustic waves is recent. A relationship between moving striations and acoustic waves was suggested by Watanabe and Oleson [11] in 1955. Wojaczeck [12] reported observations of a sound interaction in 1960 during experiments in Xenon. He noted on effect in his main discharge which occurred when an auxiliary discharge was pulsed, and he identified the effect as due to sound waves generated by the pulsed discharge.

Since that time, many workers have reported observations of sound waves generated by discharges. The source and type of disturbance in the discharges, which were observed to produce sound, have been sufficiently varied to conclude that it is a general phenomenon. Sound has been observed [1-3] whose source was interpreted to be the current fluctuations associated with moving striations. Sound production by artificially introduced current fluctuations has been reported [4,13-15] for a variety of conditions. Modulation of the electron temperature in a discharge by an R.F. field was observed by Fitaire and Mantei [16] to produce sound. Multiple pulse emission from an HCN laser, reported by Turner, et.el., [17], was interpreted by Born [18] as due to sound production by the discharge.

The variety of techniques used to study the sound produced by pulsed discharges is almost as interesting as the observations reported [4,5,12,19-25]. The pulses ranged in duration from one to fifty microseconds [23,18], in pressures ranging from 5×10^{-2} torr[19]

to 20 torr [18]. In some experiments, the sound was detected by observing its effect on some property of the discharge which produced the sound. An example of this is the work reported by Berlande, et.al. [24], in which they observed perturbations in the light of the afterglow of the plasma which produced the sound. Nygaard [21] utilized the light perturbation effect by using one discharge to produce the sound while he observed the afterglow of a second discharge. Goldstein et.al. [23] used a mobility-limited thermionic diode as a microphone. These and other techniques were used in some cases because of the problems associated with conventional acoustic detection techniques under the conditions involved. In other cases, they were used because the sound and its detection was an unexpected result in an experiment.

Only a few papers have been published concerning the effect of a plasma on sound propagating through it [5,8,9,26], as opposed to the effect on the discharge. Because of their relevance and sparsity, these papers will be discussed in detail in the next section.

C. SPECIFIC EXPERIMENTS OF INTEREST

The two aspects of this experiment are the creation of sound and its modification in a gas discharge. Earlier experiments have examined both of these and as the experimental results have been reported, theories have been developed to explain the experimental results. The theoretical aspects of the experiment will be discussed in the next chapter.

1. Sound Production

A review of the existing experimental evidence concerning sound production can point out features which must be explained by any theoretical model of the process.

Wilson [3] determined from phase measurements of the sound produced by moving striations, that the only sound source position consistent through the experiment was at or near the cathode. By comparing the current and sound waveforms, he concluded that the sound was produced by fluctuations in heating processes occurring near the cathode due to current fluctuations. He suggested that the mechanism must involve an interaction between the fluctuations in ion density and temperature and the neutrals.

Nygaard and Meltz [21] are more specific as to the location of the source. They state that the acoustic disturbance from their H.V. pulse discharge originates in the negative glow region. They postulate a high pressure driver region near the cathode maintained by electron heating and momentum transfer from the ions.

Hayess [20] also interpreted the sound production as arising from localized heating of the neutral gas. However his experiment brings in a different aspect. He used a high voltage pulse applied to an electrode near a discharge already running, so that the other electrode of the circuit had a much greater charge carrier concentration than the exciting electrode. He found that the sound source was always at the exciting electrode, regardless of the polarity of the voltage pulse. By varying the rise time of the

voltage pulse, Hayess established that it had particular importance in the sound excitation process. Pulses with rise times of 5×10^9 V/sec produced sound, those with rise times of 1.4×10^6 V/sec did not. In addition, sine waves with an average rise time of 2×10^7 V/sec did not lead to sound production. Hayess also established that the presence of charge carriers at the exciting electrode reduced the sound produced. From consideration of these factors, Hayess concluded that energy gained in the high field by the charge carriers is transferred to the neutrals. He further concluded that the ions were responsible for the inertial phenomena, i.e. dependence on rise time.

In contrast to the above experiments, the observation of sound production by modulation of the electron temperature in a discharge, reported by Fitaire and Mantei [16], may be deemed as experimental confirmation of the roll of the electron temperature in the acoustic source term of Ingard and Schulz's equations [7]. In interpreting these experimental results, it must be borne in mind that there is a distinction between the energy of electrons in a low field region, such as the positive column and a high field region such as the cathode fall. In the latter, the motion is highly directional and can not be considered thermal.

Upon considering the above experimental results, the following conclusions may be drawn. There are two mechanisms through which sound is produced in a discharge. One mechanism occurs near the cathode and probably involves ions in a high field, the cathode fall. Nygard's contention that the source is the

negative glow region is in contradiction with the results of Hayess concerning the high field. The other mechanism occurs in the positive column and involves the electron temperature. The former mechanism appears to dominate the production process. Further comment shall be reserved for a discussion of sound production in Chapter II.

2. Sound Modification

The experimental evidence concerning the effect of the plasma on sound is not so conclusive. Wojaczek [12] observed the perturbation, produced by the sound, in the light emitted from a Xenon gas discharge. On the basis of his calculations, he concluded that the attenuation was much greater than expected. He attributed this to possible interaction with the discharge.

Later Hayess [19] pointed out that the attenuation Wojaczek predicted was in error because the dominant loss mechanism, wall effects, was neglected. Hayess recomputed the predicted values. With the wall losses taken into consideration, the experimental values agreed with the predicted values within the experimental uncertainty. Wojaczek's experiment was conducted at pressure from .07 torr to 1.5 torr with currents from 1.5 to 0 amperes.

Working in Argon, Yatsui et.al. [8,9] studied the effects of a discharge on ultrasonic sound. They used barium titanate transducers with resonant frequencies of 50 kHz, 100 kHz and 200 kHz for transmitters and receivers. The signal received with no discharge, as a function of transducer input voltage, was the

reference. By dividing this into the results obtained with the discharge on, a "spatial growth rate" was obtained. A definite change in the growth rate was observed. It was found to be dependent on the current and pressure of the discharge and on the polarity with respect to the propagation direction. The polarity effect was so strong that under conditions such that while propagation in the direction of electron drift motion enhanced the signal by 50%; no signal was received when propagated contra to the electron drift. The variation of the growth rate with pressure and current was not monotonic, as the signal exhibited a maximum enhancement at intermediate values of the range investigated. The conclusion drawn by the authors was that strong damping occurred for contra-propagating signals under all conditions. For parallel propagation, there is a critical pressure p_c above which attenuation occurs and below which amplification occurs. They attributed the directional effect to coupling between the sound and the drift motion of the electrons, a coupling which is strongest when the sound velocity is nearly equal to the electron drift velocity.

Their experiment provides experimental support to the concept of energy transfer from the electric field to the neutrals via the electrons. It should be pointed out that the acoustic frequency is of the order of the collision frequency at the low end of their pressure range, 10^{-2} to .5 torr. Indeed it was at this end that the maximum effect was observed.

Macon [26] used a Helium discharge to investigate the effect of the discharge on sound. He employed resonant cavity

techniques with frequencies below 2000 Hz. The sound source was calibrated to provide constant amplitude deflections over a range of frequencies. A rigidly mounted microphone received the signal at the other end of the tube. By comparing the ratio of pressures at adjacent pressure maxima and minima, and assuming the net loss was dominated by boundary effects, the attenuation constant was determined. The value for the "discharge off" condition was compared with the "discharge on" condition. Measurements for the discharge off condition were taken one-second after turning the discharge off in order to have comparable temperature. The temperatures, as determined from sound velocity measurements, dropped from 450°K with the discharge on to 360°K with the discharge off, with one-second. The results indicated a decrease in attenuation rate of 30%; a value too large to be accounted for by the pressure and temperature differences. Although the experimental results for attenuation and amplification rates were both in poor agreement with theoretical predictions, Macon concluded that amplification by the electrons was definitely occurring.

These experiments indicate that there are amplification and attenuation effects. Wojaczek's experiment does not hint of any directional effect. Macon did not look for any. The directional effect observed by Yatsui is explainable by models for other fields, namely electronics and solid state. The Ingard-Schulz model to be discussed in the next section does not take directional effects into consideration.

II. THEORY

Physical theories go hand in hand with experiments. Theories are developed to account for experimental results. Experiments are conducted to evaluate theories by testing their predictions. In the previous chapter, the experimental evidence regarding production and modification of sound by a discharge plasma was reviewed. In this chapter, the theories will be examined.

A. SOUND PRODUCTION BY DISCHARGE PLASMAS

After several investigators reported observation of sound produced by electrically modulated discharges, Ingard [6] performed a theoretical analysis of the problem. He derived the wave equation for the pressure in the neutral gas in which the interactions with the electrons and ions were expressed in terms of sources in the wave equation. Neglecting the fluctuations in neutral particle density resulting from the imbalance of ionization and recombination rates, Ingard obtained the following wave equation:

$$\frac{1}{c^2}\frac{\partial^2 p}{\partial t^2} - \nabla^2 p = \frac{\gamma-1}{c^2}\frac{\partial H}{\partial t} - \nabla\cdot\vec{F} \quad . \tag{2.1}$$

In this equation, p is the acoustic pressure, defined as the time-dependent pressure variation about the ambient pressure; c, the speed of sound; and γ is the ratio of specific heats. "H" is the energy source term, representing the rate of energy transfer to the neutral gas from the charged particles per unit volume. The rate of transfer of momentum to the neutral gas per unit volume is represented by the momentum source term $\vec{F}$.

Ingard considered the effect of momentum transfer represented by $\nabla\cdot\vec{F}$ as negligible for two reasons. First the electron and ion contributions tend to cancel each other. Second, only the spatial variation of $\vec{F}$ leads to sound, and for most cases, this is very small. For the energy source term, he wrote

$$H = \frac{4m_e}{m_n}\left(\frac{m_e v_e^3}{2}\right) N_e N_n \langle\sigma\rangle \qquad (2.2)$$

where v_e is the average electron velocity and $\langle\sigma\rangle$ is the average collision cross section for elastic scattering. Ingard considered the ion contribution negligible due to its much lower mean energy. Ingard pointed out that since the electrons were in an equilibrium state, the energy lost to the neutrals, represented by H, was the same as the energy gained from the field. Therefore

$$H = N_e e E(\mu_e E) \qquad (2.3)$$

where μ_e is the electron mobility and E the electric field.

Schulz [10] used equation (2.1) as a basis to develop an expression for the sound field produced by current-modulating a discharge operating between two planar electrodes. He considered the effects of the two source terms separately in calculating the pressure response. For both, a one dimensional problem was assumed and it was assumed that the time dependence was given by $\exp(-i\omega t)$. Under these assumptions, the wave equation inside the source region becomes

$$\frac{d^2p}{dz^2} + \left(\frac{\omega}{c}\right)^2 p = i\left(\frac{\omega}{c^2}\right)(\gamma-1)H. \qquad (2.4)$$

If H is assumed to be spatially constant within the region, then the general form of the solution inside of the region is

$$P_{in} = Ae^{-ikz} + Be^{ikz} + i\frac{\gamma-1}{\omega}H. \tag{2.5}$$

With the additional assumption of symmetry about the origin, chosen to lie between the two electrodes which are separated by a distance a, Schulz's expression for the pressure field outside the source region for the energy source is obtained.

$$P_E = \frac{(\gamma-1)}{\omega} H \sin\left(\frac{\omega a}{2c}\right) \exp\left(i|z|\frac{\omega}{c}\right). \tag{2.6}$$

Schulz assumed that the momentum transfer acoustic source arose from an unbalanced fluctuation between the forces exerted by the ions and the electrons on the neutral gas. He stated that this force per unit volume was given by

$$\vec{F} = N_i\omega_{in}\frac{q\vec{E}}{\omega_{in}-i\omega} - N_e\frac{\omega_{en}q\vec{E}}{\omega_{en}-i\omega}. \tag{2.7}$$

With the assumptions $\omega_{in} \gg \omega$ and $\omega_{en} \gg \omega_{in}$, this simplifies to

$$\vec{F} \simeq iN_i q\vec{E}(\omega/\omega_{in}). \tag{2.8}$$

If the electric field $\vec{E}$ is assumed to be constant between the two electrodes and zero outside, then $\nabla\cdot\vec{F}$ can be expressed as

$$\nabla\cdot\vec{F} = F\left[\delta(z+\frac{a}{2}) - \delta(z-\frac{a}{2})\right]$$

where $\delta(z)$ is the Dirac delta function. This leads to a pressure field of:

$$P_F = \pm i\left(\frac{cqN_i}{\omega_{in}}\right) E \sin\left(\frac{\omega a}{2c}\right) \exp\left(\pm i\omega\frac{z}{c}\right). \tag{2.9}$$

Schulz concluded that the momentum source term would be negligible. He compared the two sound fields and found that the ratio was of the order of $\frac{\omega_{in}}{\omega}\left(\frac{T_e}{T_n}\right)^{\frac{1}{2}}$ in favor of the energy transfer process.

Schultz's results predict that the energy transfer mechanism dominates. This result is in agreement with Ingard's earlier [6] conclusion. Schulz's expression for the sound field predicts that the frequency dependence is like $\frac{\sin x}{x}$ where $x = \nu \frac{a\pi}{c}$. Heretofore this frequency dependence has not been experimentally investigated. However there is experimental evidence which refutes Schulz's results and contradicts Ingard's assumptions concerning the energy source term.

As mentioned earlier, the experimental evidence suggests that the principal source term lies near the cathode and involves the field. Schulz's analysis implied that the positive column was the source region. The $\frac{\sin x}{x}$ frequency dependence also shows that the sound produced by high frequencies will be small. The effective frequencies of the sound pulses mentioned earlier have been in the range of 20 kHz to 1 MHz, all of which are high acoustic frequencies. Perhaps the comparison with pulsed discharges is not a valid one because of the difference between the experiments and the conditions assumed for the derivation. The derivation presumes small perturbations yet the current changes in a pulsed breakdown discharge can not be small perturbations.

Since sound production appears to occur in the vicinity of the cathode and appears to be associated with high fields, a possible

source term compatible with experimental results would be a field-dependent energy source term. A field-dependent source is one in which the energy for the acoustic wave comes from the field. The dependence on this term enters through the energy equation in contrast to Schulz's treatment, in which the field entered through the momentum equation.

When the processes occurring in the region of the cathode are considered, a mechanism for the production of sound suggests itself to the author. The contribution of ions to the energy transfer is usually neglected. Due to their higher mobility the electrons transfer energy from the field to the neutral particles much more readily. It should be recognized that due to their common masses, the ions and neutrals will be at essentially the same temperature. The unity mass ratio means that during a collision, an ion will transfer a large fraction of its energy. In the cathode region, this factor becomes important. There the ions are the majority carriers of the discharge current. Their density is higher and they accelerate toward the cathode under the high field of the cathode fall. The increased energy will be transferred to the neutrals through collisions. There will also be a net momentum transfer since the ions acquire momentum from the field and transfer it also.

A rough approximation for the strength of such a source term can easily be developed. The average energy gained from the field between collisions is $eE\ell_{in}$ where E is the electric field strength and ℓ_{in} is the mean free path of the ions. Since approximately half of the ions energy would be transferred in a collision, the

energy transfer rate per unit volume is

$$H_i \simeq \frac{1}{2} eE\ell_{in} \omega_{in} N_i. \qquad (2.10)$$

This approximation is low because it uses the average energy that would be transferred if the ions were stopped after a collision. It does provide an order of magnitude estimate. If ℓ_{in} is approximated by $\bar{v}/\omega_{in}$, then

$$H_i \approx \frac{1}{2} eE \bar{v}_i N_i . \qquad (2.11)$$

The ratio of this term, where $E = E_c$, the field in the cathode fall to the electron source term, $E = E_p$, the field in the positive column is

$$\frac{H_i}{H_e} \approx \frac{\frac{1}{2}eE_c \bar{v}_i N_i}{N_e eE_p(\mu_e E_p)} . \qquad (2.12)$$

Now $eN_e\mu_e E_p$ is the current density in the positive column, and $e\bar{v}_i N_i$ is approximately the current density in the cathode region. Since the two current densities should be the same,

$$\frac{H_i}{H_e} \simeq \frac{1}{2} \frac{E_c}{E_p} . \qquad (2.13)$$

The approximations used in arriving at this result are equivalent to saying that in the positive column, all of the power delivered goes into heating the neutral gas and in the cathode region, part goes into heating the neutral gas. The ions accelerate under the action of the field in the cathode fall and gain kinetic energy.

The difference between the energy taken from the field and the kinetic energy gained represents the energy transferred to the neutrals through collisions. Since the current density is constant but the field varies throughout the length of the discharge, the energy transfer rate is a function of the field and the fraction of energy lost in collisions.

B. SOUND MODIFICATION BY THE DISCHARGE

The theoretical problem of acoustic waves in a weakly ionized gas has been studied by several authors other than Ingard [27-33]. Without exception, the work of these authors needs modification before it can be used to predict the results of an experimental study in a laboratory. This is because they neglect boundary loss effects; yet at the low pressures of most discharge experiments with typical tube diameters of less than, or of the order of, 5 cm, boundary losses are dominant. The work of Ingard and Schulz [7] is the most applicable to an experiment. In addition, it is a general treatment and is reasonably susceptible to numerical evaluation.

The mechanism of amplification is embodied in the concept of energy transfer from the electrons to the neutrals through collisions. In the absence of an acoustic wave, the energy transferred is spatially uniform and merely serves to increase the temperature of the neutral gas. In the presence of an acoustic wave, the energy transfer becomes time dependent and spatially non-uniform. This produces an acoustic wave which can be in phase with the initial wave, leading to amplification.

Ingard's initial analysis of the problem [6] followed the experimental observations of sound produced by electrically modulated discharges [2,12,13,24]. He treated the problems as belonging to two categories, sound produced by current fluctuations, or an acoustic wave instability. For the first category, he derived equation (2.1). To treat the second category, he placed a term representing the electron density perturbation into the energy source term of equation (2.1). His results indicated that the acoustic signal from a current fluctuation and also the growth of an acoustic fluctuation would be small at room temperatures but enhanced at cryogenic temperatures.

Although published in May 1966, the development of reference 6 was done in early 1965. In the fall of 1966, Macon [26] completed his investigation. A thesis student of Ingard's, he attempted to conduct his experiment at cryogenic temperatures but had to use room temperatures because of noise due to moving striations. He concluded that amplification was taking place at temperatures greatly above room temperature ($450^{\circ}K$). His values of growth and attenuation rates were not in agreement with theory but he attributed this to his experimental arrangement. The more comprehensive treatment of the problem by Ingard and Schulz [7] was published in 1967.

The Ingard-Schulz analysis is based on a three fluid model of the ionized gas with both energy and momentum transferred between the fluid components. The effects of viscosity and heat conduction within each component and with the walls are also taken into

consideration. The conditions assumed in making approximations may be considered typical for a glow discharge: gas pressures of 1-10 torr, electron densities of 10^{10}- 10^{12} cm^{-3}, and acoustic frequencies $10 \leq \omega \leq 10^5$.

The equations forming the basis for the analysis are introduced as linearized space-time Fourier transforms of the continuity equation (2.14), the momentum transfer equation (2.15), the energy balance equation (2.16) and the equation of state (2.17) for each fluid component (these equations are presented here for completeness and all items will not be defined at this time).

$$- i\omega n_j + ikN_j v_j = 0 \qquad (2.14)$$

$$- i\omega v_j + i\frac{k}{\rho_j} p_j = \omega_{jk}(v_k - v_j) + \omega_{j\ell}(v_\ell - v_j) + (q_j/m_j)e - f_{1j}(k,\omega)v_j \qquad (2.15)$$

$$(j,k,\ell = n,i,e \text{ and permutations})$$

$$-i\omega\, c_{vj}\theta_j = \alpha_j(n_e/N_e) + \beta_j(\theta_e/T_e) - ik(KT_j/m_j)v_j - f_{2j}(k,\omega)c_{vj}\theta_j \qquad (j=n,i) \qquad (2.17)$$

$$-i\omega\, c_{ve}\theta_e = - ik(KT_e/m_e)v_e - f_{2e}(k,\omega)\, c_{ve}\theta_e - \rho_e^{-1}\left[(\beta_n\rho_n + \beta_i\rho_i)\theta_e/T_e + \alpha_n\rho_n(n_n/N_n) + \alpha_i\rho_i(n_i/N_i)\right]$$

$$p_j = \left(\frac{\partial P}{\partial \rho}\right)_T m_j n_j + \left(\frac{\partial P}{\partial T}\right)_\rho \theta_j = c_j^2 \frac{m_j n_j}{\gamma_j} + N_j K\theta_j \qquad (2.18)$$

$$(j=n,i,e)$$

The frequency ω is understood to be real and positive with the waveform taken as $\exp(ikx - i\omega t)$. This means that a sign difference

between the real and imaginary components of the wave propagation constant k corresponds to amplification. Amplification occurs when the amplification mechanism dominates and net growth of the wave occurs.

In the momentum transfer equations (2.15), the term $f_{1j}(k,\omega)v_j$ represents the viscous stress in the j-th fluid component. A similar term $f_{2j}(k,\omega)\theta_j$ accounts for heat conduction in the j-th component, where θ_j is the temperature perturbation. Poisson's equation is used to relate the electric field perturbation to the density perturbation.

Ingard explicity assumed that inelastic collisions and ion-neutral energy transfer could be ignored. Other assumptions are implicit in the analysis because of neglected terms; the d.c. electric field is not present in the energy balance equation, and ambipolar diffusion to the walls is neglected.

By algebraic methods, the equations were reduced to a set of three homogeneous equations for the component velocity perturbations, written here in matrix form.

$$\begin{bmatrix} A & B & C \\ D & E & F \\ G & H & I \end{bmatrix} \begin{bmatrix} v_n \\ v_i \\ v_e \end{bmatrix} = 0 \qquad (2.19)$$

Approximate expressions for these co-efficients were given by Ingard and Schulz, in the main body of their paper, as being

consistent with the acoustic mode of motion in a gas with a low degree of ionization. These equations are:

$$A \simeq 1 - \left(\frac{c_n k}{\omega}\right)^2 + i\left(\frac{\omega}{\omega_{nn}} + \frac{\omega_{ni}+\omega_{ne}}{\omega}\right); B \simeq -i\omega_{ni}/\omega;\ C \simeq -i\frac{\omega_{ne}}{\omega} + \frac{1}{\omega\tau};$$

$$D \simeq -i\omega_{in}/\omega;\ E \simeq -\frac{\omega_i^2}{\omega^2} + i\left(\frac{\omega}{\omega_{ii}} + \frac{\omega_{in}+\omega_{ie}}{\omega}\right);\ F \simeq \left(\frac{\omega_i}{\omega}\right)^2 - \left(\frac{\omega_{ie}}{\omega}\right); \quad (2.20)$$

$$G \simeq -i\omega_{en}/\omega;\ H \simeq \left(\frac{\omega_e}{\omega}\right)^2 - i\frac{\omega_{ei}}{\omega};\ I \simeq -\left(\frac{\omega_e}{\omega}\right)^2 - \frac{1}{\gamma_e}\left(\frac{c_e}{c_n}\right)^2 + i\frac{\omega_{en}+\omega_{ei}}{\omega}.$$

Using the co-efficients given in equation (2.20), Ingard and Schulz made additional approximations and expressed the dispersion relation in the form:

$$k^2 \simeq \left(\frac{\omega}{c_n}\right)^2 \left[1 - \left(\frac{\Omega_n}{\omega} + \frac{1}{\omega\tau}\right)\frac{\delta}{1+\delta^2} + i\left(\frac{1}{\omega\tau_n} + \frac{\Omega_n}{\omega}\frac{\delta^2}{1+\delta^2}\frac{1}{\omega\tau}\frac{1}{1+\delta^2}\right)\right], \quad (2.21)$$

where

$$\Omega_n = (\omega_{ni} + \omega_{ne}) \quad \delta = \frac{1}{\gamma_n}\frac{T_e}{T_n}\frac{N_i}{N_n}\frac{\omega}{\Omega_n},$$

$$\frac{1}{\tau_n} = f_{1n} + \frac{\gamma_n - 1}{\gamma_n} f_{2n} = (\omega/c)^2\left[\frac{4\eta}{3\rho} + (\gamma-1)K_T/\rho c_p\right] + (\omega\eta/2pr^2)^{\frac{1}{2}} + (\omega K_T/2\rho c_p r^2)^{\frac{1}{2}}.$$

It was stressed that this expression was valid only if the second and third terms in the brackets were small with respect to unity.

In the above expressions, the adiabatic speed of sound for the j-th component, c_j, is defined as:

$$c_j = (\gamma_j KT_j/m_j)^{\frac{1}{2}} ,$$

where: $\gamma_j = c_{pj}/c_{vj}$, the ratio of specific heats; K, the Boltzman constant; T_j and m_j are the temperatures and mass of the j-th component. The term $\omega_{j\ell}(j\neq\ell)$ is a constant of proportionality which is related to the effective collision frequency of a particle of the j-th type moving through the fluid component ℓ with N_ℓ particles per unit volume.

The Kirchoff wave attenuation caused by viscosity and heat conduction, which was introduced through the terms f_{1n} and f_{2n} in a neutral gas is taken into account by use of the characteristic frequency ω_{nn}; defined by

$$\frac{\omega}{\omega_{nn}} = \frac{1}{\omega\tau_n} = \frac{1}{\omega}\left(f_{1n} + \frac{\gamma-1}{\gamma} f_{2n}\right) . \qquad (2.22)$$

The characteristic frequency for ions, ω_{ii}, is defined in a similar manner. The ion and electron plasma frequencies are denoted by ω_i and ω_e. The term $1/\omega\tau$ expresses the effect of the heating of the neutrals by the electrons.

In the analysis of their results, Ingard and Schulz point out that wave amplification will occur if the term in the imaginary part of k^2, Eq. (2.21), involving τ dominates. They give a simple argument and develop a criterion for amplification involving the electron-neutral collision frequency ω_{en}.

$$\left(\frac{m_e}{m_n}\right)\left(\frac{N_e}{N_n}\right)\left(\frac{T_e}{T_n}\right) > \frac{1}{\tau_n \omega_{en}} \qquad (2.23)$$

They also point out that contrary to the result obtained by Ingard [6] earlier, this more general treatment indicates that a decrease in neutral gas temperature does not always increase the amplification. They show that the optimum temperature can be close to room temperature, based on the approximate expression Eq. (2.20).

Solving equation (2.19) for the ion and electron perturbation velocities in terms of the neutral velocity and using approximations, it is shown that the assumption often used, that v_e, v_i and v_n are all the same in the acoustic mode, is not generally valid. It is true only for frequencies below some characteristic frequency. At higher frequencies, the ion and electron velocities decrease in amplitude and are brought out of phase with the neutrals.

Macons observation of an amplification effect at increased temperatures does not contradict the Ingard-Schulz development; the observations of Yatsui et.al. do. Since Ingard-Schulz did not consider directional effects, and did not set up the equations so as to include any drift motion, their results could not have predicted Yatsui's results. The question arises whether the directional effects are present at lower frequencies and higher pressures. In the Yatsui experiment, the frequencies were high and the pressures low, resulting in conditions where the wavelengths were on the order of the mean free paths.

III. NUMERICAL EVALUATION OF INGARD-SCHULZ EQUATIONS

The despersion relations developed by Ingard and Schulz predict a change in attenuation, possibly even amplification for an acoustic wave in a weakly ionized gas. To improve the chances of observing what might be a small effect, it was felt that the optimum conditions must be determined and the experiment conducted under similar conditions. "Conditions" here refers to the values of controlable discharge parameters.

The purpose of the experiment was to measure a change in the attenuation constant. When the terms in Ingard and Schultz's expressions were analyzed, the obvious variables were the microscopic parameters: neutral particle density N_n, electron density N_e, neutral temperature T_n, and electron temperature T_e and the angular frequency of the acoustic wave ω. The problem of determining the optimum conditions was thus the mathematical problem of minimizing a general function of five variables with the variables constrained to a certain region, the region of experimental feasibility. This is best done with a computer.

Since as presented, the Ingard-Schulz equations were not suited to such an analysis, the process was one of analysis and synthesis. Analysis was needed to express the terms as relations involving only the above variables and physical constants of the gas such as cross section or molecular diameter. These terms were then evaluated numerically and combined with each other to compute the predicted value of the attenuation constant for the input values of the variables.

Using a computer, the equations were evaluated for a wide range of values of the input variables. This provided a more thorough evaluation of the Ingard-Schulz equations than they had made. The results showed that their approximate expression, equation (2.21) predicted net amplification over a large region of variable space although the more complete expressions never did, even when Ingard's criterion for the validity of the approximation was satisfied.

The process of analysis is described in Section IIIA following. The procedure used in evaluating the terms and determing the optimum values for the variables is described in section IIIB. The results of the evaluation are presented and discussed in section IIIC.

It should be pointed out that this section discusses the evaluation of the Ingard-Schulz equations before the experiment was conducted. Afterwards, the program was used to compare the predicted values of the attenuation constant with the observed values by substituting known or estimated values for the variables.

A. ANALYSIS

1. Obtaining the Attenuation Factor

The system of homogenous equations (2.19) has a non-trivial solution only if the co-efficient matrix is singular, i.e. its determinant is zero [34]. We can therefore write:

$$\|\text{co-efficients}\| = A(EI-HF)+B(GF-DI)+C(DH-GE) = 0 \qquad (3.1)$$

We define the complex quantity $n = ck/\omega$. It can be considered an acoustic index of refraction. Since in Eq.(2.20) n^2 appears only in the co-efficient A, we may solve for it by defining A_1 as:

$$A_1 = A+n^2 = 1 + i\left(\frac{\omega}{\omega_{nn}} + \frac{\omega_{ni}+\omega_{ne}}{\omega}\right)$$

and substituting this into equation (3.1). After a rearrangement of terms, n^2 is found to be:

$$n^2 = A_1 + \frac{C(DH-EG)}{EI-HF} + \frac{B(GF-DI)}{EI-HF} . \qquad (3.2)$$

Now n^2 can be written in the form

$$n^2 = \lambda+i\mu \qquad (\lambda,\mu \text{ real})$$

and the desired result is the wave propagations constant k in the from:

$$k = \alpha+i\beta, \qquad (\alpha,\beta \text{ real}) \qquad (3.3)$$

so that the problem reduces to solving for the square root of a complex number. In particular, since α is defined to be positive, the root of interest is the one for which β has the same sign as μ. This means that if n^2 is written in polar form:

$$n^2 = |n^2| e^{i\theta},$$

the solution is the root at $\theta/2$, i.e. the principal root. The attenuation factor, β, the ultimately desired result, is given by

$$\beta = \frac{\omega}{c} \mathrm{Im}(n_1) \qquad (3.4)$$

where n_1 is the principal root of n^2.

2. Acoustic Losses

An acoustic wave is damped through two physically different mechanisms, viscosity and thermal conductivity. The damping can also be distinguished by the location where the losses occur, i.e. at the boundaries or in the bulk of the gas. The latter characterization has the advantage that it divides the losses into two terms of different frequency dependence. When the losses are high, the two effects are not simply additive but instead are coupled together in the differential equations for an acoustic wave. As this would only be the case for viscous fluids or for tubes of small diameter, neither of which are treated here, we shall consider the effects to be additive. Since the mean free path and therefore the boundary layer is inversely proportional to density, at sufficiently low pressures the assumption of additive effects may have to be re-examined.

A plane wave traveling in a duct attenuates expontentially with distance with attenuation co-efficient "a". With small losses, a is the sum of the bulk attenuation co-efficient a_B and the wall attenuation co-efficient a_ω. For a circular pipe, these co-efficients are given by Morse and Ingard [35,p989] as:

$$a_\omega = \frac{\omega/c}{2r}\left[\sqrt{\frac{2\eta}{\omega\rho}} + (\gamma-1)\sqrt{\frac{2\mathcal{K}}{\rho c_p \omega}}\right]$$

$$a_B = \frac{\omega^2}{2c^2}\left[\frac{4}{3}\frac{\eta}{\rho c} + (\gamma-1)\frac{\mathcal{K}}{\rho c c_p}\right] \qquad (3.5)$$

where $\mathcal{K}$, the thermal conductivity, is given by:

$$\mathcal{K} = \frac{5}{3}\eta C_v$$

and

$$\eta = \frac{\ell \rho c}{\sqrt{\gamma}} \quad \text{is the co-efficient of viscosity.}$$

The mean free path ℓ is

$$\ell = \frac{1}{\sqrt{2}\,\pi D^2 N_n} \quad . \tag{3.6}$$

In these expressions, ρ is the mass density, c the adiabatic speed of sound and D the atomic diameter. When these expressions are used for a three component fluid, c will be written c_n; however there is no difference between the two, $c_n \equiv c$.

Since the energy of a wave is given by the square of its amplitude, the energy of a wave attenuates with co-efficient 2a. With a velocity of c_n, the characteristic time for energy dissipation by the neutral component, τ_n, is related to the attenuation co-efficient a by:

$$\frac{1}{\tau_n} = 2ac \quad . \tag{3.7}$$

Therefore, for the small damping approximation of a plane wave in a circular pipe, the characteristic time for energy dissipation is given by[3]:

$$\frac{1}{\tau_n} = \left(\frac{\omega}{c_n}\right)^2 \left[\frac{4}{3}\frac{\eta}{\rho} + (\gamma-1)\frac{\mathcal{K}}{\rho C_p}\right] + \frac{\omega}{r}\left[\sqrt{\frac{2\eta}{\omega\rho}} + (\gamma-1)\sqrt{\frac{2\mathcal{K}}{\rho C_p \omega}}\right]. \tag{3.8}$$

---

[3]The expression does not exactly agree with the expression in Ref. 7 but it is consistent with the derivation there and agrees with the same expression in Morse and Ingard [35]. The difference may be due to an error in typesetting.

Substituting for $\mathcal{K}$ and η, using $\gamma = 5/3$ (a good approximation for a noble gas), the above expression simplifies to:

$$\frac{1}{\tau_n} = \sqrt{2.4}\,\omega^2 \frac{\ell}{C_n} + \frac{5}{3r}\sqrt{\sqrt{2.4}\,\omega\ell C_n} \quad . \tag{3.9}$$

This term enters the dispersion relation as ω/ω_{nn} defined by equation (2.22),

$$\frac{\omega}{\omega_{nn}} = \frac{1}{\omega\tau_n} \quad .$$

3. Zero Ionization Limit

In order to be consistent, the attenuation predicted by Ingard's equations, for the limiting case of zero ionization, should be comparable with previous results for acoustic attenuation. For the standard of comparison we shall use the attenuation co-efficient "a" which was used as an input in these equations.

$$a = a_\omega + a_B$$

$$a = \frac{1}{2}\sqrt{2.4}\,\ell\,\frac{\omega^2}{c_n^2} + \frac{5}{6r}\sqrt{\sqrt{2.4}\,\omega\,\frac{\ell}{c_n}} \quad . \tag{3.10}$$

For zero ionization, equations (2.21) and (3.2) reduce to the same expression for n^2,

$$n^2 = 1 + i\,\frac{1}{\omega\tau} \quad . \tag{3.11}$$

Now, both equations (2.21) and (3.2) were based on approximations. When the expressions for the co-efficients, Eq. (2.20), were presented, Ingard and Schulz had already made several approximations. Going back to the full expressions for

the co-efficients, which are contained in the appendix of Ingard and Schulz's paper, an examination shows that when the ionization goes to zero, only one independent co-efficient A_o remains, given by:

$$A_o = 1 - \left(\frac{c_n k}{\omega}\right)^2 \left[1 - \frac{\gamma-1}{\gamma} \frac{i\, f_{2n}/\omega}{1+i\, f_{2n}/\omega}\right] + i\, \frac{f_{1n}}{\omega} .$$

Even though there is only one co-efficient, it must equal zero for the equations to have a non-trivial solution for V_n. Setting A_o equal to zero, and solving for $n^2 = \frac{k^2 C_n^2}{\omega^2}$, we obtain

$$n^2 = \frac{1+i\, f_{1n}/\omega}{1 - \frac{\gamma-1}{\gamma} \frac{f_{2n}/\omega}{1+i\, f_{2n}/\omega}} , \qquad (3.12)$$

where f_{in} and f_{2n} are the viscous and thermal conduction components of the acoustic losses given earlier in section IIA. They are hidden in the expression for the attenuation co-efficient. The attenuation time τ_n can be expressed in terms of these components as

$$\frac{1}{\tau_n} = f_{1n} + \frac{\gamma-1}{\gamma} f_{2n} .$$

Using the same expressions and approximations as before they can be written as:

$$f_{1n} = \sqrt{\frac{16}{15}}\, \omega^2 \frac{\ell}{c} + \frac{1}{r} \sqrt{\sqrt{2.4}\, \omega \ell c}$$

$$f_{2n} = \sqrt{\frac{5}{3}}\, \omega^2 \frac{\ell}{c} + \frac{5}{3} \sqrt{\sqrt{2.4}\, \omega \ell c} .$$

Since there were fewer approximations involved in Eq. (3.12), the value of β obtained is a stronger comparison test then the use of equation (3.11). Using both equations (3.11) and

(3.12), β was calculated for several different values of N_n, T_n and ω. The results were compared with the value of "a" calculated for the same input values using equation (3.10). In all cases, the results agreed within less than 1%. It is therefore concluded that in the limit of zero ionization, the Ingard-Schulz dispersion relations predict the correct attenuation.

4. Neutral Heating by Electrons

The effect of energy transfer to the neutrals by the electrons is expressed through the term $1/\omega\tau$. Ingard and Schulz define τ by the relation:

$$\frac{1}{\tau} = (\gamma-1)\frac{H}{c^2} . \tag{3.13}$$

The rate of energy transfer per unit mass, H, is defined by:

$$H = \left(\frac{8}{\pi^3}\right)^{\frac{1}{2}} \left(\frac{m_e}{m_n}\right)^2 \left(\frac{KT_e}{m_e}\right)^{3/2} N_e \sigma_{en} \tag{3.14}$$

where σ_{en}, the average cross section for energy transfer, is defined as:

$$\sigma_{en} = \left(\frac{\pi^3}{8}\right)^{\frac{1}{2}} \left(\frac{KT_e}{m_e}\right)^{-3/2} \int_0^\infty \int_{-1}^{1} v_e^3 (1-\cos\theta) \frac{d\sigma_{en}}{d\Omega} d(\cos\theta) f(v_e) v_e^2 dv_e .^4 \tag{3.15}$$

The integral over cos θ is the total cross section (velocity dependent) for momentum transfer, q_D, as defined by Present [36]. It is given by:

---

[4] This is the correct expression for σ_{en}, vice the expression given in [7] as confirmed by private communication with M. Schulz (due to a typographical error).

$$q_D(v_e) = \int_{-1}^{1} 2\pi(1-\cos\theta)\,\frac{d\sigma_{en}}{d\Omega}\,d(\cos\theta) \qquad (3.16)$$

Therefore:

$$\sigma_{en}(v_e) = \left(\frac{\pi}{8}\right)^{\frac{1}{2}}\left(\frac{KT_e}{m_e}\right)^{-3/2}\int_o^{\infty} v_e^5\, q_D(v_e) f(v_e)\,dv_e \ . \qquad (3.17)$$

A Maxwellian distribution of electron velocities is a good approximation to the actual distribution in a gas discharge only at extremely low values of E/p [39]. It is recognized that E/p is not low in the usual case as evidenced by figures 125 and 126 of von Engle [40]. However the Maxwellian distribution is computationally convenient to use and is valid as a first approximation to the real distribution function. It is felt that the improvement in accuracy resulting from the use of a better approximation such as the Druyvesteyn distribution does not justify the increased computational difficulties. The value obtained for σ_{en} under this approximation is smaller than the actual value because the approximation indicates a greater number of high energy electrons than actually exist and the cross section decreases at higher electron energies. Substituting the expression for the Maxwellian distribution into Eq. (3.17) gives:

$$\sigma_{en} = \left(\frac{KT_e}{m_e}\right)^{-3}\frac{1}{8}\int_o^{\infty} v_e^5 q_D(v_e) e^{-\frac{m_e v_e^2}{2KT_e}}\,dv_e \ .$$

The cross section for momentum transfer is available in terms of electron energy expressed in electron volts. By defining

$E_T \equiv KT_e/e$, the energy equivalent electron temperature, and effecting a change of variable, σ_{en} can be expressed in the simple form

$$\sigma_{en} = \frac{1}{2}\int_o^\infty q_D(RE_T)R^2 e^{-R} dR \qquad (3.18)$$

where $R \equiv \frac{m_e v_e^2}{2KT_e}$ is the variable of integration by which the average cross section for energy transfer can be evaluated from the momentum transfer cross section data.

5. Collisional Losses

If we refer back to equation (2.2), we see that the terms involving the constants of proportionality ω_{jk} arise from the collision integral for momentum transfer. The collision integral can be written:

$$\int m_j(v_j - u_{jk})\left(\frac{\partial f_j}{\partial t}\right)_{coll} dv_j = \rho_j\omega_{jk}(v_k - v_j) + \rho_j\omega_{j\ell}(v_e - v_j) \ .$$

In order to give a numerical value to ω_{jk}, it must be expressible in terms of the variables and gas properties. To do that, its definition must be understood. Since the momentum transferred from species 1 to 2 through collisions is equal and opposite to that transferred from 2 to 1 through collisions, then we can equate:

$$\rho_j\ \omega_{jk}(v_k - v_j) = -\ \rho_k\omega_{kj}(v_j - v_k).$$

This shows that the constants ω_{jk} are related to ω_{kj} as:

$$\omega_{jk} = \frac{N_k}{N_j}\ \frac{m_k}{m_j}\ \omega_{kj} \ . \qquad (3.19)$$

Notice that due to the mass ratio factor, ω_{jk} and ω_{kj} cannot both be collision frequencies. If in Eq. (3.19) the j-th component is taken to be the heavier component and the k-th component the ion or electron component, the resulting expressions will be consistent with the relations given by Ingard and Schulz. In addition, when the heavier component is the neutral gas, this is consistent with the picture of ω_{jk} being the collision frequency of a particle of the j-th type moving through the k-th fluid component since the neutrals are much more numerous. We can therefore develop analytical expressions for ω_{en}, ω_{in} and ω_{ei}. The other terms will be related by Eq. (3.19).

a. Ion-Neutral Collision Frequency

If it is assumed that the ion-neutral collision cross section is essentially the same as for a neutral-neutral collision, then it follows that the ion-neutral collision frequency is the same as the neutral-neutral collision frequency. The neutral-neutral collision frequency is very closely approximated by the elementary kinetic theory result for a hard sphere ideal gas. The ion-neutral collision frequency can therefore be expressed by:

$$\omega_{in} = \frac{\bar{v}}{\ell} = \sqrt{\frac{8}{\gamma\pi}}\,\frac{c}{\ell} \quad . \tag{3.20}$$

b. Electron-Neutral Collision Frequency

In order to obtain an expression for the electron-neutral collision frequency, we must start with the integral form of the expression given by Present [36] for the collision rate for two intermixed species.

$$\theta_{EN} = \int d^3v_e \int d^3v_n \frac{d\sigma(|\vec{v}_e - \vec{v}_n|)}{d\Omega} |\vec{v}_e - \vec{v}_n| f_n(v_n) f_e(v_e)$$

For electron-neutral collisions, $|\vec{v}_e - \vec{v}_n| \simeq v_e$ and the integrals can be separated. The frequency of collision of an electron with a neutral particle, ω_{en}, is θ_{EN}/N_e. Substituting also the expression for the Maxwellian distribution for $f(v)$, the collision frequency can be written:

$$\omega_{en} = \frac{N_n}{\sqrt{2\pi}} \left(\frac{m_e}{KT_e}\right)^{3/2} \int_o^\infty v_e^3 \sigma(v_e) e^{-\frac{mv^2}{2KT}} dv_e .$$

Finally this can be expressed in a form similar to the expression for σ_{en} as:

$$\omega_{en} = N_n \sqrt{\frac{2KT_e}{\pi m_e}} \int_o^\infty \sigma(E_T R) R e^{-R} dR \qquad (3.21)$$

c. The Electron-Ion Collision Frequency

The electron-ion collision frequency for momentum transfer ω_{ei} is given by Tanenbaum [41] as:

$$\omega_{ei} = 3.62 \times 10^{-12} N_i T_e^{-3/2} \ln \Lambda \quad (N_i \text{ in } cm^{-3}) \qquad (3.22)$$

where $\Lambda = 12\pi r_D^3 N_e$ is the Coulomb cutoff parameter, and r_D, the Debye length is given by:

$$r_D = \left(\frac{KT_e}{m_e}\right)^{1/2} \frac{1}{\omega_e} .$$

Expressions for the plasma frequencies for electrons ω_e, and for ions ω_i,

$$\omega_e = \left(\frac{q_e^2 N_e}{m_e \epsilon_o} \right)^{\frac{1}{2}}$$

$$\omega_i = \left(\frac{q_e^2 N_e}{m_n \epsilon_o} \right)^{\frac{1}{2}} = \sqrt{\frac{m_e}{m_n}} \; \omega_e$$

are well known and present no computational difficulty.

6. Ion-Acoustic Losses

Losses caused by viscosity and thermal conductivity in the ion fluid component are represented by the term ω/ω_{ii} which is defined by

$$\frac{\omega}{\omega_{ii}} = \frac{1}{\omega} \left(f_{1i} + \frac{\gamma_i - 1}{\gamma_i} \; f_{2i} \right) .$$

The quantity $f_{1i} v_i$ represents viscous stress in the ion fluid. The other term f_{2i}, when multiplied by θ_i, the ion temperature perturbation, accounts for heat conduction in the ion fluid. Adapting a heuristic approach, assume that ω/ω_{ii} has the same form as ω/ω_{nn} given by equation (3.9). Under such an assumption, it can be expressed as:

$$\frac{\omega^2}{\omega_{ii}} = \frac{1}{\tau_i} = \sqrt{2.4 \; \omega^2 \frac{\ell_i}{c_i}} + \frac{5}{3r} \sqrt{\sqrt{2.4 \; \omega \ell_i c_i}} \qquad (3.23)$$

where the subscripts indicate that these are ion terms.

It is not unreasonable to assume that, since their masses are essentially the same and their temperatures nearly the same, the

ion sound speed c_i is the same as the neutral sound speed c_n. However the mean free path for ions ℓ_i, must be unlike that for neutrals, since one must consider the effect of Coulomb interactions. Wu [42] expresses the mean free path for Coulomb interactions, which have been corrected for Debye screening, as:

$$L_i = \frac{1}{N_e r_m^2 \ell n(r_p/r_m)} , \qquad (3.24)$$

where $r_m = \frac{q^2}{4\pi\epsilon_o KT}$ is the mean distance of closest approach for two like charges q. Wu refers to T as the mean plasma temperature. Since we are considering ion losses, the temperature to be used in the expression for r_m is the ion temperature. However the Debye length is determined by the electrons due to their higher temperature and greater mobility.

Because the mean free path of ions in a weakly ionized gas is limited not by Coulomb interations but through collisions with neutrals, this expression alone would give erroneous results. The mean free path, λ, can be expressed in terms of the mean velocity v and collision frequency ν as

$$\lambda = \frac{v}{\nu} .$$

In a mixture of gaseous components, the total collision frequency of one component is the sum of the partial collision frequencies. This leads to the result:

$$\frac{1}{\lambda_{eff}} = \frac{1}{\lambda_{ie}} + \frac{1}{\lambda_{ii}} + \frac{1}{\lambda_{in}} .$$

Ignoring $1/\lambda_{ie}$ and making the approximation that $\lambda_{in} = \lambda_{nn}$, the mean free path for ions can be written as:

$$\ell_i = \frac{1}{1/L_i + 1/\ell} \cdot \qquad (3.25)$$

B. COMPUTATION AND EVALUATION

1. Defining the Limits of the Variables

Since the goal of the analysis is a prediction of results for a given experimental arrangement, it would have been desirable to formulate the problem in terms of filling pressure p_o, filling temperature T_o; tube radius r, frequency v and current I_o. Unfortunately the conversion of p_o, T_o, and I_o to the variables T_e, T_n and N_e is not a trivial problem. For that reason, the independent variables chosen were: neutral density N_n, neutral temperature T_n, electron density N_e, electron temperature T_e and angular frequency ω. The limits of these variables were then chosen to correspond to the values expected in a feasible experiment.

A practical range of values for the tube radius is from .5 cm to 10 cm. This value was fixed at 2 cm except when investigating its effects.

The lower limit of the angular frequency was fixed at 100 radians/second because it was experimentally possible and numerically convenient. The assumption of plane waves was implicit in the formulation of the problem by Ingard and Schulz. From an experimental point of view, in order to avoid the effect of higher modes propagating in a tube, this sets an upper limit for ω of the

order of $2\pi c/r$ [35]. However most pulse experiments involve higher frequencies and Yatsui, et.al. [8,9] worked with 50, 100 and 200 kilocycle continuous and burst sineisoidal signals. The limit of validity of the continuum description is when the wavelength is of the order of the mean free path. This corresponds to about 10^5 radians/sec. at room temperature and pressures around 1 torr and was selected as the upper limit for ω.

The neutral density limits were set at $3.5 \times 10^{14} cm^{-3}$ and $1.5 \times 10^{18} cm^{-3}$, corresponding approximately to filling pressures of .01 torr and 50 torr at room temperature respectively.

The electron-density limits relative to the neutral density were selected arbitrarily, with a logical basis, as $10^{-8} N_n$ to $10^{-3} N_n$ with absolute limits of $10^8 cm^{-3}$ to $1.5 \times 10^{13} cm^{-3}$. For currents of milliamperes at low pressures around 1 torr, the degree of ionization is about 10^{-6} [40,43]. A lower limit two orders of magnitude below this is reasonable and a higher limit of three orders of magnitude greater would correspond to ampere currents. These relative limits were tempered by the current densities which they implied for large pressure changes.

The neutral gas temperature is not truly independent but actually depends on the discharge current, pressure, tube radius, and external cooling effects. For the purpose of this analysis, it is sufficient to assume the temperature can range from the boiling point of the gas to the upper limit of temperature which can reasonably be obtained in an oven, approximately 700 Kelvin.

The electron temperature T_e is definitely not an independent variable, being determined by the discharge conditions specified through the other variables [40]. The only analytical expression available implies that the electron temperature is a function only of the gas and the similarity parameter pR. The expression is of limited validity, falling at very low values of pR and high p. Rather than restrict T_e with an artificial constraint, it was felt that treating it as an independent variable would yield more valid results. The limits were chosen to correspond to those normally encountered experimentally [40,44], 10^4 to 10^5 Kelvin.

It should be pointed out that permitting these variables to move freely within their limits places less constraints on their possible values than actually exist. The result may predict physically unrealizable results.

2. Computation of Attenuation and Determination of Minimum

For the computation, the formulas were first placed in the order in which their values were needed. They were then translated for computer processing and a program written using the FORTRAN IV programming language. The values for the fundamental constants are from [45], data for Argon are from Cook [46] except the atomic diameter and scattering cross section for momentum transfer which are from McDaniel [39].

The scattering cross section data were taken from figure 4-3-1(c) of McDaniel, using a transparent overlay grid and dividers to establish a table of values of q_D versus electron energy in electron volts. A subroutine was written to use this table to

perform the numerical integration to determine σ_{en} using Eq. (3.18) and to determine ω_{en} using Eq. (3.21). In computing ω_{en}, the momentum transfer cross section data were used to approximate the collision cross section. The momentum transfer cross section is from 20% to 50% smaller than the collision cross section for all values of electron energy. This substitution causes the electron collision frequency to be low by $\approx$ 25%. If this was found to be critical, a correction could be applied. This procedure was considered to be justified by the increased convenience in setting up the problem and in reducing the number of complete integrations required by a factor of two.

A set of fixed values: $\omega = 10^3$, $N_n = 10^{16}$, $N_e = 10^{10}$, $T_n = 300^{\circ}K$ and $T_e = 10^4 K$ were used to evaluate all expressions with an electronic calculator. This served as a cross check on the computer results. To check the validity of the expressions used to calculate attenuation, a comparison was made of the attenuation factor for bulk losses with a value from another source. Using Eqn. (3.9) and (3.7), we can write

$$\frac{a_{BULK}}{\omega^2} = \frac{1}{2c\omega^2}\left(\frac{1}{\tau_n}\right)_{BULK} = \sqrt{.6}\,\frac{\ell}{c^2}\ ;$$

therefore

$$\frac{\beta'}{f^2} = 4\pi^2\sqrt{.6}\ \frac{\ell}{c^2}\ .$$

Evaluated at standard temperature and pressure, this yields

$$\frac{\beta'}{f^2} = 1.89 \times 10^{-11}\ m^{-1}/sec^{-1}$$

which agrees with the value of β'/f^2, 1.87×10^{-11}; for Argon in Kinsler and Frey [47].

3. Discussion of Results of Calculations

At the point used for checkout of the computer program, the agreement between the attenuation constant calculated using Eq. (3.1) and the Ingard-Schulz approximation, Eq. (2.21), was very good with differences on the order of a few parts per million. However the agreement was not so good in other areas. The use of Eqn. (2.21) yielded predictions of amplification over a wide range of conditions. In contrast, results using equation (3.1) show no amplification within the entire range of the variables, but merely an increase or decrease in attenuation, with respect to that without ionization. The amplification predicted by Eq. (2.21) is therefore considered erroneous, arising from factors being neglected in the approximation.

The minimum attenuation was found to occur at the limits of the allowed ranges of the variables. Those variables at their high limits were neutral density, electron density and electron temperature. The frequency and neutral temperature were at their low limits.

Figure 1 shows the attenuation as a function of angular frequency, displayed on a semi-log plot. The curve parameter is neutral density. Neutral temperature, electron temperature and degree of ionization have been held constant at their optimum values. A more revealing display is shown in Figure 2 which is a plot of the

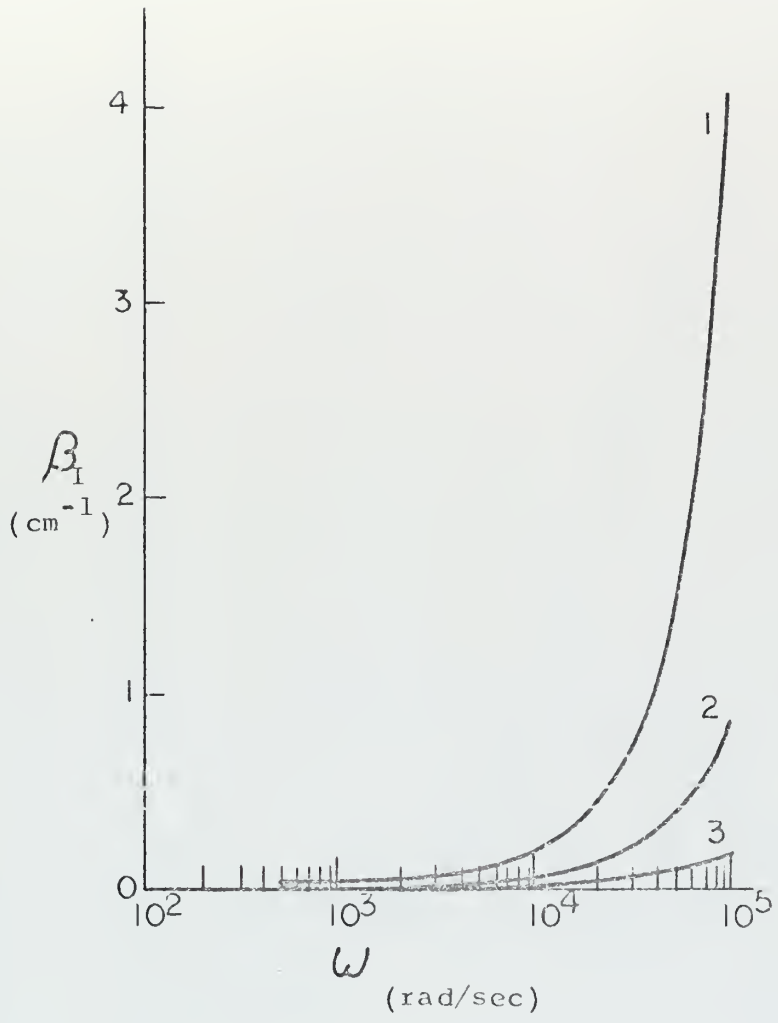

Figure 1. Predicted Attenuation Factor in Discharge Plasma in Dependence on ω for Various Values of Neutral Density. Parameters are: T_n = 88K, T_e = 10^5K, and N_e/N_n = 10^{-5}.
Curve 1: N_n = 10^{15} cm^{-3}.
Curve 2: N_n = 6.2 x 10^{15} cm^{-3}.
Curve 3: N_n = 3.9 x 10^{16} cm^{-3}.

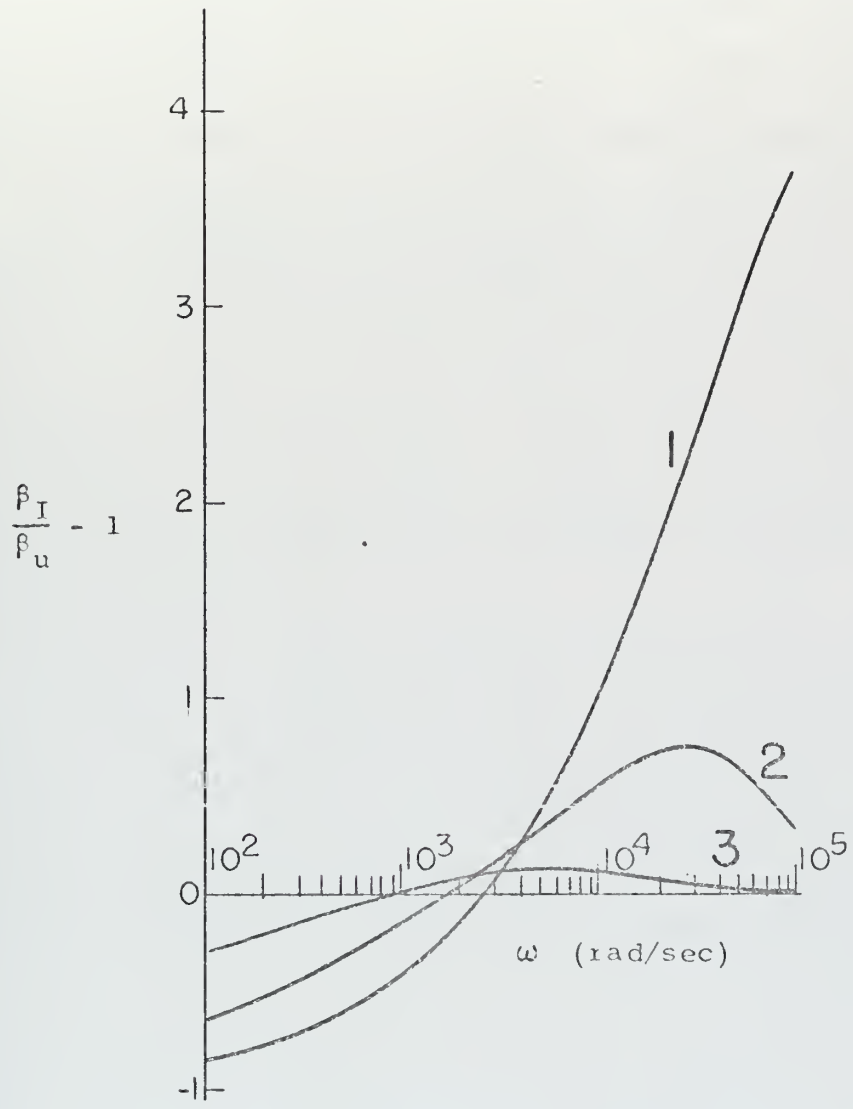

Figure 2. Relative Change in Attenuation due to Ionization in Dependence on ω for Various Values of Neutral Density.

Values calculated using Ingard-Schulz equations with parameters $T_n = 88K$, $T_e = 10^5K$, and $N_e/N_n = 10^{-5}$. The values of neutral density for the curves are:

1. $N_n = 1.5 \times 10^{18}$ cm^{-3};
2. $N_n = 2.4 \times 10^{17}$ cm^{-3};
3. $N_n = 3.9 \times 10^{16}$ cm^{-3}.

fractional change in attenuation due to ionization. The curve parameters are the same as for Figure (1). Positive values correspond to an increase in attenuation; negative values, a decrease.

The ion perturbation velocity was found to remain the same magnitude as the neutrals and in phase. The electron perturbation velocity was the same magnitude as the neutrals, and in phase, at low frequencies, and decreased to zero and went out of phase at high frequencies. The frequency at which the transition began shifted to higher frequencies as the density increased. This is displayed in Figure 3.

The results of the computation indicate that net amplification is a false prediction, arising from approximations; however, attenuation is affected to a measurable degree. The maximum decrease occurs with high pressure, low temperature, low frequency and a high electron temperature, highly ionized discharge.

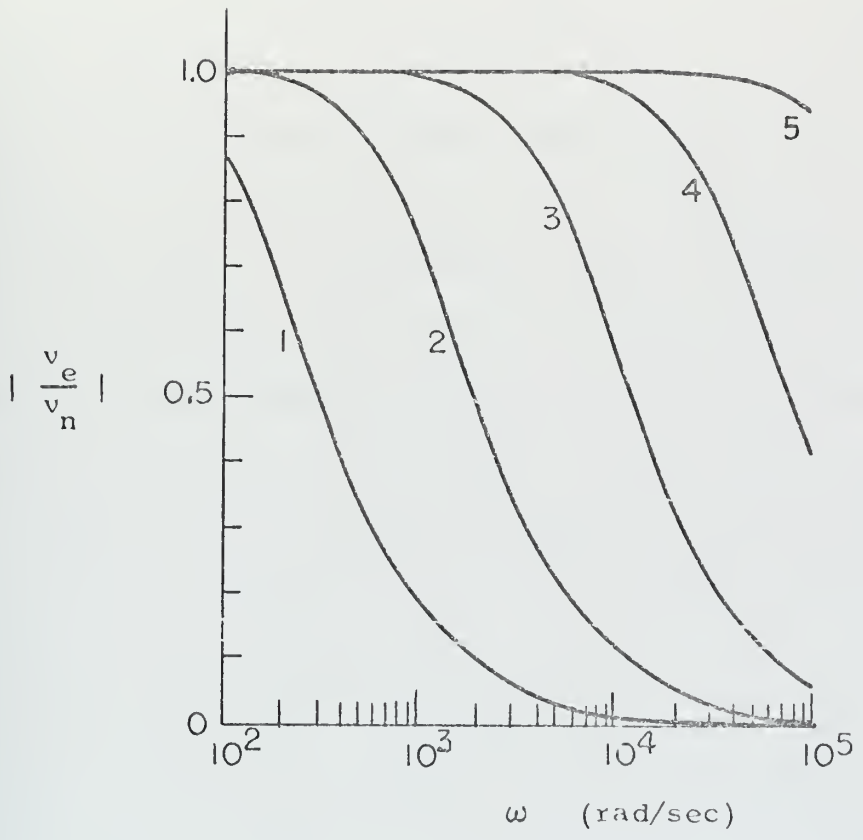

Figure 3. Magnitude of Ratio of Electron to Neutral Perturbation Velocity in Dependence on ω for Various Values of Neutral Density.

Values computed using Ingard-Schulz equations with parameters: $T_n = 88K$, $T_e = 10^5K$, and $N_e/N_n = 10^{-5}$. The values of neutral density for the various curves are:

1. $N_n = 10^{15}$ cm^{-3}; 2. $N_n = 6.2 \times 10^{15}$ cm^{-3};

3. $N_n = 3.9 \times 10^{15}$ cm^{-3}; 4. $N_n = 2.4 \times 10^{17}$ cm^{-3};

5. $N_n = 1.5 \times 10^{18}$ cm^{-3}.

IV. EXPERIMENTAL ARRANGEMENT AND PROCEDURE

The original concept was to use an auxiliary discharge, with a gated sine wave of current to produce gated sine waves of sound. the sound amplitude was to be measured before and after passing through the main discharge area. From a comparison of the signal amplitudes at the two points for various frequencies, the attenuation factor and its variation with current magnitude and polarity would be determined. The analysis of a preliminary experiment showed that other factors had to be considered and that a Fourier analysis of the signals was needed. Compromising between the need for a signal with low frequency components and one with all significant features appearing before the reflection of the signal from the tube ends, a one millisecond current pulse was selected to provide the sound pulse. Although a two ampere power supply was available for the main discharge, the high temperature of the main discharge column limited the experiment to half an ampere.

A. SOUND SOURCE

The sound source was a small auxiliary discharge far removed from the main discharge and the two diodes bounding the main discharge. The auxiliary discharge was always on when in operation. The quiescent state was a normal glow with a current of less than 10 ma. The peak current during a pulse was around 150 to 200 ma. which corresponded to an abnormal glow. The current in the auxiliary discharge was controlled through a transistor load. During preliminary work, it was ascertained that the sound produced was

closely related to the current in the auxiliary discharge but not to the voltage or to the power dissipated. Therefore only the current was controlled and monitored.

Although a pulse was used for the final data, the current control circuitry was designed for sinusoidal currents, either continuous or gated. To avoid extinguishing the discharge, a minimum current flow was required at all times. This required a bias signal equal to the sinusoidal signal. The continuous mode was not operational due to rapid deterioration (in times less than or of the order of one-second) of the discharge current when run at the high currents required for a good acoustic signal. The cause was not thoroughly investigated, but was believed due to excessive power dissipation.

The current control circuitry is shown (enclosed in dashed lines) in Figure 4. It consists essentially of two circuits feeding the base side of two transistors operating in parallel. One circuit consists of a small d.c. battery with a variable resistor for controlling the quiescent state of the discharge. The other circuit sums two input signals to provide the a.c. signal.

Because of their high voltage capability (300 V), and their high dynamic resistance, Motorola MJ3202 transistors were used. Parallel operation was chosen to give a greater current range to the discharge while remaining within the power rating and linear range of the transistors. Emitter biasing resistors were used to balance the load between the two transistors. Although some

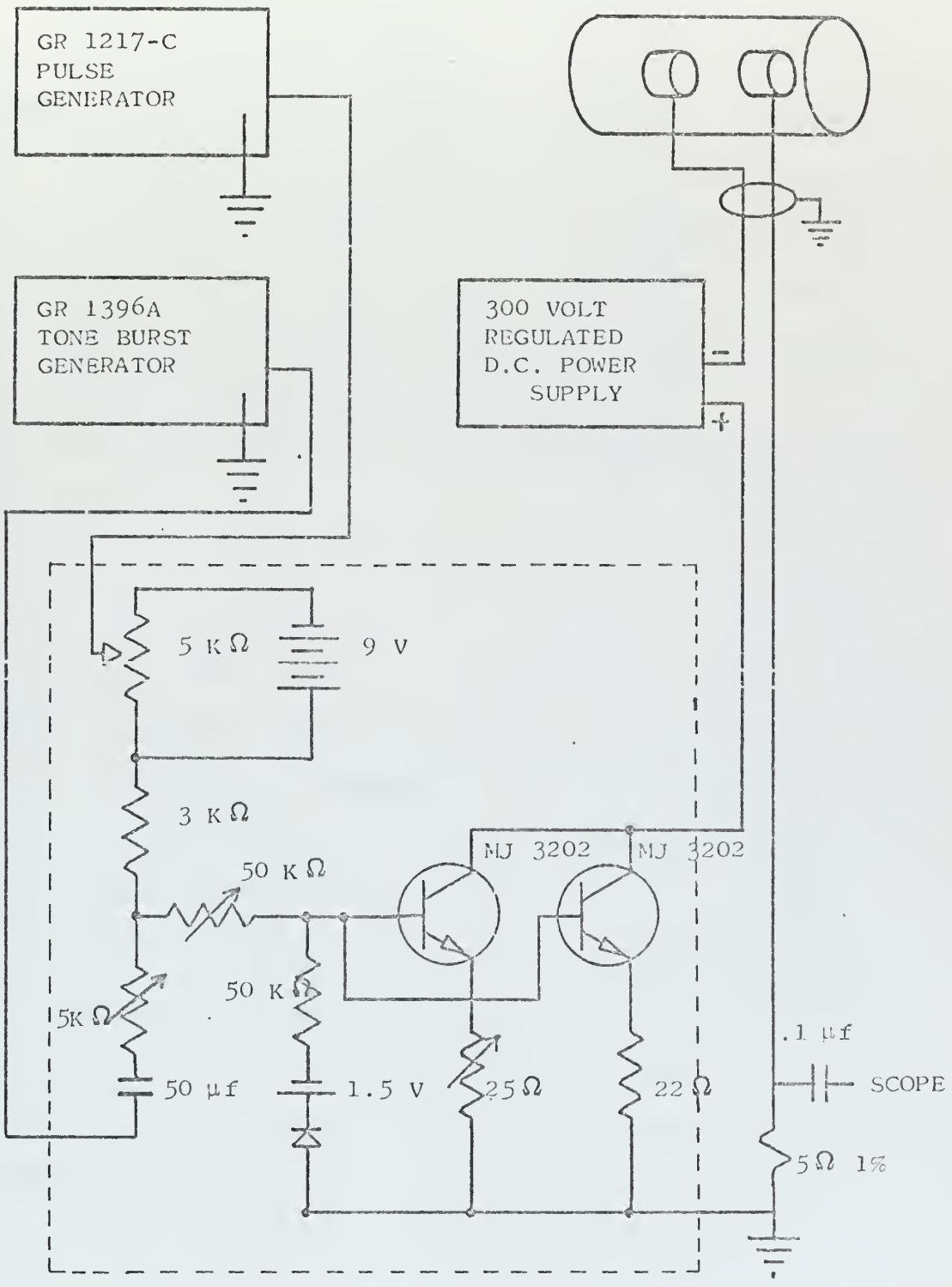

Figure 4. Sound Source Circuit.

negative feedback occurred due to the absence of bypass capacitors, it did not have a noticeable effect.

A General Radio GR1217-C Unit Pulse Generator provided the d.c. pedestal for the gated sine wave. The degree of modulation by the gated sine wave and the amplitude of the a.c. discharge currents were adjustable through variable resistors. For ease of control, multiturn potentiometers were used for control of bias, quiescent current and a.c. current amplitude.

The General Radio equipment used required the low side of the transistor circuit to operate at ground potential. To minimize electrostatic interaction with the diode microphones, the anode of the auxiliary discharge was grounded. This meant that both terminals of the d.c. power supply were floating above ground. Since the floating potential varies greatly during the current modulation, capacitive coupling of the terminals to ground was found to distort the discharge current waveform. The power supply used (Universal Electronics Model G3050M) was chosen because of its low coupling. However its maximum voltage was 300 volts. This did not permit using the full current capability of the circuit at low pressures. Consequently operation was limited to pressures above 5 torr for good acoustic signals, although use of another power supply would have extended the operating range. Figure 5(a) shows a typical discharge current pulse waveform with a gated sine wave.

The electrodes for the auxiliary discharge were two tantalum cylinders ($1\frac{1}{4}$ cm long by 2 cm dia.) with faces separated by $3\frac{1}{2}$ cm. They were mounted axially in the tube, supported by .070 inch diameter KOVAR leads. The leads were beaded with glass for electrical insulation.

(a)

(b)

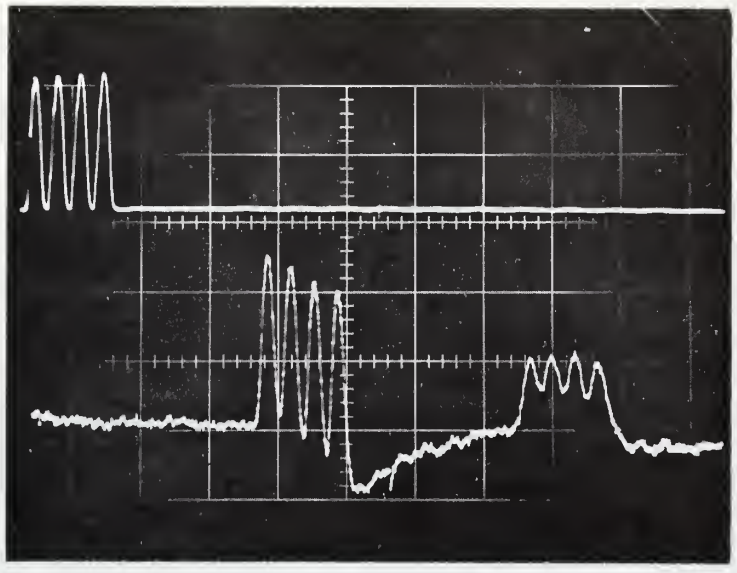

Figure 5. Sound source current waveform and resultant sound. Ambient pressure is 8.7 torr. Gas is Argon. Frequency of sine wave being gated is 3000 Hz. Time scale is .5 ms/cm.

(a) Sound source current. Vertical scale is 100 ma/cm.

(b) Sound produced by discharge current. Vertical scale is uncalibrated. The second pulse of sound is the reflection from the near end of the tube.

B. SOUND DETECTION

Mobility-limited thermionic diodes were used to detect the sound waves. They were mounted axially, one on each side of the discharge region. Electrostatic shielding was provided by a cylinder of heavy, 2.3 mil., copper foil which was wrapped around the tube at the location of the diode. The shield extended several inches on both sides of the diode and was connected to ground. Since the cables and connectors were shielded, the only part of the circuit not shielded was a small portion of feedthroughs where they penetrated the glass. Also the diode was not shielded on the ends. For a more complete discussion of the diode and its susceptibility to noise, see Appendix A. Figure 5(b) shows a typical diode response signal.

For the experiment, filament power for both diodes was provided by the same power supply, a Power Designs 3610OR regulated power supply operating in the constant voltage mode. Figure 6 shows the circuit employed for power and signal detection.

C. TUBE DESIGN AND CONSTRUCTION

There are two features of the tube used in the experiment which are worthy of note. One is the method of mounting the elements. The other is the length of the tube and the placement of the elements therein.

The tube elements were mounted on feedthroughs which did not distort the tube walls significantly. The feedthroughs were

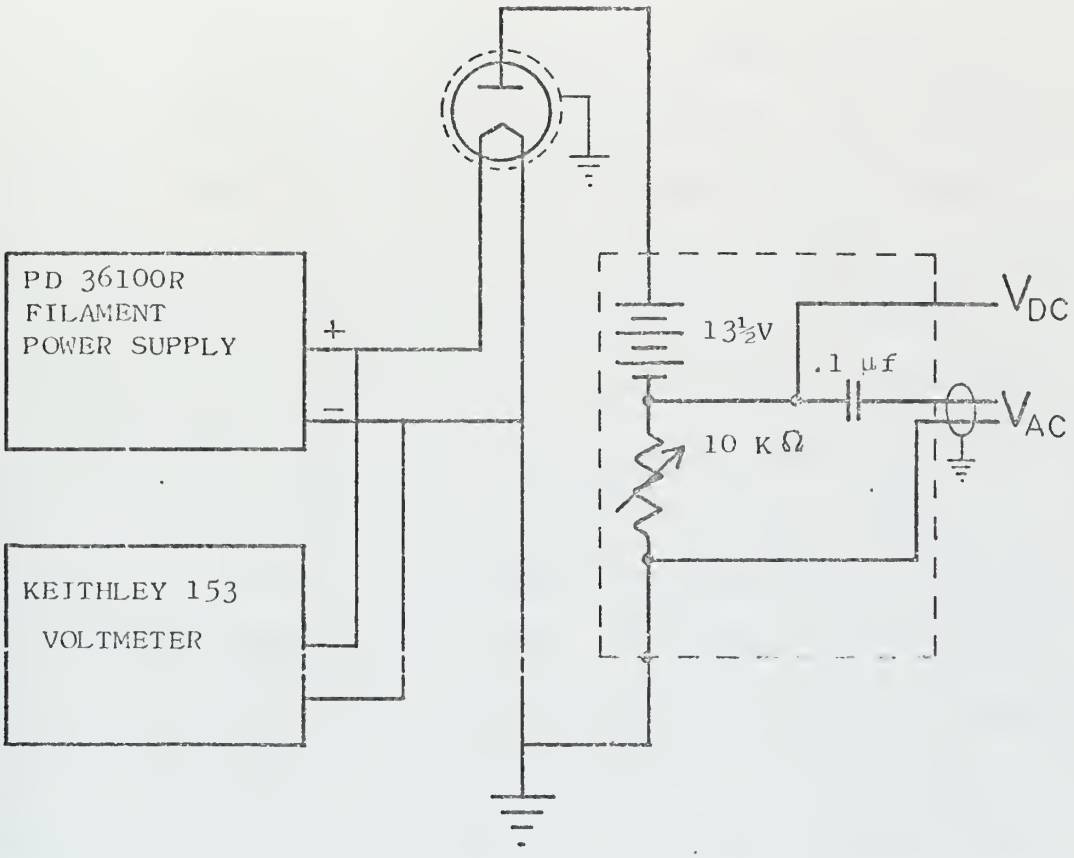

Figure 6. Sound Detection Circuit.

sealed with a special glassblowing technique which is discussed in the appendix. The result was a tube which could be treated as an acoustic waveguide for frequencies much higher than those used.

To reduce the effects of reflections and electrostatic interactions, the elements were physically separated so that the acoustic time of flight separated the unwanted, from the wanted, signals. This required a half meter buffer region at the tube ends and a one meter region between the sound source and the nearest diode.

In addition, it was discovered during preliminary experiments, that there were positively and negatively charged particles extending into the supposedly neutral region far beyond where they were expected. A series of experiments established that they were real and that both types were present. The buffer region reduced the effect but screening electrodes were used for further reduction. Since with cold filaments, any diode signal was attributable to charged particles rather than sound, the screnning effectiveness was studied with cold filaments, in which case, the diodes acted like double Langmuir probes. The cold filament effect was strong in Neon but barely noticeable in Argon. Although interesting in itself because these signals were detected at distances from the discharge of 30, 40 and 50 cm in Neon at pressures $\approx$ 10 torr, the phenomenon was studied only enough to eliminate its interference. A schematic drawing of the tube appears in Figure 7 and the locations of the tube elements appear in Table 1.

Copper-constantan thermocouples, of 5 mil wire, were used to measure the temperature on the tube axis at three points. For

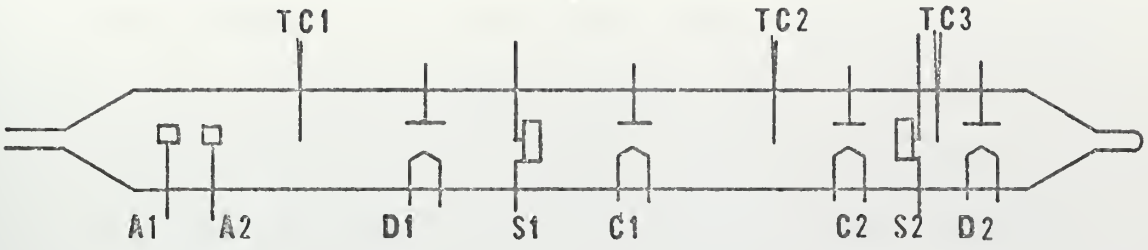

Figure 7. Schematic Drawing of Discharge Tube. Identification of Symbols and Locations are Shown in Table I.

TABLE I

LOCATION OF TUBE ELEMENTS

ITEM	SYMBOL	LOCATION*(cm)
End 1 †		-149.7
Anode 1	A1	-103.4
Anode 2	A2	-98.7
Thermocouple 1	TC1	-50.3
Diode 1	D1	0
Screen 1	S1	26.3
Cathode/Anode 1	C1	37.3
Thermocouple 2	TC2	102
Cathode/Anode 2	C2	122.2
Screen 2	S2	133.4
Thermocouple 3	TC3	139.3
Diode 2	D2	152.5
End 2		203 ‡

* Location given is location of center of element

† Tube ends taper from 4 cm to 1 cm diameter over 5 cm. Distance refers to beginning of taper.

‡ For calculating tube volume, the effective length is 363 cm.

support and insulation, the leads were first sealed in fine twin capillary glass tubing with ULTEK VACSEAL epoxy. The wire to extend into the tube was left exposed. During construction of the main tube, a small piece of tubing, large enough to hold the capillary tubing, was attached. The capillary tube was sealed inside of this tube with the epoxy. The seal was good and the thermocouples worked well. Such a method is not recommended for the main discharge area. This is because the temperatures encountered in the vicinity of the discharge may exceed the maximum recommended for the epoxy, 150°C. In this experiment, such heating caused contamination of the discharge and limited operation of the main discharge to currents below .5 ampere.

The pumping train used for evacuating the tube consisted of a VEECO Model EP2A1 diffusion pump, rated at 85 ℓ/sec, pumping to a DUOSEAL forepump. A NRC model 720 ionization gauge control with a type 536-SK ionization gauge was used to monitor the pressure above the trap, which was kept filled with liquid nitrogen. A one inch line was used between the trap and the high vacuum isolation valve (a GRANVILLE PHILLIPS type C value) used to connect the discharge tube to the pumping system. The ultimate vacuum obtained was around 5×10^{-8} torr as measured by the gauge.

The gas filling system was connected to the tube via a (CEC type 25) high vacuum valve. Pressure was measured with a manometer filled with Octoil S. A trap located between the filling system and the tube was partially filled with liquid nitrogen whenever the connection to the tube was open.

D. MAIN DISCHARGE

In order to determine the effect of polarity, the electrodes at both ends of the main discharge needed to serve as cathode or anode. Therefore they were of identical design, consisting of a filament and a cylindrical anode. The filament was used as the hot cathode for the main discharge or as the hot cathode for a "Pupps discharge" at the anode of the main discharge. It was a ¼ inch diameter, 7 turn helix, directly heated tungsten dispenser cathode designed for laser work and produced by SPECTROMAT. It is rated at an emission current of $5A/cm^2$ at $1150^{o}C_{B}$. The anode cylindrical electrode which was mounted concentric with the filament, was located so that the first two turns of the filament, on the discharge side, were exposed. This was done so that the Pupps discharge would tend to go toward the leading edge of the anode, and thus eliminate anode oscillations. A small low ripple (20V, 1.5A) D.C. power supply was used for the Pupp's discharge power source.

Filament power for the main discharge cathode was supplied by a KEPCO KS-8 100M power supply. Filament power for the Pupps discharge cathode was supplied by a POWER DESIGNS PD36100R unit. The load for the main discharge was two high power variable resistors connected in parallel. The main discharge power supply was a KEPCO 770B, 600 V d.c. supply.

A reasonably simple, yet effective system was used to electrically isolate the main discharge system from the remainder of the circuitry. The 60 cycle input power for all units was isolated

using transformers. All equipment for the main discharge was mounted on the same rack, which contained no other equipment. The chassis ground for all of this equipment was connected to a common point which was then connected to ground via a one megohm resistor in parallel with a 10 μf capacitor. The a.c. and d.c. potentials across these points were monitored with high impedance devices. This precaution was taken to prevent the buildup of a high electrostatic potential between the two ground points. The a.c. current in the discharge was monitored by using a current probe with a sensitivity of 1 mv/ma. To prevent a large potential difference between the two ground systems, arising from interaction of the fields, a potentiometer was used to vary the potential of the main electrodes with respect to the secondary ground. This is shown in Figure 8 as part of the main discharge circuit.

The discharge was ignited with a Tesla coil in conjunction with a copper wire wrapped around the discharge tube between the anode and the cathode. This was necessary because of the high breakdown voltages required at the pressures used.

E. ELECTRONIC MEASUREMENTS

The three waveforms of interest - the sound source current, and the two diode signals - together with a trigger signal were recorded on a four channel FM tape recorder (Precision Instrument Co., PI-6200) for later analysis. Recording was done at 37.5 ips. Record and playback specifications are contained in Appendix C. The frequency response did not appear to distort the two diode

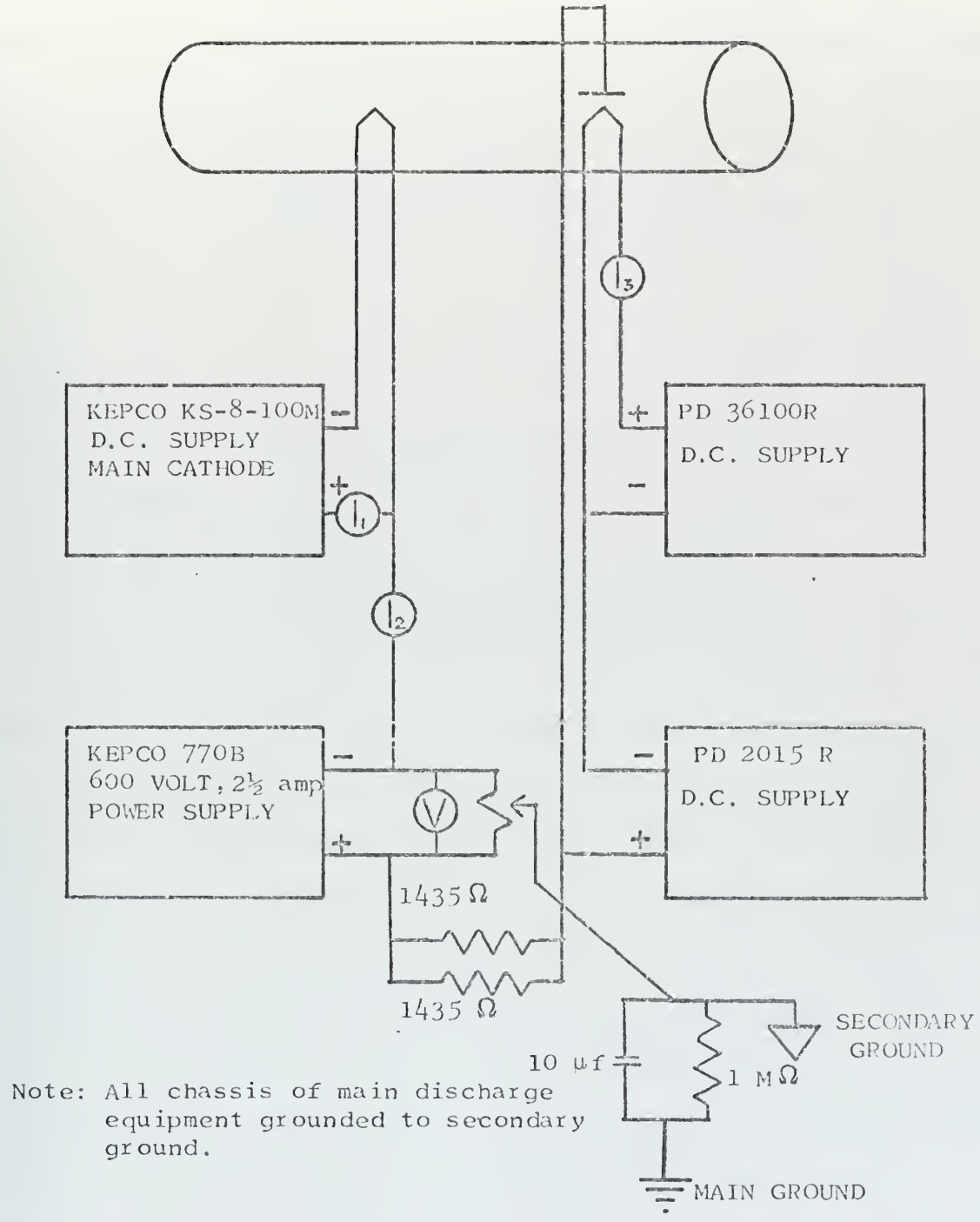

Figure 8. Main Discharge Circuit.

signals but it did affect the trigger and discharge current signals since these had significant high frequency components. Figure 9(a) shows a typical diode signal. Figure 9(b) shows a typical playback of a diode signal. It should be noted that these figures are not derived from the same sample.

The trigger signal was provided by a General Radio GR 1217-C Unit Pulse Generator operating at a pulse repetition rate of 10 Hz. The output signal was a one millisecond rectangular pulse which was used to trigger the scope and was also recorded. The "delayed sync" output was used to trigger another unit pulse generator from which a one millisecond pulse was fed to the current control circuit. The discharge current was observed by measuring the voltage across a 5 ohm precision resistor.

The output signals from the diodes were amplified with two differential amplifiers, TEKTRONIX RM122, with an input impedance of 10 megohms. The amplifiers could provide amplification of either 100X or 1000X. Both output signals were recorded on tape. The diode output contained very sharp noise spikes which, after amplification, adversely affected the recorder operation. To eliminate this, a slicing circuit, which clipped all signals whose value exceeded $\pm$ 1.5 volts, was employed between the amplifier output and the tape recorder. This circuit permitted an improvement in the signal to noise ratio since the noise could not exceed 1.5 volts and the signal could be amplified to a level just below that.

(a)

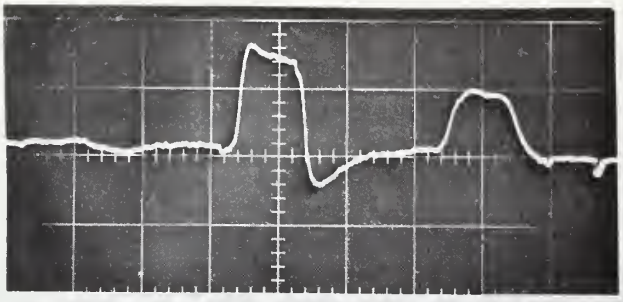

(b)

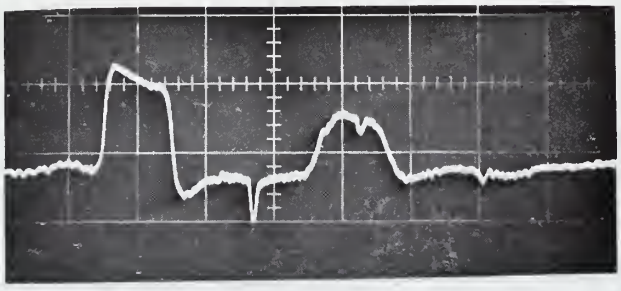

Figure 9. Comparison of Typical Diode Signal with Playback of Diode Signal.

(a) Direct display of diode signal.

(b) Playback of diode signal. Due to triggering problems, the playback is not a playback of (a). The playback does show how little the recording process distorted the signal.

F. EXPERIMENTAL PROCEDURE

After preliminary experimental work had established the background, the progress of the experiment can be divided into five stages: (1) construction of the tube, (2) preparation of the tube, (3) calibration of the diodes (4) data accumulation, and the last stage, (5) analysis of results. The analysis of results will be discussed in the next chapter.

1. Construction

Due to its great length, the tube was constructed in three sections. After construction and before annealing, each section was leak tested with a helium mass-spectrometer. The sections were annealed in a vacuum and then sealed under vacuum until time for assembly. The support system built for the tube consisted of a long aluminum beam with six rigid tube supports. This permitted the sections to be rotated while being sealed together so that the joint was reasonably smooth with no sags or large irregularities. After the sections were joined together, the tips of the thermocouple support tubes were broken, the thermocouples inserted and sealed with epoxy. The epoxy was then cured for two hours with heat lamps. After curing, the tube was placed in its final position and sealed to the system via a section of glass tubing containing a metal bellows.

2. Preparation

Preparation of the tube involved bakeout and outgassing of the tube and its elements so that a high vacuum could be obtanied followed by filament activation. Bakeout was perfo ed

with heating tapes at 200°C for over 24 hours with the system under evacuation. The cold trap was kept filled with liquid nitrogen following bakeout. Outgassing was performed by induction heating, after bakeout. Since the leads were KOVAR, with a much lower melting point than the tantalum cylinders, outgassing of the tantalum at elevated temperatures was done in short bursts. In the case of the diodes and main discharge electrodes, the filaments were activated first and then the anodes were outgassed. Filament activation consisted of slowly raising the temperature by varying the filament voltage until the temperature, as measured with an optical pyrometer, was at a certain value. For the diode filaments, this temperature was 1750°C_B, (subscript B denotes brightness temperature)the recommended temperature for thoriated filaments. Following the manufacturers instructions, the main cathode filaments were only heated to 1190°C_B. This temperature was held for five minutes.

Following outgassing and filament activation, the filaments were aged for several hours at their normal operating temperatures. Then the main discharge anodes were cleaned by electron bombardment. This was accomplished by applying 300 volts to the anode, at which time the anodes turned bright red under the absorption of 45 watts of power.

3. Calibration of the Diodes

After the tube was prepared, with all elements outgassed, the diodes had to be calibrated. Since the mobility-limited current is less than the space-charge limited current, and the

transition is a function of gas pressure, it is best first to attain space charge limited operation. This was easily determined by preparation of a log-log plot of the plate current versus plate voltage to a value of plate voltage (30 volts), well in excess of that to be used (13½ volts). This was found to be a straight line, indicating that the filament voltage selected provided a good operating point.

Calibration consisted of varying the pressure in the tube and measuring the plate current as the plate voltage was varied. The filament voltage was held constant. As the pressure increases, there is increased filament cooling. It is not practical to use an optical pyrometer to maintain constant filament temperature at all pressures. Since the power applied increases as the temperature decreases for constant voltage, the constant voltage mode is semi-compensatory.

The filaments were thoriated tungsten and at first operated extremely well. After the main discharge was first run, which overheated the epoxy seal at the thermocouple, the diode current became noisy and started to decrease. It became necessary to increase the current to a high value and operate the diode filaments as pure tungsten. This required a recalibration.

4. Data Accumulation

It was decided to take data at three pressures. The low pressure was selected to be around 8 torr because a larger power supply was needed to obtain a good current pulse at pressures much

lower than that. The high pressure was 16 torr because of the difficulty in getting the main discharge started at higher pressures. The third pressure chosen was 12 torr.

In order to be able to detect the existence of any trends (in the data), due to time the order of experiments was chosen with a random number table. First the order of the pressures was chosen and then the order of the polarity of the main discharge. The order of runs is shown in Table II. Due to the difficulty of filling to the same pressure, the runs were not completely independently ordered.

TABLE II

ORDER OF RUNS

Polarity / Pressure	ALL	+1	0	-1
8	1	2	1	3
12	3	3	2	1
16	2	1	3	2

A set procedure was followed when taking the final data. First all equipment was turned on and allowed to warm up. Then the tape recorder was calibrated. The calibration of the oscilloscope was checked. For each pressure, the steps were the same except for minor variations due to the different order of the polarities within each pressure. The trap in the filling line was partially filled with liquid nitrogen. After the tube was filled with Argon at the desired pressure, the valve to the filling

manifold was secured. The diode and main discharge filaments were given plenty of time to warm up. When the main discharge was on, the Pupps discharge was adjusted for minimum AC current variation in the main discharge. This was observed on the oscilloscope using the current probe. The d.c. diode signal was measured after adjustment so that the amplified a.c. signal did not exceed the clipping level of the slicing circuit. When everything was ready, the tape recorder was started. While it was running, the temperatures were recorded. Between runs, the tape recorder calibration was checked and the output zero adjusted, but the input gain was not touched. After the experiment was over, a 5000 Hz tone burst sine wave, stepped down to 2 millivolts peak to peak was fed to the amplifiers in parallel. This was recorded for later use as a calibration aid. After each set of runs at a single pressure, the tube was pumped down to a hard vacuum and refilled for the next set of runs.

V. THEORETICAL ANALYSIS

This section treats the analysis of data theoretically. It develops the expressions needed to utilize the data to obtain information from it concerning the processes under investigation. In doing so, it takes into consideration the progagation of errors.

A. ENSEMBLE AVERAGING

Nine experimental runs were made, each with different conditions. An event, or experiment, consists of a current pulse, and the subsequent sound production. An experimental run consists of many events or replications of the experiment. The data recorded for each event were the triggering signal and the waveforms at three points. After conversion to digital form, each waveform was represented by a set of samples. Since a run consists of a set of events, the data consists of a set of sets of samples which shall be referred to as an ensemble of sample sets.

Consider just one of the signals. The samples in any one of the sets were not taken randomly, but have fixed relationships to each other which reflects their time dependence. For the set of samples, the zero of time is chosen to correspond to the triggering event. Thus, the n-th sample represents the value of the signal at time $t = nT$ where T is the period of the sampling frequency.

This sample represents not only the time signal at that time, but also something else. It represents the value of the cross correlation between the signal at that time and a Dirac delta

function signal which coincided with the triggering event. This is a subtle point which was used for advantage in eliminating noise.

The cross correlation function $f(x)$ of two real functions $g(x)$ and $h(x)$ is given by:

$$f(x) = \int_{-\infty}^{\infty} g(u-x)h(u)du$$

Let g be the Dirac delta function $\delta(t)$ and h be the signal $s(t)$. Then

$$f(t) = \int_{-\infty}^{\infty} \delta(u-t)s(u)du$$

and therefore,

$$f(t) = s(t).$$

By ensemble averaging the sets of samples, we obtain the ensemble average of $f(t)$, which is the cross correlation function of the signal with the triggering event. For a large enough ensemble, this should approach the time average of the cross correlation function. In the time average, contributions from non-correlatable portions of the signal, such as those due to noise, random or non-random, will vanish.

Because of their intimate relation, $f(t)$ and $s(t)$ may be used interchangeably except that it must be recognized that in each sample set, $s(t)$ has a different reference time while $f(t)$ has the same reference (for this reason, $s(t)$ will be used for $f(t)$ except when the special features of $f(t)$ are needed).

When $f(n\tau)$ is ensemble averaged, the mean value and its standard deviation are obtained. Since there is no reason to assume that the distribution of noise or fluctuations in value of $f(n\tau)$ should depend on n, the standard deviation is considered a constant. Then, if $f_i(n\tau)$ represents the value for the i-th set of samples, the process of ensemble averaging can be represented by

$$f(n\tau) = \frac{1}{N} \sum_{i=1}^{N} f_i(n\tau) \tag{5.1}$$

$$\sigma_n^2 = \frac{1}{N-1} \left(\sum_{i=1}^{N} f_i^2(n\tau) - N f^2(n\tau) \right)$$

and

$$\sigma^2 = \frac{1}{M} \sum_{n=1}^{M} \sigma_n^2 \tag{5.2}$$

where M is the number of points in the sample. It is possible to consider this ensemble average $f(n\tau)$ and the standard deviation σ as the expected value of the signal, $s(n\tau)$ and its standard deviation, σ.

B. FOURIER TRANSFORMATIONS

When a harmonic waveform is fed into a linear time-invariant device, the output is also harmonic but in general with a different amplitude and phase [48]. This is true whether the device be a filter, or transducer or some other system with an input and an output. Such a device can be completely specified by a frequency dependent complex quantity $Z(\nu)$ given by the ratio of the

output to the input. If the input $v_1(t)$ is given by

$$v_1(t) = Ae^{i2\pi\nu t}$$

and the output by

$$v_2(t) = Be^{i2\pi\nu T+i\phi},$$

then

$$Z(\nu) = \frac{B}{A} e^{i\phi} .$$

If an arbitrary input $v_1(t)$ is applied to the device and it is desired to calculate the output $v_2(t)$, $v_1(t)$ is analyzed into its spectrum; each spectral component multiplied by the corresponding transfer factor to obtain the spectrum of the output, and then $v_2(t)$ is synthesized from its spectrum. Thus

$$V_2(\nu) = Z(\nu)V_1(\nu)$$

and

$$v_2(t) = \int_{-\infty}^{\infty} Z(\nu)V_1(\nu)e^{i2\pi\nu t}d\nu.$$

(Here and elsewhere, where a quantity is viewed in both the frequency and time domains, the upper case symbol will be used for the frequency domain and its lower case for the time domain.)

If the process of convolving $g(x)$ and $h(x)$, is represented by $g*h$, defined by

$$f(x) = g*h = \int_{-\infty}^{\infty} g(u-x)h(u)du,$$

and the process of Fourier transformation is represented by $\supset$, the determination of $v_2(t)$ can be presented by the diagram below.

$$
\begin{array}{ccc}
v_1(t) & \supset & V_1(\nu) \\
* & & \times \quad \text{(multiplication)} \\
z(t) & \supset & Z(\nu) \\
\downarrow & & \downarrow \\
v_2(t) & \supset & V_2(\nu)
\end{array}
$$

In this experiment, there are three time dependent waveforms, $i(t)$, $s_1(t)$ and $s_2(t)$, corresponding to the sound-producing discharge current, the sound at point 1 and the sound at point 2 respectively. The object of the experiment was to obtain the transfer function of the conversion of current to sound, $Z_s(\nu)$, and the transfer function of the spatial region between points 1 and 2, $Z_{12}(\nu)$. The entire process can be represented by the diagram below, where the time representation of the transfer functions and the convolution process has been omitted for clarity.

$$
\begin{array}{ccc}
i(t) & \supset & I(\nu) \\
 & & \times \\
 & & Z_s(\nu) \\
 & & \downarrow \\
s_0(t) & \supset & S_0(\nu) \\
 & & \times \\
 & & Z_{01}(\nu) \\
 & & \downarrow \\
s_1(t) & \supset & S_1(\nu) \\
 & & \times \\
 & & Z_{12}(\nu) \\
 & & \downarrow \\
s_2(t) & \supset & S_2(\nu)
\end{array}
$$

The application of Fourier transform theory to this problem assumes linearity of the processes. That is, if $s_{21}(t)$ is the output at point 2 to an input of $i_1(t)$ and if $s_{22}(t)$ is the response to $i_2(t)$, then the response to $i(t) = i_1(t)+i_2(t)$ is $s_2(t)= s_{21}(t)+s_{22}(t)$, regardless of the choice of i_1 and i_2. In the transform domain, the process from current to sound at point 2 is represented by the set of equations:

$$S_0(\nu) = I(\nu)\ Z_S(\nu)$$

$$S_1(\nu) = S_0(\nu)\ Z_{01}(\nu)$$

$$S_2(\nu) = S_1(\nu)\ Z_{12}(\nu)$$

Since $i(t)$, $s_1(t)$ and $s_2(t)$ are known, their respective transforms are known. Therefore these constitute three equations with four unknowns, $S_0(\nu)$, $Z_{12}(\nu)$, $Z_{01}(\nu)$ and $Z_S(\nu)$. For the case where the main discharge is on, only $|Z_{12}(\nu)|$ is desired. This can be solved for easily,

$$|Z_{12}(\nu)| = \frac{|S_2(\nu)|}{|S_1(\nu)|} \quad .$$

To determine Z_S, when the discharge is off, acoustic theory provides a model from which a fourth equation can be obtained. For sound propagating in a tube, the transfer function between two points is given by

$$Z_{12}(\nu) = e^{ik(\nu)d_{12}}$$

where d_{12} is the distance between 1 and 2. With this equation and the additional assumption that, in the absence of a discharge in

the intervening space, $k(\nu)$ is the same throughout the tube, the system reduces to two equations in two unknowns,

$$S_1(\nu) = I(\nu)\, Z_S(\nu) e^{ik(\nu)x_1}$$

$$S_2(\nu) = I(\nu)\, Z_S(\nu) e^{ik(\nu)x_2} \quad .$$

The propagation constant $k(\nu)$ is complex,

$$k(\nu) = \alpha(\nu) + i\beta(\nu).$$

Under the experimental conditions, boundary losses dominate. In this case, $\beta(\nu) = \beta_o \sqrt{\nu}$. If phase information is neglected, meaning that the delay between $i(t)$, $S_1(t)$, and $S_2(t)$ is neglected, then β_o can be obtained from $S_1(\nu)$, $S_2(\nu)$ by

$$\beta_o = \frac{-1}{x_2 - x_1} \frac{d}{d(\nu^{\frac{1}{2}})} \ln \left\{ \frac{|S_2(\nu)|}{|S_1(\nu)|} \right\}$$

and

$$|Z_S(\nu)| = \frac{|S_0(\nu)|}{|I(\nu)|} \quad .$$

C. ACOUSTIC TRANSFER FUNCTION

After ensemble averaging, the two diode signals are represented by sample sets and standard deviations

$$s_1(n\tau),\ \sigma_1$$

$$n = 1, M$$

and $$s_2(n\tau),\ \sigma_2$$

Since the standard deviations are considered time independent, each represents a constant signal in time, the transform of which, Σ,

is a zero frequency component of the same magnitude as σ. Therefore, in the transform domain, the two diode spectra are

$$S_1(\nu_i)$$

and

$$S_2(\nu_i)$$

where Σ_1^2 and Σ_2^2 affect only $S(\nu_o = 0)$.

The standard deviation or error in $S_1(\nu_i)$ and $S_2(\nu_i)$ is that due to the noise, plus that due to other sources. (The error in the value of a quantity such as S_1 is represented by Δ preceeding the symbol for the primary quantity, e.g. ΔS_1.)

Let $Y(\nu_i)$ represent the natural logorithm of $Z_{12}(\nu_i)$.

Then

$$Y(\nu_i) = \ell n \frac{|S_2(\nu_i)|}{|S_1(\nu_i)|} \tag{5.3}$$

and

$$\Delta Y(\nu_i) = \left\{ \left(\frac{\Delta S_2}{S_2} \right)^2 + \left(\frac{\Delta S_1}{S_1} \right)^2 \right\}^{\frac{1}{2}} . \tag{5.4}$$

For the discrete case, the earlier expression for β_o is not very useful. Another expression which can be written containing β_o is

$$Y(\nu_i) = - \beta_o (x_2 - x_1) \nu_i^{\frac{1}{2}} . \tag{5.5}$$

This expression can be solved for β_o at each value of ν_i. However a better approach is to use all the information available and minimize the error in β_o. If all values of $Y(\nu_i)$ were known to the same degree of accuracy, then a simple linear least squares fit would provide the optimum estimate for β_o. However, from the ensemble average and another consideration to be discussed

later, the error in $Y(\nu_i)$ is known. A weighted average will therefore improve the estimate for β_o. The values of $Y(\nu_i)$ are best weighted with a weighting function

$$W_i = \frac{A}{\Delta Y(\nu_i)^2} \tag{5.6}$$

where A is a normalizing constant given by

$$A = \sum_{i=1} \Delta Y(\nu_i)^{-2} .$$

D. SOURCE TRANSFER FUNCTION

When there is no discharge between points 1 and 2, it is assumed that the transfer function is the same throughout the tube. This means that the value of β_o may be used to extrapolate the sound spectrum observed at points 1 and 2 to the origin. There it may be compared with the current spectrum of the sound source discharge to obtain the source transfer function.

The spectral components of S_1 and S_2 projected to the origin are given by:

$$S_{jo}(\nu_i) = S_j(\nu_i) e^{\beta_o x_j \nu_i^{\frac{1}{2}}} . \qquad (j=1,2) \tag{5.7}$$

If β_o is used, the implication is that the estimate of β_o is independent of the S_j. But since β_o was derived from the estimates for S_2 and S_1, this is not true. Recall that

$$\frac{S_1}{S_2} = e^{\beta_o \nu^{\frac{1}{2}}(x_2 - x_1)} . \tag{5.8}$$

therefore

$$e^{\beta_o} = \left(\frac{S_1}{S_2}\right)^{\frac{1}{\nu^{\frac{1}{2}}(x_2-x_1)}} . \qquad (5.9)$$

This can be substituted into Eq. (5.7) to give

$$S_{10}(\nu_i) = S_1\left(\frac{S_1}{S_2}\right)^{\frac{x_1}{x_2-x_1}}$$

and

$$S_{20}(\nu_i) = S_2\left(\frac{S_1}{S_2}\right)^{\frac{x_2}{x_2-x_1}} .$$

Since these are equivalent, the estimate for S_0 is

$$S_0 = S_1^{\frac{x_2}{x_2-x_1}} S_2^{\frac{-x_1}{x_2-x_1}} . \qquad (5.10)$$

The standard deviation for S_0 is given by

$$\Delta S_0 = S_0\left\{\left(\frac{x_2}{x_2-x_1}\right)^2\left(\frac{\Delta S_1}{S_1}\right)^2 + \left(\frac{x_1}{x_2-x_1}\right)^2\left(\frac{\Delta S_2}{S_2}\right)^2\right\}^{\frac{1}{2}} . \qquad (5.11)$$

The transfer function of the source is obtained with a simple division,

$$Z_S(\nu_i) = \frac{S_0(\nu_i)}{I(\nu_i)} \qquad (5.12)$$

whereby

$$\Delta Z_S^2(\nu_i) = \left(\frac{\Delta S_0(\nu_i)}{I(\nu_i)}\right)^2 + \left(\frac{Z_S(\nu_i)}{I(\nu_i)}\right)^2 \Delta I(\nu_i)^2 . \qquad (5.13)$$

E. EFFECT OF THE DISCHARGE

In order to make a valid comparison between experimental results and theoretical predictions, the predictions should be based on values which represent the experiment. In this case, to compare

the Ingard-Schulz predictions with experiment, the effects of longitudinal and radial thermal gradients must be taken into consideration. Since the electron temperature and electron density are not known, they must be estimated. Also it should be noted that the discharge does not fill the region between the two diodes but, using the values from Table 1, occupies only 55.6% of the space. When there is no discharge, this does not affect results but when the discharge is on, the region is inhomogenous and the attenuation constant obtained is the average value for the entire space between the diodes.

Several assumptions must be made in order to predict the experimental results. The first is that there is no transition zone at the ends of the discharge region. This means that the predicted value for the effective attenuation constant should be the average of the value for no discharge and that in the discharge, where the values are weighted by the lengths of the two regions. Due to the nature of the interface between the regions, reflections are considered negligible. Temperature measurements taken between the discharge and diode 2 support this assumption. They showed only a one-degree higher temperature than measurements far removed from the discharge. The two diodes are separated by a distance d_0 and the main discharge elements by d_1. Thus, if β_{01} and β_{02} denote the attenuation constant in the discharge and outside of the discharge respectively, the effective attenuations constant β_0' is given by

$$\beta_0' = \frac{d_1}{d_0} \beta_{01} + \frac{d_2}{d_0} \beta_{02}$$

where $d_2 = d_0 - d_1$.

Other assumptions concern the effects of the discharge through thermal gradients. During their investigation of the neutral temperature in medium pressure discharges, Hayess, et.al. [49] observed a radial temperature gradient under all discharge conditions. This will affect the propagating sound. Hayess [50] considered the problem in conjunction with his experiment. He concluded that for frequencies below the first radial resonant frequency, only the fundamental mode, a plane wave would propagate. He further concluded that the temperature difference would not affect the attenuation greatly since only its square root appears in the attenuation factor. The cut off frequency for this experiment is about 9 kHz. The discharge region can be characterized by two temperatures for two different purposes. The longitudinal gradient in the tube affects the pressure in the tube. For this purpose, the discharge can be characterized by its mean temperature T_M. Since the temperature outside of the discharge, T_o, did not change, the tube pressure with the discharge on is given by

$$p' = p_o \frac{1}{1 - \frac{d_l}{d_t}\left(1 - \frac{T_o}{T_M}\right)} = p_o \frac{1}{1 - .234\left(1 - \frac{T_o}{T_M}\right)}$$

where d_T is the length of the tube. The uncertainty in the pressure is given by

$$\Delta p'^2 = \left(\frac{\partial p'}{\partial T_M}\right)^2 \Delta T_M^2 + \left(\frac{\partial p'}{\partial p_o}\right)^2 \Delta p_o^2 .$$

Since $\frac{\partial p'}{\partial T_M} = p' \frac{d_2}{d_0} \frac{T_o}{T_M^2}$, this can be expressed as

$$\left(\frac{\Delta p'}{p'}\right)^2 = \left\{ \frac{1}{1 - \frac{d_2}{d_0}\left(1 - \frac{T_o}{T_M}\right)} \frac{d_2}{d_0} \frac{T_o}{T_M} \right\}^2 \left(\frac{\Delta T_M}{T_M}\right)^2 + \left(\frac{\Delta p_o}{p_o}\right)^2 .$$

Under the assumption that boundary effects are the dominant loss mechanism, the temperature at the wall, T_W, is important for the discharge region. This is because these losses occur within two or three mean free paths of the boundary.

To calculate the predicted attenuation constant with the Ingard-Schulz equations, the experimental parameters must be converted to the variables used in the computer program: ω, N_n, N_e, T_e, and T_n. The wall temperature can be used for T_n. The neutral density can be calculated from p' with T_W, using the expression

$$N_n = 9.6642 \times 10^{18}\ p/T$$

where p is in torr and N_n in cm^{-3}. The relative uncertainty in the density is given by

$$\left(\frac{\Delta N_n}{N_n}\right)^2 = \left(\frac{\Delta p}{p}\right)^2 + \left(\frac{\Delta T}{T}\right)^2 .$$

Since they were not measured, estimates must be used for the electron temperature and the electron density. With the similarity parameter Rp as an entry, T_e may be obtained from von Engle [40] with an estimated uncertainty of 10%. Estimating the electron

density requires a more complicated process. Venzke [51] has plots which give E/p as a function of i/R with Rp as a curve parameter. The value of E/p thus obtained can be used to obtain the electron drift velocity from page 525 of MdDaniel [39]. With the assumption of a uniform current density across the tube, the electron density is given by

$$N_e = \frac{I}{2\pi r_o v_D q_e} .$$

Of course it is known that the current density is not uniform across the tube but neither are other factors such as neutral density. The entire acoustic problem is treated in a one-dimensional sense. Because of the approximations involved, the electron density is assumed to be uncertain by 50%.

The relation of β_o, the attenuation constant, to β, the attenuation co-efficient, can be viewed in two different ways. If $\beta = \beta_o \sqrt{\omega}$, the two ways are equivalent. One way is to write

$$\beta_o = \beta(\omega = 1).$$

The other way is to write

$$\beta_o \equiv \beta(\omega)/\sqrt{\omega}.$$

The latter form is preferred since a departure from the assumption of boundary loss domination will be readily apparent from a plot of β_o as a function of ω. It should be noted that Figure 2, which is a plot of $\frac{\beta_I - \beta_{UI}}{\beta_{UI}}$, would not be changed by switching β_o for β. Since β_o should have no dependence on ω, the value of ω should not be important. To be certain, the value corresponding to the highest

and lowest experimental values of ω should be used and the dependence checked.

Since all of the input quantities are estimates, with an uncertainty which can be treated as a standard deviation, the estimate of β_o obtained will be uncertain. The uncertainty in β_o is given by

$$\Delta\beta_o^2 = \left(\frac{\partial\beta_o}{\partial T_n}\right)^2 \Delta T_n^2 + \left(\frac{\partial\beta_o}{\partial T_e}\right)^2 \Delta T_e^2 + \left(\frac{\partial\beta_o}{\partial N_e}\right)^2 \Delta N_e^2 + \left(\frac{\partial\beta_o}{\partial N_n}\right)^2 \Delta N_n^2 + \left(\frac{\partial\beta_o}{\partial\omega}\right)^2 \Delta\omega^2 \ .$$

The partial derivatives can be obtained with the computer program by the expression

$$\frac{\partial\beta_o}{\partial x_i} \simeq \frac{\beta_o(x_i=X_i+\Delta X_i) - \beta_o(x_i=X_i)}{\Delta X_i} \ .$$

If $\Delta\beta_o$ is particularly sensitive to any of the variables, the process of evaluation should be reviewed to see if the uncertainty can be reduced.

VI. TREATMENT OF DATA

The choice of data handling procedure was strongly influenced by problems associated with the experiment. The strong reflection from the tube ends was one of the most important factors in all considerations. The need for gated signals rather than continuous waves, in order to study the effect of the discharge, meant that the data could not be taken with meters. The multi-component spectrum associated with the bias for the gated sine waves meant that the signal had to be Fourier analyzed.

Due to the strong reflections, the signals could not be analyzed in the continuous mode with a Correlation Function Computer such as the PAR 100A. When the gated mode was used, the time base was limited to the period from the triggering signal to the start of the reflected signal. Since this time base was sampled only 100 times, the resolution was very poor. Preliminary analysis of the signals indicated that the source transfer function decreased at low frequencies. Since this could help to check theories of the production mechanism, the low frequency components were of particular interest and resolution was needed.

A Boxcar integrator was also used to recover the signal on a scale compatible with transcription into numbers. However like the Correlator, this utilized only one signal waveform at a time and it wasted most of that. In addition, the data had to be converted into numbers, and card punched for computer processing.

Even using digital voltmeters to obtain the data, obtaining more than one hundred twelve points from a waveform was very difficult.

For these reasons, the process of recording on tape and direct conversion to digital form was finally selected. It offered the greatest resolution, processing possibilities and error recovery capability.

A. DATA REDUCTION PROCEDURE

1. Analog to Digital Conversion

After completing the data recording, the data tapes were reviewed with an oscilloscope. One minute segments were cut from each of the original tapes and spliced together. They were separated by long sections of white leader tape for easy identification of the segments.

A hybrid computer composed of a COMCOR 5000 analog computer interfaced with an SDS 9300 digital computer was used for the conversion of the analog data to digital form. The analog side of the hybrid computer was set up to receive the analog signal and provide the appropriate signals to the digital portion for digitizing the information. The gain of the data channels was 50. A channel corresponds to the waveform recorded on it. Logic boards were used to start sampling at a frequency of 10 kHz when the trigger signal reached a variable trigger level. Two switches were used to start and stop the conversion process. The number of samples taken following each trigger signal was controlled by the digital program. After converting 1200 samples of each of the

three data channels to digital form, the information was written on a magnetic tape. The program used for the conversion is a standard program available to all users of the hybrid computer. The parameters for the program are the number of channels to be sampled and the number of samples per channel to be made for each record. The logic involved in the sampling process is different for most conversions and this required a slight amount of patching on the logic patch boards.

2. Seven to Nine Track Conversions

The information written on the 7 track magnetic tape by the hybrid computer is in the form of 24 bit binary words. To be processed by the IBM 360, these must be converted to 32 bit binary words. The only programming involved in this is a program to read the 7 track tape, call a conversion routine and write the information on another tape, usually 9 track for increased efficiency, for later processing. For this job, this step was also used to separate the samples by channel.

3. Ensemble Averaging with Data Rejection

The diode signals contained noise. The noise was random and consisted chiefly of positive-going spikes. A low pass filter could not eliminate them without distorting a significant portion of the acoustic waveform. In addition there were a few bad trigger signals recorded. Thus it was known from the beginning that some of the data records were bad and should not be included in the processing but it was not known which they were. Since the entire data set consisted of ten files, each of which contained from 80 to 120

records of 3600 words, screening became a major task. The following procedure was finally found to be most efficient and effective.

Each file corresponded to an experimental run and all records in that file represented the same waveforms plus noise. The records in a file were all averaged together and the standard deviation for each channel was obtained. Following this, all records were compared with the average. Those with less than 75% of their points within 2.8 standard deviations of the average were dropped from further processing. Using only the acceptable records, a new ensemble average and standard deviation was obtained for each channel. These were used in a final ensemble averaging process in which only those points within 2 standard deviations of the average were used. This provided an ensemble average of the waveform and the standard deviation of the points involved.

4. Delay, Overlay and Zero

At this point, the data consisted of 1200 samples for each of the three waveforms, representing their average values, and the standard deviation of the waveforms. For the sampling process 1200 samples were taken so that all of the desired waveform of the signal at point 2 was sampled. This meant an undesired signal was included in the samples of the signal at 1, namely the reflected signal. In order to make a valid comparison of spectral components, the time samples of the waveform which is transformed must contain the same number of samples. Reducing the number of samples of s_2 to

those necessary to avoid the reflections in s_1 means the starting point for the transformation must be delayed. Since phase information was not going to be considered in the analysis, and time delay merely changes the phase of the components, delaying the signals would not affect the results. Therefore the signals s_1 and s_2 were delayed by choosing a starting point for each such that 600 samples included the waveform up to the point where the reflection started.

The diodes interacted electrostatically with discharge. This caused a small coherent square wave in the diode output which coincided with the time of the current pulse. Its' inclusion in the waveform to be transformed would give erroneous spectral components for the acoustic signal. Delaying was sufficient to eliminate this unwanted signal from s_2. In order to eliminate it from s_1, without introducing unwanted spectral components, the values of the samples in the region containing this unwanted signal were replaced with values taken at random from the adjacent region. Since this adjacent region contained only samples of the waveform before arrival of the acoustic signal, they only represented background noise.

Since the initial portions of the signals S_1 and S_2 represent no signal, i.e. the period before arrival of the acoustic signal from the sound source, its average value should be zero. The signals were offset to zero by first determining the average value of the no signal region and then subtracting it from all

values. For the current waveform, this region followed the current pulse. The three operations of delaying the signals, overlaying the electrostatic signal and establishing the zero level were performed in one program.

B. OPERATIONS ON THE TRANSFORM

Two sequential programs were used to transform the waveforms and obtain acoustic informations from them. The first program took the input waveforms, corrected them for gain and diode sensitivity and determined their spectra. The second used the spectra to determine the transfer functions of the discharge region and the source.

Input data for the transform program were the three ensemble-averaged waveforms, $i(n\tau)$, $s_1(n\tau)$, $s_2(n\tau)$ and their standard deviations, Δi, ΔS_1, ΔS_2, and the diode sensitivities.

Two uncalibrated amplifiers were used in amplifying and recording the diode signals. These were calibrated as part of the processing. While recording data, both amplifiers were fed a common signal consisting of 2 millivolt peak to peak, 5000 Hz, tone burst. This calibration signal was processed in the same manner as the other signals. In the first part of the transform program, the spectrum of this signal, in the diode channels, was Fourier analyzed. Then the spectral component closest to 5000 Hz (5040) was used to calibrate the gain for each diode channels so that this component was equal to one.

The diode sensitivities, supplied as inputs, were calculated earlier from experimental data and expressed in terms of millivolts/torr. The sensitivity of the current detector was 5×10^{-3} volts/milliamp. The sensitivities and corrected gain factors were used to convert the values into the correct magnitudes of the physical quantities involved, milliamps for the current and torr for the acoustic signals.

The transforms of the corrected waveforms were then calculated using a computer library subroutine "RHARM". This program requires that the number of points be an integer power of two. There were 600 points available and the nearest power of two was 512, leaving 88 excess points. This means that there is some uncertainty as to where to start the analysis. For this reason, the waveforms were analyzed five times, each time advancing the starting position by 10 places. The average value and variance of each component was calculated from the five spectra.

The output of the transform program was the average spectrum and the variance of its components. Only the first twenty five of these were passed to the next program. The magnitudes of the remaining components were less than 5% of the fundamental and were characterized by a great deal of scatter.

The next program used this data, and calculated the acoustic and source transfer functions. The equations of Chapter V were used for the calculations. A computer library subroutine "LSQPL2" was used to obtain the least squares determination of β_o. For this

calculation, the data was weighted inversely proportionally to the square of its uncertainty, with weights normalized such that their sum was equal to the number of points.

For the data corresponding to no discharge, Eq. (5.10) was used to obtain an estimate for the sound spectra at the source. This was divided by the sound source current spectra to obtain the transfer function of the sound source.

VII. PRESENTATION AND DISCUSSION OF RESULTS

A. AVERAGE WAVEFORMS

The averaging and screening method worked very well although the program could be rewritten to perform the job more efficiently. The three waveforms for the discharge-off case at 7.65 torr are shown as Figures 10, 11 and 12 just before being transformed. For contrast, the first 2/3 of the average waveform for s_1 for the same run is shown as Figure 13 with the same scale. The second pulse is the reflected signal from the end close to the sound source. This shows the effect of the delaying, overlay and zeroing operations. Unless otherwise specified, the remainder of the figures displayed in this chapter were derived from these waveforms.

B. ACOUSTIC TRANSFER FUNCTION

The points of the acoustic transfer function showed a reasonable amount of scatter about the predicted form. The greatest degree of scatter was found to be associated with those components whose contributions to the signal were small. Figure 14 shows the first twenty five spectral components of the sound at point 2. Figure 15 shows the transfer function in a linear form. Figure 16 is the same information expressed as attenuation of sound in decibels per meter as a function of frequency. The curve represents the least squares fit to the data under the assumption that boundary losses dominate. The goodness of fit found in all cases supports the validity of this assumption.

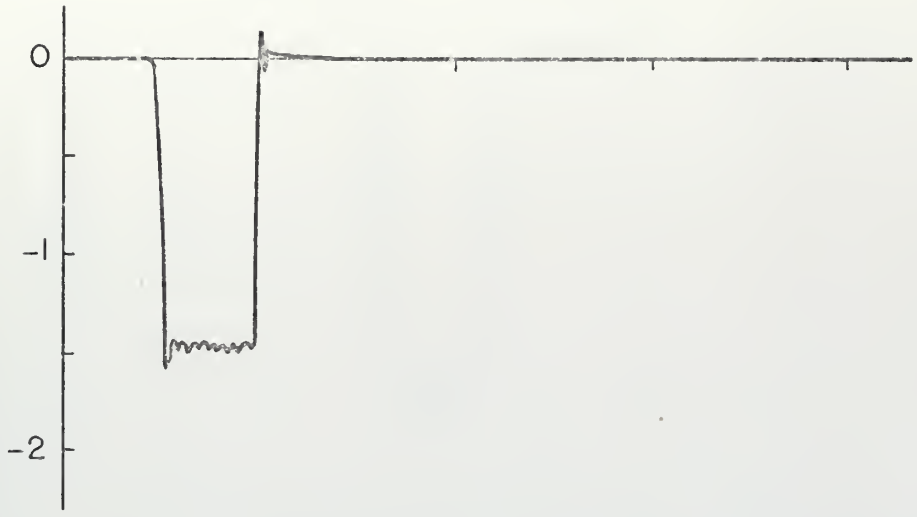

Figure 10. Sound Source Discharge Current. P = 7.65 torr. Main Discharge off. Time Scale: 2.048 msec/in. Vertical scale is arbitrary.

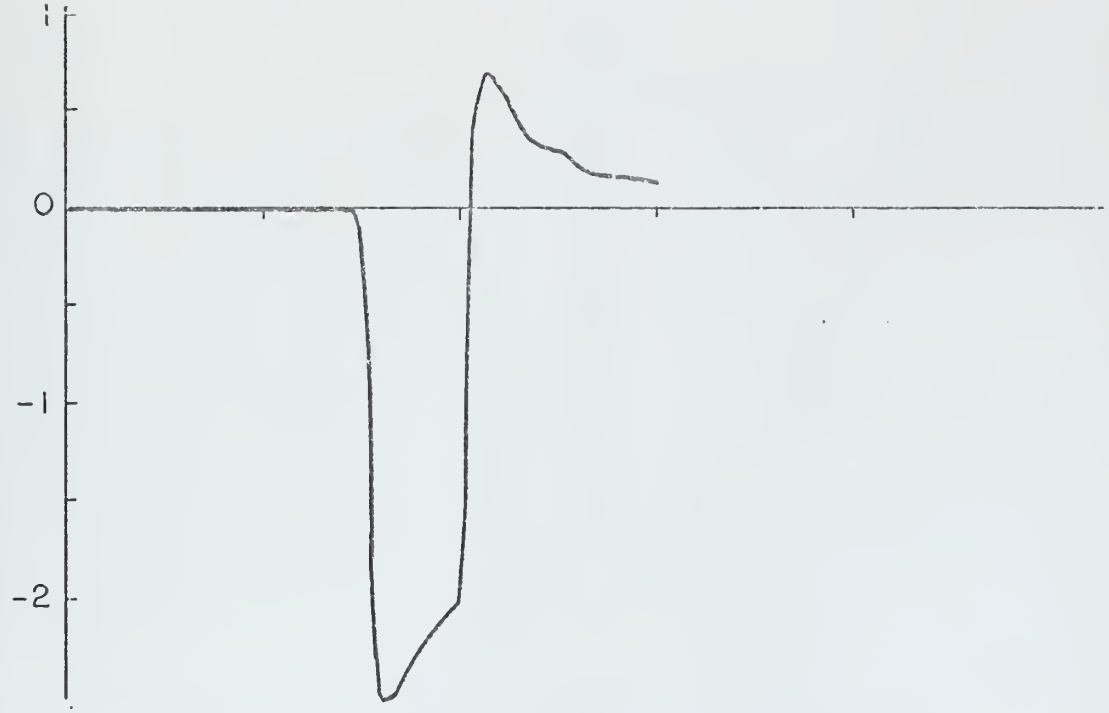

Figure 11. Sound Signal at Point 1. (delayed, overlayed and zeroed). P = 7.65 torr. Main discharge off. Time scale: 2.048 msec/in. Vertical scale is arbitrary.

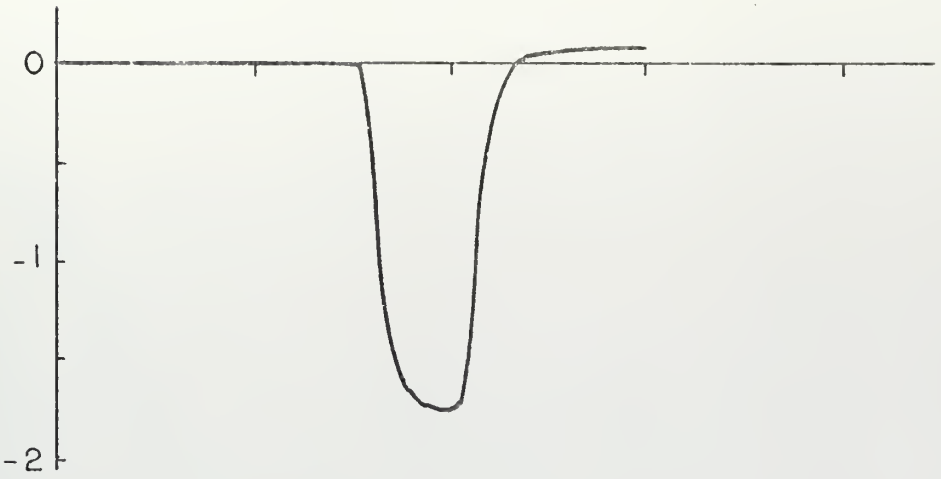

Figure 12. Sound Signal at Point 2. (delayed, overlayed and zeroed). P = 7.65 torr. Main discharge off. Time scale: 2.048 msec/in. Vertical scale is arbitrary.

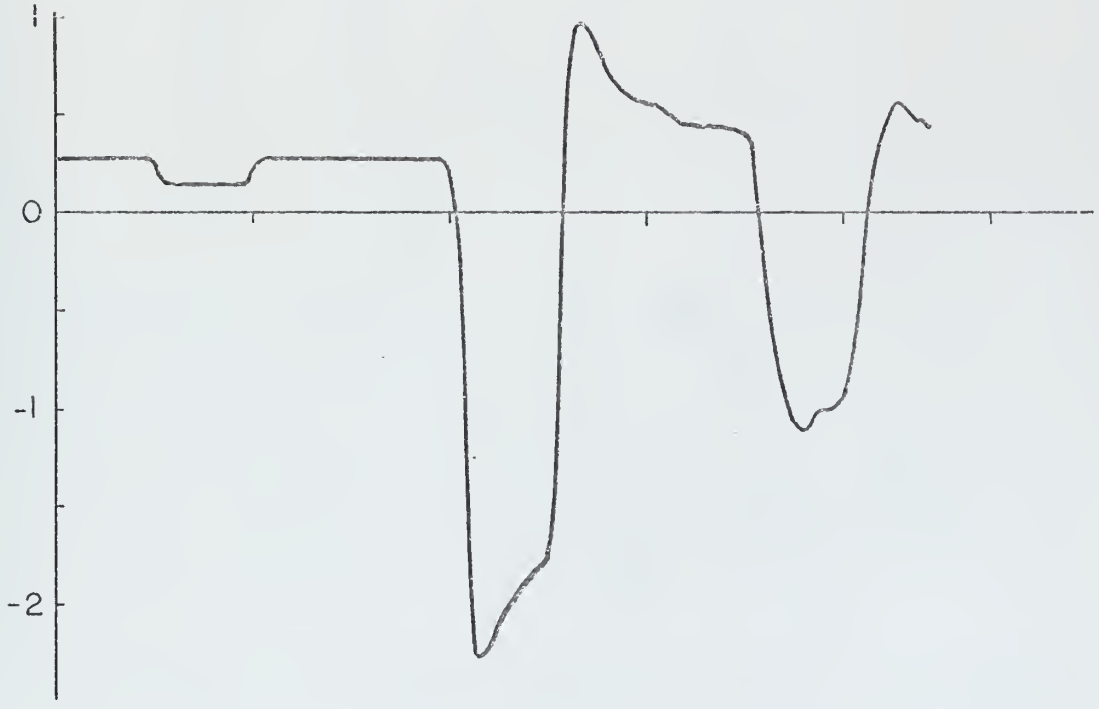

Figure 13. Sound Signal at Point 1. (Uncorrected). P = 7.65 torr. Main discharge off. Time scale = 2.048 msec/in. Vertical scale is the same as Figure 11.

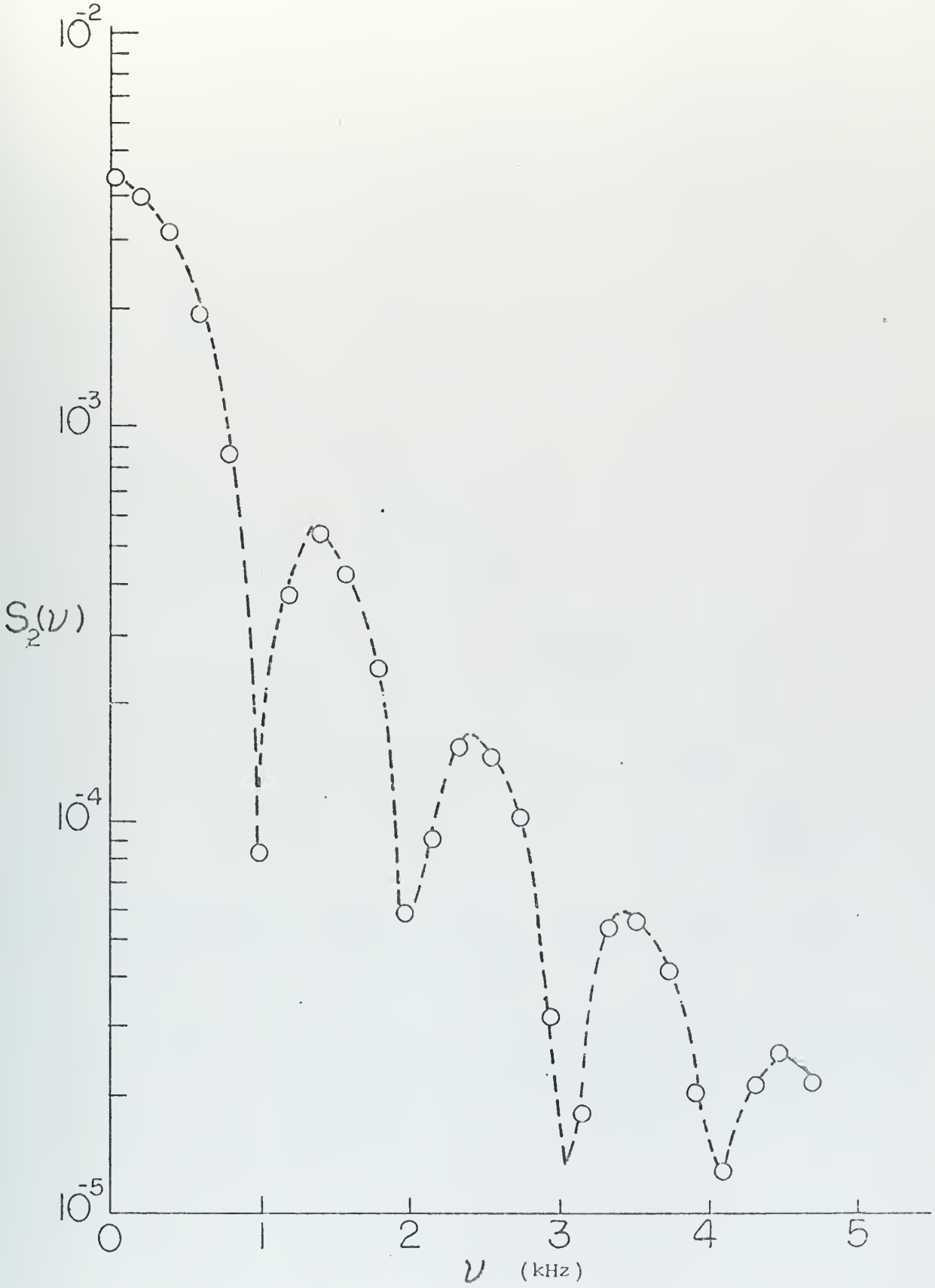

Figure 14. Spectral Decomposition of Sound Signal at Point 2. This is the spectral decomposition of the [illegible] form shown in Figure 13. Dashed line is a simple connection of points.

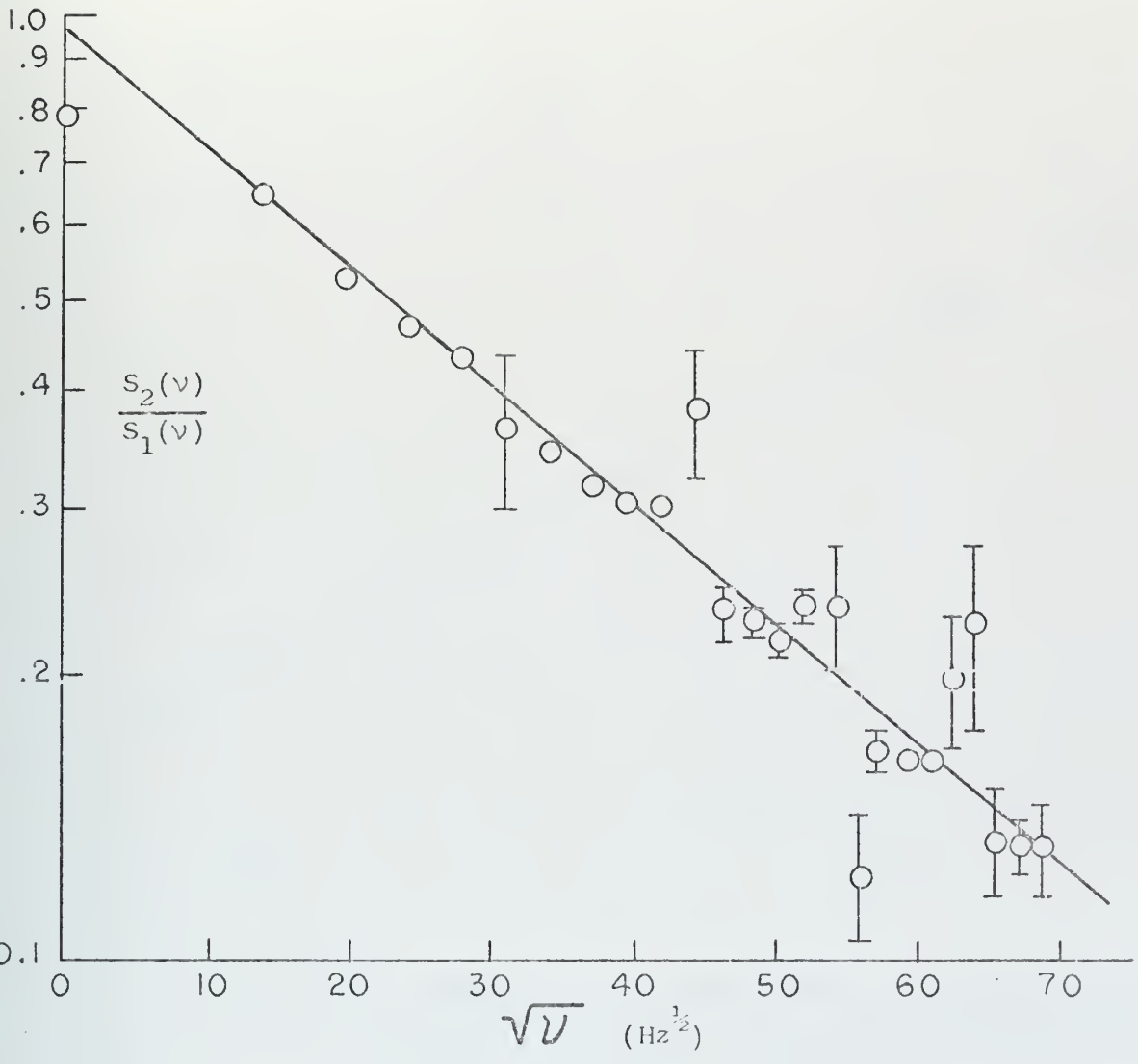

Figure 15. $S_2(\nu)/S_1(\nu)$ in Dependence on $\nu^{\frac{1}{2}}$ for a Pressure of 7.65 torr. Main discharge off. Error bars represent one standard deviation. Curve represents the weighted least squares fit to the data.

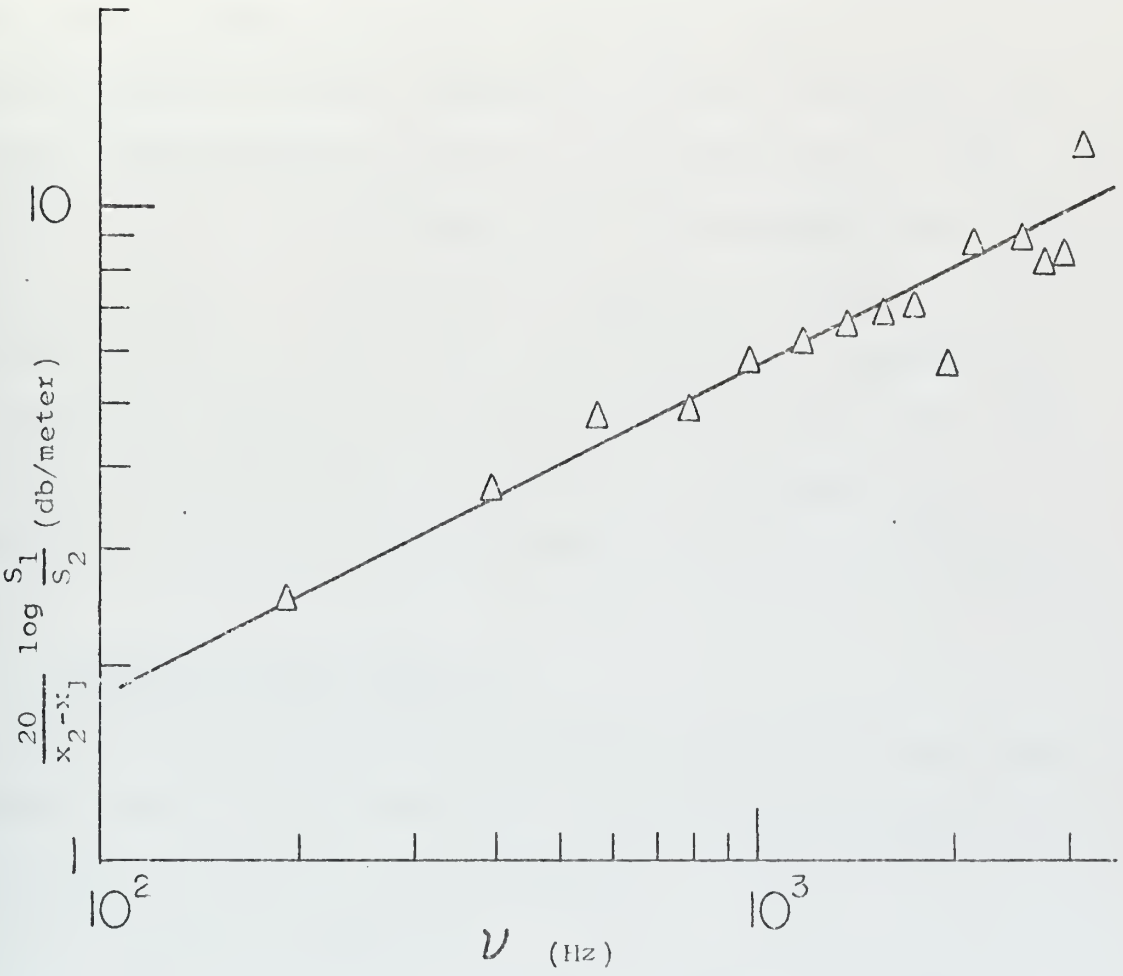

Figure 16. Attenuation in Dependence on Frequency for a Pressure of 7.65 torr. Main discharge off. Curve represents the least squares fit to the data. This figure corresponds to Figure 15.

C. SOURCE TRANSFER FUNCTION

The source transfer function was found to have the low frequency drop off indicated by the preliminary observations. At frequencies above a pressure-dependent transition frequency, the frequency characteristic did follow the predicted form. The magnitude was also found to agree with the predicted values. The transfer functions are displayed as Figures 17, 18 and 19 for the filling pressures 7.65 torr, 12.7 torr and 16 torr respectively. The structure is believed to be due to scatter in the data since the points with the greatest departure from the smooth curve correspond to those spectral components with the largest relative error.

1. Agreement with Prediction

Two aspects of the results can be used to test the theory of sound production from a discharge. One is the frequency dependence and the other is the magnitude.

a. Frequency Dependence

The low-frequency drop off is contrary to the frequency dependence predicted by Schulz's results. This effect is believed to be due to neutral particle diffusion under the influence of thermal gradients. It is a low-frequency, low-pressure effect which should appear only when thermal energy sources provide the acoustic energy. This will be discussed later.

According to Schulz's prediction, the transfer function should vary as

$$\frac{\sin\left(\frac{\omega a}{2c}\right)}{\omega} .$$

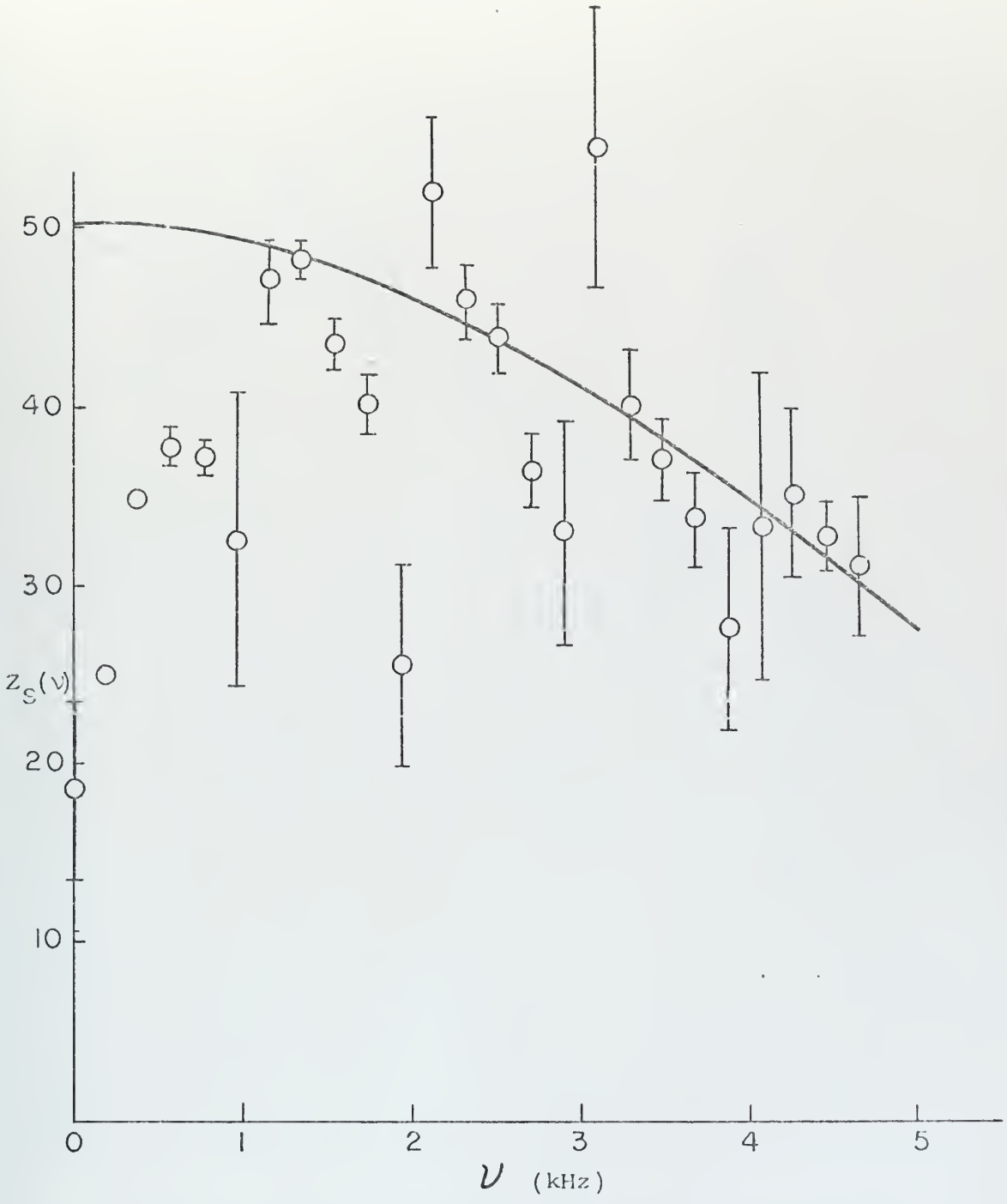

Figure 17. Source Transfer Function in Dependence on Frequency for p = 7.65 torr. Main discharge off. Vertical scale in units of (newton/m^2) per ampere. Solid curve represents predicted form fitted at one point.

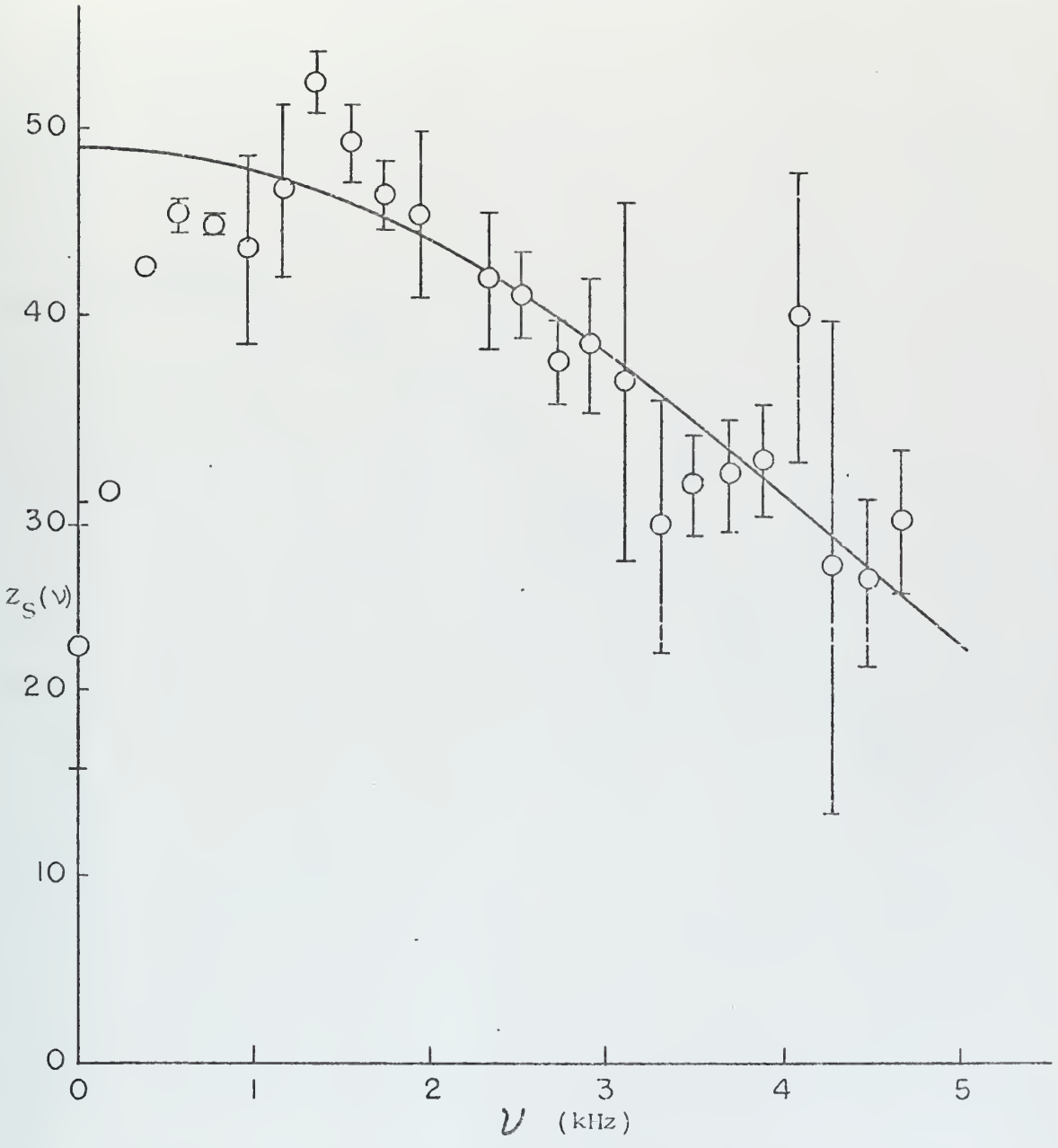

Figure 18. Source Transfer Function in Dependence on Frequency for p = 12.7 torr. Main discharge off. Vertical scale in units of (newtons/m^2) per ampere. Solid curve represents predicted form fitted at one point.

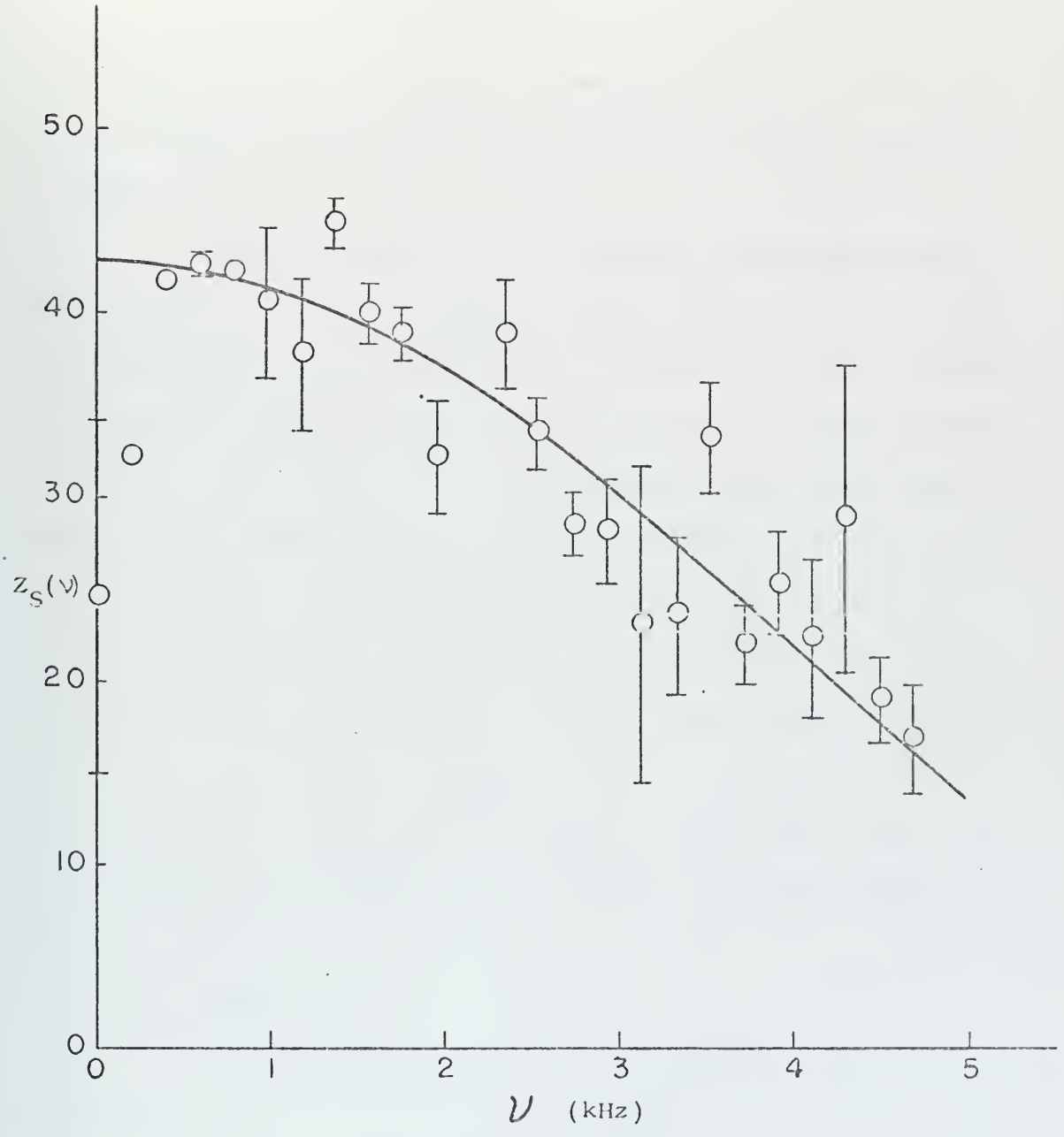

Figure 19. Source Transfer Function in Dependence on Frequency for p = 16 torr. Main discharge off. Vertical scale in units of (newton/m^2) per ampere. Solid curve represents predicted form fitted at one point.

This prediction was tested by fitting a curve given by

$$y = \frac{C_1}{\omega} \sin\left(\frac{\omega a}{2c}\right) \qquad (7.1)$$

through the transfer function data points. The coefficient C_1 was evaluated by causing the curve to pass through the point at ν = 2450 Hz.

Schulz's derivation was based on planar electrodes separated a distance "a". The experiment used cylindrical electrodes of length 1½ cm separated by a distance of 3 cm. Therefore the effective length of the discharge could lie anywhere between 3 and 6 cm. The value of "a" was adjusted within these limits to obtain a curve which fitted the data reasonably well. For 7.65 torr, the value of a was 3.5 cm; for 16 torr, the value was 4.6 cm. Since the pressure affects the discharge, there was a possibility that the value of "a" for 12.7 torr could be interpolated from the other two values. The value obtained by interpolation was 3.93. This gave a good fit to the data. The smooth curves shown in the figures are the fits of equation (7.1) to the data.

b. Magnitude

Using Schulz's equation, the source transfer function is predicted as

$$Z_S = (\gamma-1)H \frac{\sin(\frac{\omega a}{2c})}{I\omega} .$$

The energy transfer rate from the electrons H is the same as used earlier in conjunction with wave amplification. It

may be expressed in terms of the characteristic time for electron heating as

$$H = \frac{c^2}{\tau(\gamma-1)} .$$

The calculated value of c^2/τ was obtained with the computer program used for evaluating the Ingard-Schulz equations. This was accomplished for the transfer function at ν = 2540 Hz and p = 16 torr. The discharge current spectral component at this frequency was 6.4 ma which was estimated to correspond to an electron density of 2×10^{10} cm^{-3}. In determining this density, the cross sectional area of the electrodes was used since the discharge did not extend, in the radial direction, significantly beyond them. The procedure used was the same as outlined in Sec. V.E. The predicted value of Z_S obtained was

$$Z_S = 43.5 \frac{nt/m^2}{ampere} . \quad (\nu = 2540 \text{ Hz}, p = 16 \text{ torr})$$

The corresponding value, experimentally obtained, was

$$Z_S = 33.2 \frac{nt/m^2}{ampere} .$$

The agreement of the two values is good. Considering the number of approximations made, order of magnitude agreement would have been considered satisfactory. No error analysis was conducted on this computation for that reason.

Except for the departure at low frequencies, the results are consistent with the theoretical predictions based on the assumption of energy transfer by the electrons in the positive

column. There are aspects of the problem which were not examined by this experiment but which should be studied to gain complete understanding and to understand other experimental results. A more complete investigation would include phase as well as magnitude information in the transfer function. In addition, the source of the sound could be localized and momentum transfer aspects investigated. Although this experiment indicates that electron heating of the neutrals in the positive column provides a mechanism for sound production in glow discharges, it has not discounted the roll of ions in sound production under other circumstances.

2. Low Frequency Departure

During preliminary work in conjunction with this experiment, a large number of acoustic waveforms were observed. One characteristic of the sound signal produced by a pulse was noticed, which is reflected in the drop-off of the transfer function at low frequencies. Figure 20 shows part of the waveform received at point 1 during one of the runs. Due to attenuation of the high frequency components, the features are not as sharp as some which were observed at closer positions during earlier work. The main features are visible however.

The first and most significant feature is that the vertical distance from 1 to 2 is approximately equal to the distance from 3 to 4, with the latter always slightly greater. The next feature is that the slope and curvature of the curve from 2 to 3 is approximately the negative of that for the curve from 4 to 5. The two

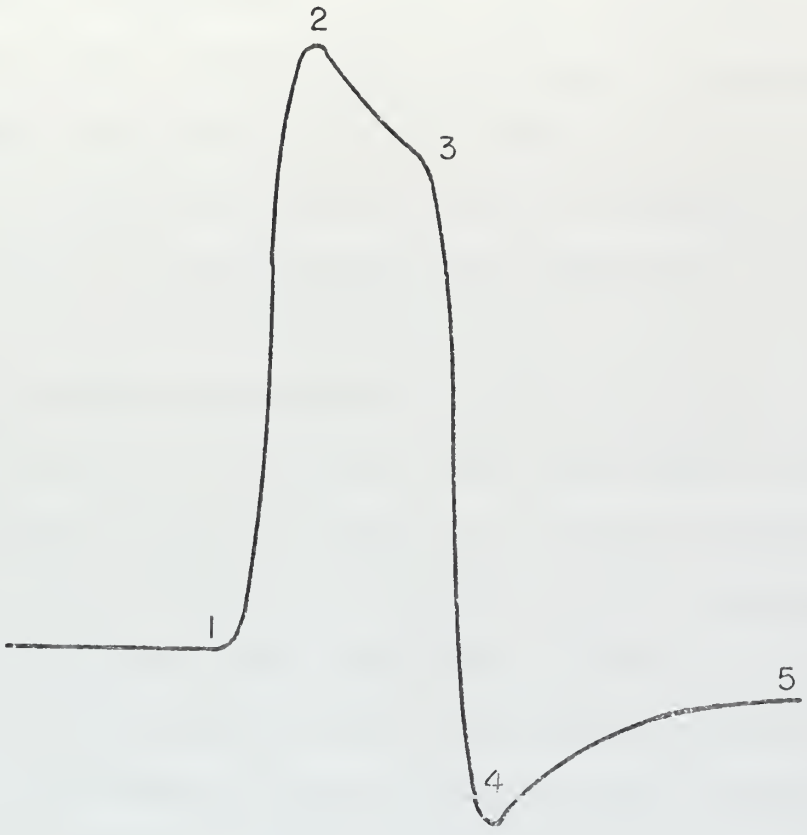

Figure 20. A Typical Sound Pulse Produced by a Rectangular Current Pulse.

curves suggest an exponential process with a long time constant. A last point is that point 5, where the slope is approximately zero, is lower than point 1, the level before the signal. The polarity of the figure is such that point 1 corresponds to the ambient pressure with upward deflections indicating an increase in pressure in the discharge region.

The following description of events occurring in the discharge region during the creation of the sound pulse is postulated. When the discharge current increases, the energy transferred to the neutral gas increases, thereby increasing the temperature of the neutral particles. This temperature increase is so rapid that the netural particle density remains essentially constant. As a consequence, the pressure changes almost directly with the temperature. The neutral particles move away from the discharge, radially as well as axially, under the temperature and pressure gradients. As the concentration decreases, the pressure decreases toward the ambient value. The pressure change, Δp_1, which would take place because of the diffusion is

$$\Delta p_1 = K\Delta NT_1$$

where ΔN is the change in density.

When the heating processes are removed, the neutral gas cools rapidly to the ambient temperature. Since the cooling process is much more rapid than the particle diffusion, the pressure at ambient temperature would be the equilibrium pressure

minus the pressure difference caused by the density change. This pressure difference, Δp_2, is given by

$$\Delta p_2 = K\Delta NT_2.$$

Since $T_1 \simeq T_2$, $\Delta p_1 \simeq \Delta p_2$. The neutral particles would then diffuse back in, to return the region to the ambient density.

The diffusion process is slow, with a long time constant. Under the action of a high frequency signal, there would not be time for a significant amount to occur between cycles. Consequently, the acoustic pressure would not reflect any density changes. At the other extreme, for very low frequency temperature variations, the pressure changes would be negligible but the density changes would be large. Therefore it can be predicted that the effect will become appreciable at low frequencies.

Notice that in the postulated process, no assumptions were made concerning the heating process except that it is spatially uniform in one region and that particles are free to move in and out of the region. Thus the assumption of one dimensionality for such a process occurring in a tube could be a valid assumption. Therefore Schulz's assumptions will be considered valid and the failure of the prediction at low frequency attributed to the wave equation. The wave equation fails because it does not take diffusion into consideration.

If diffusion is the important factor in the discrepancy at low frequencies, then the effects will become important for frequencies whose period is of the order of or longer than a characteristic diffusion time τ_D. This time is the time for particle

diffusion for a mean displacement of some characteristic dimension of the discharge region. Therefore, the characteristic frequency is given by McDaniel [39] as

$$\nu_c = \frac{1}{\tau} = \frac{D}{\zeta^2}$$

where ζ is the characteristic dimension. The effective diffusion coefficient D is given by Present [36] as $D = \frac{\bar{v}\ell}{2}$ where $\bar{v}$ is the mean velocity and ℓ is the mean free path.

Since the mean free path varies inversely with pressure, this predicts that the frequency at which the effect occurs will vary inversely with pressure. An examination of Figures 15, 16 and 17 shows that this is the case: at 16 torr, $\nu_c \simeq 500$ Hz; at 12.7 torr, $\nu_c \simeq 750$ and at 7.65 torr, $\nu_c \simeq 1000$ Hz, the product $p\nu_c$ being roughly constant as it would for the predicted dependence on density. However, substitution of the discharge length "a" for the characteristic dimension gives a frequency which is three orders of magnitude too low. Thus, although diffusion effects may be responsible for the low frequency effects, the simple argument used to determine the critical frequency did not predict the correct result.

This diffusion effect is a new problem for acoustics. It is a low frequency, low pressure effect and will probably only occur in conjuction with a thermal acoustic source. The excitation of sound by a heat or energy source is self-rectifying since the energy transfer into the system cannot be balanced by the removal

of heat or energy from the system by the same process. This means that the energy source term H in equation (2.1) can not be represented by the form

$$H(r,t) = H(r)e^{i\omega t}$$

since such a representation implies that energy can be removed by the source with the same efficiency that it transfers energy into the source.

To predict the correct low frequency characteristics of sound produced by a discharge plasma, the derivation of the wave equation must take diffusion and heating effects into consideration. The results of the derivation should be a differential equation capable of predicting the neutral density and temperature when solved for the zero frequency case. Such a derivation is considered beyond the scope of this investigation.

D. EFFECT OF THE DISCHARGE

1. Predicted Attenuation

When the measured values of axial temperature were compared with the predictions of Venzke et.al. [51], the agreement was within 7%. This verification of the predictions of that paper was considered sufficient justification to use its predictions for T_w, the wall temperature and T_M, the mean temperature with the same relative error. These values were substituted into the expressions of Section V.E. to obtain the neutral density in the two regions for each run. The steps outlined in that section were followed to obtain estimates for N_e and T_e. With the density,

wall temperature, electron temperature and electron density as inputs, the attenuation constant was calculated using the Ingard-Schulz equations for ω = 31,400 and ω = 600.

The results obtained were that the zero ionization value of the attenuation constant was essentially the same as the value predicted for a discharge under the experimental conditions. The value of β_o calculated in the manner mentioned earlier was larger at the higher frequency, which indicated that bulk losses were not completely negligible. The largest difference between the values of β_o for the two frequencies occurred at 7.65 torr where the difference was slightly less than 3% for the un-ionzed value. The greatest ionization effect predicted was a .5% reduction in attenuation for the two discharge runs made with a filling pressure of 7.65 torr. In other words, the Ingard-Schulz equations predicted that no plasma effects would be discernable under the experimental conditions.

For the plasma associated with a filling pressure of 7.65 torr, the electron temperature T_e was estimated to be 1.4×10^4K and the electron density was 5×10^{11} cm^{-3}. With these values and the values for the neutrals, $N_n = 2.4 \times 10^{17}$ cm^{-3} and T_n = 323K, the values of some of the plasma parameters were calculated. The characteristic collision frequencies are; $\omega_{en} = 2.9 \times 10^9$, and $\omega_{in} = \omega_{nn} = 5.87 \times 10^7$ sec^{-1}. The electron and ion plasma frequencies (ω_e, ω_i), are 4.00×10^{10} and 1.5×10^8 cm^{-1}. The mean

free path of a neutral particle is 7.0×10^{-4} cm. While these values are different for the other discharges, the values are representative of the orders of magnitude of the various parameters.

2. Comparison of Predicted and Experimental Values

The assumption of boundary loss domination was made earlier. Since the failure of this assumption would occur at higher frequencies, where the data were weighted the least due to their larger relative error, the fit to the data should reflect the low frequency characteristics. This was tested at the value for β_o predicted for $\omega = 600$. The predicted values are shown in Table III under the column marked β_o'. The experimentally determined value of β_o and its standard deviation are shown in the columns marked β_o and $\Delta\beta_o$.

The ratio of the difference, between the predicted and experimental value of β_o, to the standard deviation of β_o is shown in the column headed $\frac{\beta_o - \beta_o'}{\Delta\beta_o}$. The magnitude of these numbers are all less than unity, indicating that the differences between the predicted and the experimental value are all within one standard deviation of the result. The greatest difference between the predicted and experimental values is 13%.

However the signs of the difference are correlated. The second column, headed "polarity", indicates the polarity of the discharge with respect to sound propagation. A plus sign means sound propagation in the direction of electron drift motion. A

TABLE III

COMPARISON OF PREDICTED AND EXPERIMENTAL VALUES OF ATTENUATION CONSTANT

RUN	POLARITY	PRESSURE (CORR.) (torr)	β_o' (PRED.) ($10^{-4}cm^{-1}$)	β_o (EXPT) ($10^{-4}cm^{-1}$)	$\Delta\beta_o$ ($10^{-4}cm^{-1}$)	$\frac{\beta_o-\beta_o'}{\Delta\beta_o}$	$\frac{\beta_o}{\beta_o'}$	$\delta\beta_T$ ($10^{-4}cm^{-1}$)
1	0	7.65	1.89	1.93	.21	.19	1.02	-.04
2	+	8.1	1.86	1.7	.24	-.67	.91	-.04
3	-	8.1	1.86	1.74	.43	-.28	.94	-.04
4	+	17.2	1.287	1.12	.37	-.45	.87	-.03
5	-	17.2	1.287	1.23	.32	-.18	.96	-.03
6	0	16	1.31	1.33	.25	.08	1.02	-.03
7	-	13.5	1.44	1.4	.30	-.14	.97	-.03
8	0	12.7	1.47	1.59	.21	.57	1.08	-.03
9	+	13.5	1.44	1.41	.24	-.13	.98	-.03

β_o' Predicted value of attenuation constant for experimental conditions

β_o Experimental value of attenuation constant

$\Delta\beta_o$ Standard deviation of β_o

$\delta\beta_T$ Uncertainty in predicted value of β_o' due to uncertainty in values of wall temperature

zero is used to indicate the discharge-off state and a minus sign indicates sound propagation counter to electron drift. The sign of the differences is positive for the no-discharge cases. For the discharge cases, it is negative. The negative sign indicates that the predicted attenuation is greater than the observed attenuation.

3. Discussion of the Results of the Comparison

The results show that for the ionized cases, the predicted value of the attenuation constant is greater than the observed value. Although the two values lie within one standard deviation of the experimental value, the consistency of the result indicates that it is due to either a systematic error or to a plasma effect. The temperature dependence of the attenuation constant at constant pressure is such that if the wall temperature used for the computation were too low, the predicted values of β_o would be too high. The three parameters which influence the predicted values to any degree are ω, N_n and T_n. The error must be due to either N_n or T_n since although the value of ω is the same for the ionized and un-ionized cases, the results of the comparison show that the sense of the errors involved is different.

In calculating the predicted values, the propagation of error was followed. Although the mean temperature in the discharge was assumed to be uncertain by 10%, it did not affect the error of the corrected pressure significantly. That error was affected primarily by the uncertainty in the value of the filling

pressure, which was estimated to be 5%. If the error in filling pressure was systematic, it would have affected all cases in the same manner. Therefore neither an error in the mean temperature nor an error in the filling pressure is believed to be a source of systematic error.

The only remaining source of systematic error would be the value of wall temperature used. This affects the results through the density, calculated using T_w and p', and directly. The error in the wall temperature was conservatively over-estimated to be 10^o, which means a 25% error with respect to the increase above ambient temperature but only a 3% error with respect to the absolute temperature. Representing the error in β'_o due to the error in T_w by $\delta\beta_T$, it is given by

$$\delta\beta_T = \left(\frac{\partial\beta}{\partial N_n} \frac{\partial N_n}{\partial T} + \frac{\partial\beta}{\partial T} \right) \Delta T_\omega .$$

Since

$$N_1 = \frac{P}{KT}$$

for constant pressure,

$$\frac{\partial N}{\partial T} = \frac{-N}{T} ,$$

which gives

$$\delta\beta_T = \left(\frac{-N}{T} \frac{\partial\beta}{\partial N_n} + \frac{\partial\beta}{\partial T} \right) \Delta T_\omega .$$

Using this expression, $\delta\beta_T$ was calculated for $\Delta T_\omega = 10$. The results are displayed in Table III. It is apparent that these values are not large enough to account for the discrepancy between results except for runs 7 and 9. It should be noted that if the

value of the filling pressure used for predicting β_o for runs 7, 8 and 9, were high, then the correct value for the prediction would be higher for all three cases. This would decrease the discrepancy for the no discharge case and cause the results for the ionized cases to be more like the others. The conclusions to be drawn from this discussion are that while a systematic error in the value of the wall temperature used for predicting the results is possible, it is not likely to be the cause of the difference between the experimental and predicted results.

The two runs where this error should be the smallest are runs 2 and 3, since the temperature increase is less at lower pressures. The difference for these two runs is not significantly lower. If the results for filling pressures 7.65 and 16 torr alone are compared, then it appears that the polarity does have an effect. However, there is insufficient replication to support such a conclusion.

The conclusion supported by the results is that for these experimental conditions, amplification of the sound may have occurred and a polarity effect may be present. The observed effects are within the experimental error.

E. EVALUATION OF THE YATSUI EXPERIMENT

Yatsui, et.al. [8,9] conducted their experiment in Argon at low pressures and high frequencies. For a comparison of their experimental results with the Ingard-Schulz prediction, the Ingard-Schulz equations have now been evaluated with parameter

values corresponding to two points in the Yatsui experiment. For $\nu = 10^5$ Hz and I = 5 mA, they reported maximum amplification occurred at 1.5×10^{-2} torr and damping occurred for pressures greater than .31 torr. For the condition of maximum amplification, the ratio of the received signals with and without a discharge was 3.3. The predicted value for this set of experimental parameters will be discussed first.

Since the signal traveled only a fraction ϵ of its total travel in the discharge, the ratio of the two signals is

$$\frac{V_{S-p}}{V_S} = \frac{e^{-(\epsilon\beta_p + (1-\epsilon)\beta)d}}{e^{-\beta d}} = e^{-\epsilon(\beta_p - \beta)d}$$

where d is the total distance between source and receiver. Therefore, the difference, $\beta_p - \beta$, between the two attenuation coefficients can be determined from their data by

$$\beta_p - \beta = \frac{-1}{\epsilon d} \ln\left(\frac{V_{S-p}}{V_S}\right).$$

The denominator, ϵd, is the distance traveled in the discharge, 38 cm. Therefore the experimentally determined value is

$$\beta_p - \beta = \frac{-1}{38} \ln 3.3 = -3.12 \times 10^{-2} \text{ cm}^{-1}.$$

Using the procedures outlined in Section V.E., the electron temperature was estimated to be 5.5×10^4K and the electron density was estimated to be 5.1×10^{10} cm^{-3}. With these values, and $\omega = 6.28 \times 10^5$, $N_n = 5 \times 10^{16}$ cm^{-3}, and $T_n = 300$K; the quantity

$\beta_p - \beta$ was computed using the computer program. This calculation gave $\beta_p - \beta = -5.3 \times 10^{-4}$, which is lower than the experimental value by two orders of magnitude. Using liberal estimates of the errors in the input variables, the uncertainty of this result is $\Delta(\beta_p - \beta) = 1.52 \times 10^{-3}$. This is not enough to give order of magnitude agreement.

The Ingard-Schulz predictions were also evaluated for the discharge conditions corresponding to the critical pressure, .31 torr, using: $N_n = 1.1 \times 10^{17}$ cm^{-3}, $N_e = 5.5 \times 10^{10}$, $T_e = 1.6 \times 10^4$K and $T_n = 300$K. The value predicted was found to be

$$\beta_p - \beta = -9.54 \times 10^{-10} \text{ cm}^{-1} .$$

Since this difference would hardly be detectable, it is in agreement with the Yatsui results. Further agreement with the results is the prediction that, for pressures above this, damping occurs.

Thus, although the Ingard-Schulz equations do not predict a directional effect, its predictions are, to a certain degree, in agreement with experiment.

VIII. SUMMARY AND CONCLUSIONS

This study has examined the creation and modification of sound by a discharge plasma both theoretically and experimentally. Following a review of earlier experiments on the creation of sound, a mechanism for sound production by ions was proposed and shown to be feasible. Then a numerical analysis of the equations of Ingard and Schulz was performed. This analysis showed that net amplification would not occur. It also showed that the approximate form of the dispersion relation was not useful because the criterion for its applicability was invalid.

Incidental to the experimental study, the theory of the mobility-limited thermionic diode used as a microphone was developed beyond its previous, elementary form. This analysis and the subsequent successful usage as an acoustically transparent microphone for two point measurements has increased its usefulness as an experimental tool.

The diodes were used in an experimental investigation of the modification and creation of sound at medium pressures. Fourier transforms and computer data processing techniques were used in the analysis of the data. The investigation into the modification effect of the discharge was in a different region of current, pressure and frequency from earlier experiments. The results indicate that an amplification mechanism may be operative and that there may be directional effects. Since the Ingard-Schulz equations, evaluated for the experimental conditions, predicted

no effect would be detectable, these results do not support the equations. The Ingard-Schulz equations were also evaluated for the conditions of the Yatsui experiment. The predicted values were not found to be in agreement with the experimental results but the trend with pressure was in agreement. The conclusion drawn was that the theory needed more development.

The major contribution of this study is believed to be the information gained from what was originally the secondary experiment, the conversion of discharge current fluctuations into sound. This is the first known investigation in which the current magnitude was compared to the sound it produced. The results were in reasonable agreement with the Ingard formulation of the problem. A low frequency effect was observed which was interpreted as the first observation of the effects of particle diffusion in acoustics.

The general agreement of Ingards predictions in both areas indicates that electron heating of the neutrals is the dominant source of acoustic energy. However several experiments have raised questions not answered with the present theory. One of these is the directional effect on discharge modification. Two others, associated with sound production, are the effects of high fields and the localization of the sound source near the cathode. These stand out as subjects of further experimental and theoretical development. The interpretation of the low frequency behavior of the sound source as a diffusion effect also warrants further work, both experimental and theoretical. In addition, the study of the

Ingard-Schulz equations indicates that the increased attenuation to be expected under certain conditions could be a fruitful area for investigation.

APPENDIX A

THE MOBILITY-LIMITED THERMIONIC DIODE AS A MICROPHONE

Standard microphones have limitations which hinder their usage when studying sound at very low pressures. This is particularly true in conjunction with plasma-acoustic work. There are several reasons for this. A very important one is contamination from gassy components. Another consideration is that the microphones were designed for operation at atmospheric pressure. Operation at reduced pressures may require circuit modification since, for condenser microphones, breakdown can occur. Chalupnik et.al. [52] reported changes in sensitivity and frequency response with pressure in two commonly used condenser microphones (Western Electric 640AA, Bruel and Kjaer type 4111). The lack of a sensitive sound detector without the problems outlined above has slowed plasma-acoustic studies. Recently Dayton et.al. [53] reported the use of a mobility-limited diode as a microphone without the drawbacks of conventional microphones at low pressures. However heretofore the theory has not been developed beyond its most elementary form.

1. Theory

If the cathode is sufficently hot, so that the operation is not emission limited, the current flow in a thermionic diode, operating in a high vacuum, is limited by the effects of space charge. The current density is given by the Langmuir-Childs law which says that the density is proportional to the cathode-plate

potential to the three-halves power. The constant of proportionality is dependent on the geomentry of the current-flow situation. The three halves power dependence assumes an equipotential filament; a condition which is approximately true provided the voltage drop across the filament is small compared to the cathode-anode potential. If this condition is not met, then the current density varies with the plate potential to a higher power, up to 5/2 [54], the actual value of which is determined by the definition of the cathode to anode potential.

a. Mobility-limited Operation

In the presence of a background gas of neutral particles, the electrons will suffer collisions and their average velocity will therefore decrease. This affects the space charge field and the current density. In the limiting case, where the anode-cathode separation is much larger than a mean free path, the velocity of the electrons is limited by their mobility in the gas. Cobine [55] derives an expression for the current density in a parallel-plate diode with a mobility-limited current:

$$j = 9.92 \times 10^{-14} \frac{\mu V^2}{d^3} \quad (\text{amp-cm}^{-2}) \qquad (A.1)$$

where d is the electrode separation in cm and μ is the mobility. The derivation assumed the electron velocity is proportional to the field, i.e. the mobility is field independent. This result means that the current is proportional to the square of the anode-cathode potential. A derivation for a cylindrical situation under the same assumptions yields the same dependence on plate voltage.

Although a general treatment has not been attempted, the similarity of the derivation to that of the Languir-Childs law suggests that the result is geometry independent. With the additional assumption that the mobility μ is inversely proportional to pressure, the current in a mobility limited diode is given by

$$I \alpha \frac{V^2}{p} \qquad (A.2)$$

For weak fields, the mobility is not field-independent [40] and the drift velocity is given by

$$v_D \alpha (\frac{E}{p})^{\frac{1}{2}} . \qquad (A.3)$$

In such a case, it is easy to show that the diode current for parallel plate and cylindrical diodes is given by:

$$I \alpha \frac{V^{3/2}}{p^{\frac{1}{2}}} . \qquad (A.4)$$

The field-dependent, the field-independent and any intermediate case as well as the transition from space charge to mobility limited operation are included in the general form

$$I = Cp^{-k_1} V^{k_2} \qquad (A.5)$$

where C, k_1 and k_2 are dependent on the situation and must be empirically determined.

b. Sensitivity

To determine the sensitivity of the diode as a microphone, consider the simple circuit shown in Figure 21. If the effect of the sound on the diode is observed by measuring the

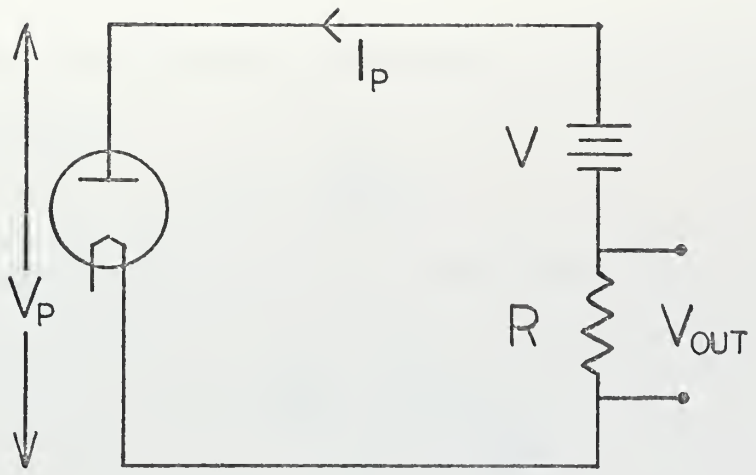

Figure 21. Diode Circuit. A simple circuit which can be used to study sound with a mobility-limited thermionic diode.

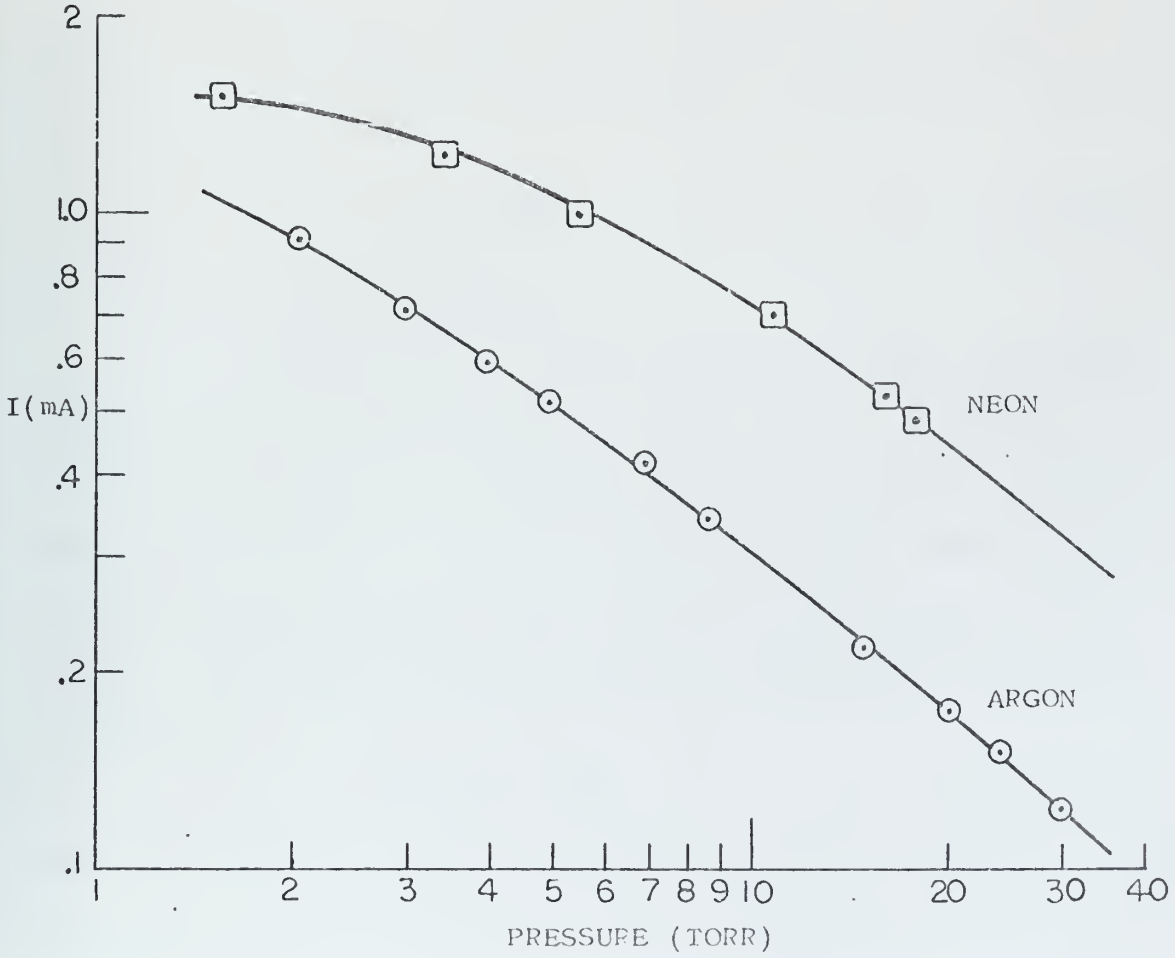

Figure 22. Diode Current in Dependence on Pressure for a Typical Diode in Argon and Neon.

voltage across R, then the sensitivity, S, of the diode circuit can be defined as:

$$S = - \frac{\delta V_{out}}{\delta p} \qquad (A.6)$$

Using equation (A.5), it is easy to show that this is given by:

$$S = \frac{k_1}{p} \frac{V_{DC}}{1 + k_2 \frac{V_{DC}}{V - V_{DC}}} \qquad (A.7)$$

where V_{DC} is the d.c. component of the output voltage. This expression shows that the sensitivity increases with the d.c. voltage across R, in an approximately linear relation, until the output voltage becomes comparable with the supply voltage V. The signal voltage $\tilde{V}$ produced by an acoustic pressure wave $\tilde{p}$ is therefore given by

$$\tilde{V} = S\tilde{p}. \qquad (A.8)$$

c. Frequency Response

Equation (A.7) is not correct for short wavelengths. Implicit in the discussion thus far has been the assumption that the finite size of the diode would not affect results. Actually the diode averages the pressure over its length. When fringing effects are ignored, the diode current is proportional to its length. Therefore a diode of length $\delta\ell$ contributes a current δi given by

$$\delta i = I \frac{\delta \ell}{\ell} \qquad (A.9)$$

where I is the current for a diode of length ℓ, considered uniform. The total current consists of the d.c. component plus the a.c.

component caused by a pressure disturbance. The current fluctuation is given by

$$\tilde{I} = \frac{S}{R} \tilde{p} \ . \qquad (A.10)$$

For a pressure wave given by $\tilde{p} = p_o e^{ikx-i\omega t}$, which is propagating in the axial direction of the diode, the total current $\tilde{I}$ is given by integrating equation (A.9) over the length of the diode, wherein the real part of the pressure must be used.

$$\tilde{I} = \frac{S}{R} \frac{p_o}{\ell} \int_o^{\ell} \cos kx \, dx,$$

therefore:

$$\tilde{I} = \frac{S}{R} p_o \frac{\sin k\ell}{k\ell} \ . \qquad (A.11)$$

The frequency response of the diode is therefore $\frac{\sin(2\pi\ell/\lambda}{2\pi\ell/\lambda}$.

d. Temperature Effect

The equations developed thus far indicate that the diodes can be calibrated in terms of absolute pressures by extrapolation from the zero frequency case, i.e. the d.c. characteristic of the diode. This requires that the pressure be varied and the current measured as a function of plate voltage at the pressures used. The pressure measurement is usually made at some point removed from the diode. Since the filament is hot, the effects of the thermal gradient between the diode and the measuring point must be considered.

Many properties of particles in gases which are frequently expressed as functions of pressure are in fact primarily dependent on the particle density. In such cases, temperature effects can be compensated for by correcting the pressure for

temperature. For example, mobility is given as a function of pressure even though it is a function of density.

$$\mu = \mu(p)$$

If the data is for pressures at temperature T_o and the temperature of the point of concern is T_2, and the pressure is p_2, then the effective pressure, p_e, for entry into the data is

$$p_e = p_2 \frac{T_o}{T_2} .$$

Now consider the effect of the temperature difference on the diode characteristics, starting from Gauss's law:

$$\nabla^2 = - \frac{\rho}{\epsilon_o} \qquad (A.12)$$

and the expression for current density

$$j = \rho v .$$

Assume electrons moving in a gas under a weak field so that

$$v_D = C_1 \left(\frac{|\nabla V|}{p} \right)^{\frac{1}{2}}$$

where C_1 is a constant peculiar to the gas. Consider cylindrical symmetry and negligible end effects. Since the current I is a constant, and related to j by geometry, the density can be expressed in terms of the current and other factors then substituted into Eq. (A.12). The result can be written in cylindrical coordinates as:

$$\frac{1}{r} \frac{d}{dr} \left(r \frac{dV}{dr} \right) = \frac{1}{2\pi r \ell} \frac{p^{\frac{1}{2}}}{C_1} \frac{1}{\left(\frac{1}{r} \frac{dV}{dr} \right)^{\frac{1}{2}}} .$$

This can be re-expressed as:

$$\left(r\,\frac{dV}{dr}\right)^{\frac{1}{2}}\frac{d}{dr}\left(r\,\frac{dV}{dr}\right)=\frac{1}{2\pi\ell}\,\frac{p^{\frac{1}{2}}}{C_1}\,r \qquad (A.13)$$

The pressure p can be expressed in terms of the pressure, p_1, at the measuring point as

$$p = p_1 f(T(r)) = p_1 f(r) \ .$$

With this substitution, Eq. (A.16) can be integrated

$$\left(r\,\frac{dV}{dr}\right)^{3/2}=\frac{3}{2}\,\frac{I}{2\pi\ell}\,\frac{p_1^{\frac{1}{2}}}{C_1}\int f^{\frac{1}{2}}(r')r'dr' \ .$$

Therefore

$$\frac{dV}{dr}=\left\{\frac{3}{2}\,\frac{I}{2\pi\ell}\,\frac{p_1^{\frac{1}{2}}}{C_1}\right\}^{\frac{2}{3}}\frac{F(r)^{2/3}}{r} \quad \text{where}$$

$$F(r)=\int_o^r f^{\frac{1}{2}}(r')r'dr'$$

from which the result

$$I=\frac{4\pi\ell C_1}{3p_1^{\frac{1}{2}}}\,V^{3/2}\left\{\int_o^{r_o}\frac{F(r)^{2/3}}{r}\,dr\right\}^{3/2}$$

can easily be obtained. This can be written as

$$I = A\,\frac{V^{3/2}}{p_1^{\frac{1}{2}}} \ .$$

A review of the steps taken to arrive at this result shows that even had some other dependence on pressure been used, the functional dependence does not change because of a temperature effect.

A theoretical treatment has given several predictions as to the operation of a mobility-limited thermionic diode as a microphone. The results may be summarized as follows.

1. The diode d.c. current will vary with pressure and plate voltage as

$$I = Cp^{-k_1} V^{k_2}$$

where $\frac{1}{2} \leq k_1 \leq 1$ and $\frac{3}{2} \leq k_2 \leq 2$.

2. For a simple circuit like Figure 21, the sensitivity, S, is given by

$$S = \frac{k_1}{p} \frac{V_{DC}}{1 + k_2 \frac{V_{DC}}{V - V_{DC}}} .$$

3. The sensitivity as a microphone will fall off with wavelength as

$$\frac{\sin (2\pi \ell / \lambda)}{(2\pi \ell / \lambda)} .$$

2. Experiment

An experiment was performed using several diodes which investigated the first two predictions. The frequency response was not tested.

a. Experimental Arrangement and Procedure

The diodes used were of similar construction. They consisted of a tantalum cylinder, 1 cm long by 1 cm diameter, as plate and a tungsten or thoriated tungsten filament as cathode. The diodes were mounted several decimeters from the tube ends and the sound source, in a tube 4 cm in diameter. A current-modulated

glow discharge acted as sound source. The a.c. signal was measured using a circuit like Figure 6 with a differential amplifier to amplify the signal which was then observed with an oscilloscope or with a boxcar integrator.

After outgassing the system and activating the filaments, space charge limited operation in a high vacuum was verified. This was done by measuring the plate current as a function of plate voltage to a value of 30 volts, which was twice the highest expected operating voltage. If a log I, log V plot gave a straight line, the selected operating point was considered valid. If not and the current dropped below a straight line at 30 volts, then the diode was considered emission limited and appropriate steps taken. If the operating point was valid, then that filament voltage was maintained throughout the calibration. For the remainder of the calibration, the pressure was changed and the I versus V measurement made. For this portion of the calibration, if the log log plot showed that the current at higher voltages was above the linear fit to the lower values, than ionization was taking place and subsequent operation below these values of plate voltage was required.

After calibration, the a.c. response to various pressure waveforms was noted. The sensitivity was measured with a boxcar integrator set to read the same point in the signal as the d.c. signal was varied by changing the resistance of the load resistor. The sound source amplitude was kept constant during the measurements.

b. Noise

The diode was found to be susceptible to electrical noise from external and internal sources. The external noise was reduced to an insignificant level by shielding with heavy copper foil. The foil was wrapped around the tube at its surface, extending beyond the diode approximately 5 cm at both ends. The shield was grounded with a separate head. All leads to the diode were also shielded.

In addition to the external noise, the diode was subject to an internal noise which seemed due to spurious ionization. This noise was characterized by fast rising positive spikes, representing a sudden increase in current, followed by a more gradual fall. These spikes always appeared when contamination was suspected.

c. D.C. Characteristics

Dayton et.al. [53] reported results for a diode operating in N_2 whereas Argon and Neon were used in this experiment. The results obtained were similar to those of Dayton. A typical plot for Argon and Neon is shown in Figure 22. The values of k_1 and k_2 obtained are displayed in Table IV along with information on N_2 taken from Dayton's paper. The values shown are the averages computed from data for several diodes for the pressure range 5 to 30 torr.

TABLE IV

Gas	k_1	k_2	k_3
Ne	.60 $\pm$ .01	1.67 $\pm$ .04	1.5
Ar	.63 $\pm$ .02	1.03 $\pm$ .09	1
N_2	.62	1.98	1.7

d. Sensitivity

A plot of signal voltage versus d.c. voltage for constant acoustic pressure constitutes a measurement of the sensitivity in arbitrary units. Figure 23 shows the results of such a plot. The solid curve was calculated using equation (A.17) with k_2 and the amplitude determined by a least squares fit to the data points. The upper half of the points were neglected in the fit because of a definite shift in the slope of a linear plot of the data when the plate voltage became comparable to the filament voltage.

3. Discussion of Results

The value of k_1 is very similar in all three gases but there is a large difference in the values for k_2. Since the theoretical treatment assumes that the pressure dependence arises from the similarity parameter E/p, if k_1 is the same, then k_2 should be the same. As this is not the case, and the analysis has also shown that the temperature gradient should not affect this, then there must be a pressure dependence other than E/p.

Von Engle [40] points out that molecular gases, such as N_2, have large in-elastic collision cross sections which causes their mobility to be constant and their drift velocity to vary linearly with E/p. This is related to the manner in which $\mathcal{K}$, the average fraction of electron energy lost in a collision, increases with E/p. Until inelastic collisions start to take place, $\mathcal{K}$ remains constant, afterwards it increases with E/p. The relation between the dependence of $\mathcal{K}$ on E/p and the dependence of the

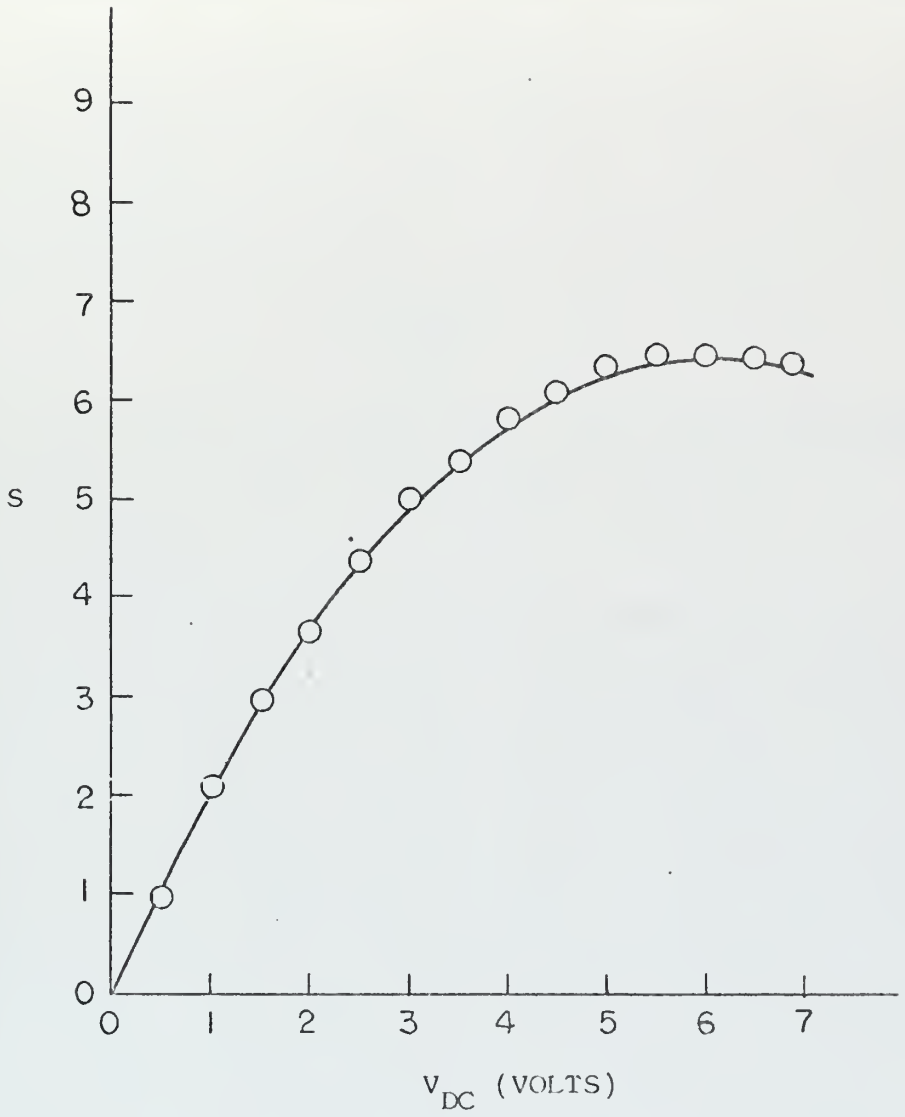

Figure 23. Diode Sensitivity in Dependence of d.c. Signal. Argon at pressure of 7.35 torr. Vertical scale is arbitrary. The ordinate is the d.c. component of the signal voltage.

mobility-limited diode current on plate potential is a complicated one and would be difficult to establish quantitatively. However there is a correlation between the experimentally determined values of k_2 and the slope of the log $\mathcal{K}$ - log E/p curves as figure 63 of Von Engle [40]. For simplicity, k_3 is defined by

$$\mathcal{K} = C \left(\frac{E}{p}\right)^{k_3}$$

which is used merely for comparison. The values of k_3 determined from Von Engle are shown in Table IV for comparison.

4. Conclusion

The mobility-limited diode nicrophone should serve to fill a need in plasma-acoustic studies. It is simple and inexpensive to construct and requires no complicated circuitry. By virture of changing the d.c. signal, sensitivities of different diodes can be matched for direct comparison of signals. It is sensitive. Sensitivities higher than .27 mV/microbar (360 mV/torr) at 5 torr ambient pressure, can easily be attained. It is transparent to sound and offers little interference to light in the axial direction. Calibration at zero frequency is simple and easy to perform.

It is susceptible to noise from contamination. This is a drawback which conventional microphones do not have. Its use would be limited to inert gases or those where chemical activity with the hot tungsten filament would not be expected. Even with these drawbacks, a diode microphone can be used for many experiments where other techniques can not.

APPENDIX B

THE USE OF BUTT SEALS FOR FEEDTHROUGHS

In order to seal electrode supports and feedthroughs into glass with a minimum disturbance of the glass surface, a special procedure was required. Kovar wire, 70 mil. diameter, was used for all supports and feedthroughs. Tantalum sheet 5 mil., was used for the electrodes. Diode filament leads were wrapped with fine rhenium wire for ease in spot welding. The electrode supports went along the electrode in the axial direction and were spot welded in several places. In addition, a small cut in the electrode was made at the edge and the support wire was bent back and crimped to hold the electrode in a mechanical grip. The small cut was made to prevent the wire from extending beyond the edge of the electrode. The materials were cleaned prior to assembly and the components were cleaned again just before sealing in accordance with procedures recommended by Rosebury [56].

For final assembly and sealing, the components of an element were assembled on a special jig. The jig was designed to hold the support wires and feedthroughs in a plane which would be normal to the axis of the glass tubing. After assembly of the components the jig was attached to one piece of the glass tubing, earlier mounted in the lathe. The jig was placed so that the feedthroughs were flush against the edge as shown in Figure 24. The edge used for the seals worked best if it was diamond cut. Fire cut edges were susceptible to leaks. The second piece of tubing was matched with

the edge of the first as shown in Figure 25. A low pressure purge of nitrogen was used to prevent the flame from penetrating the tube and contaminating the surfaces. After the purge was on and the two pieces and jib were turning in the lathe, heat was applied and the two ends pushed toward each other. When sufficiently hot, the glass would flow around the leads and the two ends would butt together, forming a butt seal. A small ring of 7052 was then beaded around the base of the leads, for insurance. The complete tube was annealed in an oven following the recommended temperature cycle. For the tube used in the experiment, due to the nature of the main discharge filaments, annealing was done with the tube being evacuated by a diffusion pump. During preliminary work, several seals were not annealed in the oven, but merely flame annealed on the lathe with no later cracking.

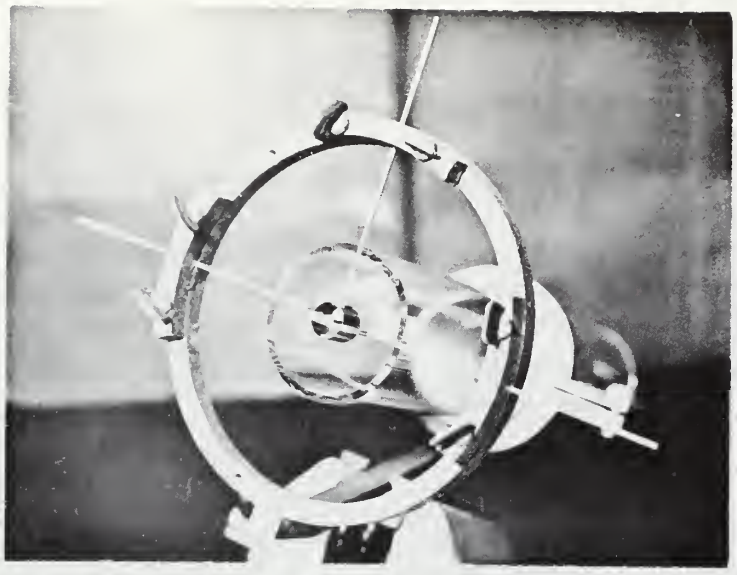

Figure 24. Diode in Process of Assembly, Showing Placement in Jig.

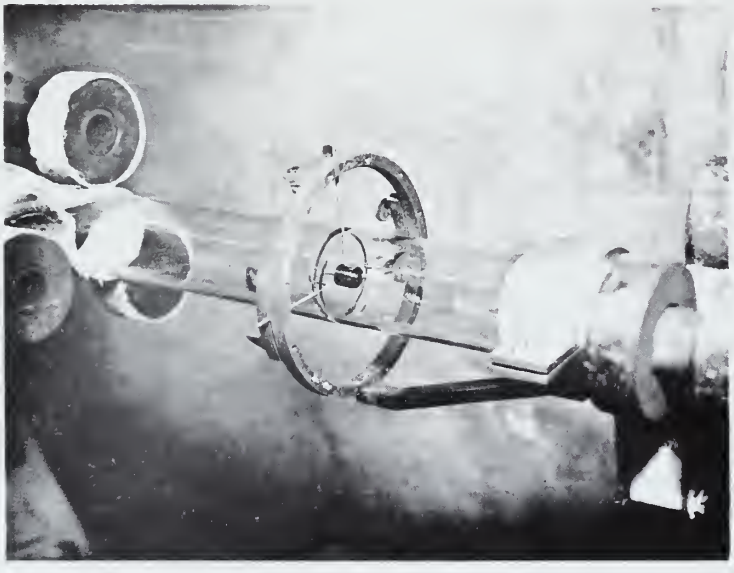

Figure 25. Diode in Process of Assembly, Showing Assembly in Lathe.

APPENDIX C

TAPE RECORDER SPECIFICATIONS

FM Record/Reproduce

Input Sensitivity:	(High Level)	1 to 20 volts peak-to-peak for ± 40% deviation
	(Low Level)	0.030 to 1 volt peak-to-peak for ± 40% deviation
Input Impedance:	(High Level)	20k ohms or greater, unbalanced to ground
	(Low Level)	50k ohms or greater, unbalanced to ground

Carrier Frequency, Response, Signal-to-Noise Ratio:

High Level	Center Frequency	Response	S/N
.375 ips	500 hz	DC to 100 hz ± 1 db	35 db
3.75 ips	5 khz	DC to 1 khz ± 1 db	38 db
37.5 ips	50 khz	DC to 10 khz ± 1 db	42 db
Low Level			
.375 ips	500 hz	5 to 100 hz ± 1 db	35 db
3.75 ips	5 khz	5 hz to 1 khz ± 1 db	38 db
37.5 ips	50 khz	5 hz to 10 khz ± 1 db	42 db

Gain Drift:	2% or less of full scale	(temp. range 35° to 110°F, line voltage range 110 vac to 125 vac)
Center Frequency Drift:	2% or less of full scale	
Linearity:	1% of best straight line through zero	
Output Level:	2.8 v p-p for ± 40% deviation into 1,000 ohms	
Output Impedance:	50 ohms or less	
Harmonic Distortion:	1.5% total (signal 1 v p-p, 3,000 hz, at 37.5 ips)	

Output Filter

Cutoff Frequency:	100 hz, .1 khz, 10 khz, 100 khz
Frequency Response:	Filter set for flat frequency response, ± 1 db -- Filter set for flat phase response -4 to -8 db at cutoff.
Overshoot:	Filter set for flat frequency response, 15% max. -- Filter set for flat phase response, 2% max.

Transport

Tape Speeds:	37.5, 3.75, 0.375 ips
Speed Accuracy:	± 0.2%, long-term

I. DATA REDUCTION

AFTER THE DATA WERE STORED ON TAPE IN 32-BIT BINARY FORM, FIVE PROGRAMS WERE USED SEQUENTIALLY TO PROCESS THE DATA. DISK STORAGE WAS USED FOR INPUT AND OUTPUT EXCEPT THE FIRST PROGRAM USED TAPE FOR INPUT DATA EACH PROGRAM MAY BE THOUGHT OF AS A STEP IN THE PROCESSING

1. STEP ONE --AVERAGE--

```
C          THIS PROGRAM TAKES THE RAW DATA AND BEGINS THE
C  PROCESSING.  THE DATA HAS BEEN PRESCREENED AND INFORMATION
C  STORED IN AN ARRAY INDICATING WHICH SETS OF WAVEFORMS ARE
C  ACCEPABLE FOR AVERAGING.  THIS ARRAY IS CALLED 'KF'.  ALL
C  ACCEPTABLE WAVEFORMS ARE AVERAGED AND THE STANDARD DEVIA-
C  TION OF EACH DETERMINED FOR EACH DIFFERENT EXPERIMENTAL
C  RUN.  THIS INFORMATION IS STORED FOR USE BY THE NEXT
C  PROGRAM.
C
C
      DIMENSION DATA(3600),AVG(3600),KSTAR(12),KF(100,12)
      DIMENSION STDEV(3600),DEV(3)
      REWIND 4
      REWIND 2
      DATA KF,NF,KSTAR/1200*0,1,3*2,3,1,1,3,1,1,2/
C
      READ(3)KF
    5 NR=0
C
      KG=0
    2 DO 7 I=1,3600
      STDEV(I)=0.
    7 AVG(I)=0.0
    1 NR=NR+1
      READ(2,ERR=1,END=50) DATA
      IF(KF(NR,NF).EQ.0) GO TO 1
C
      DO 4 I=1,3600
      STDEV(I)=STDEV(I)+DATA(I)**2
    4 AVG(I)=AVG(I)+DATA(I)
      KG=KG+1
      GO TO 1
C
   50 DIV=KG
      DO 6 I=1,3600
      STDEV(I)=SQRT((STDEV(I)-AVG(I)**2/DIV)/(DIV-1.))
    6 AVG(I)=AVG(I)/DIV
C
      DO 8 J=1,3
      DEV(J)=0.0
      DO 9 I=1,1200
      II=I+(J-1)*1200
    9 DEV(J)=DEV(J)+STDEV(II)**2
    8 DEV(J)=SQRT(DEV(J)/1200.)
C
      WRITE(4) AVG,DEV
      WRITE(6,200) NF
      WRITE(6,203) DEV
      WRITE(6,201) AVG
      WRITE(6,202) (KF(I,NF),I=1,NR)
      NF=NF+1
      IF(NF.LE.10) GO TO 5
C
      WRITE(13) KF
C
  200 FORMAT('1          FILE NO. ',I3)
  201 FORMAT(60(1X,10F12.4,/),/)
  202 FORMAT('0',10(10X,10I5,/))
```

```
  203 FORMAT('           AVERAGE DEVIATIONS  ',3F10.5)
      STOP
      END
```

2.STEP TWO --SCREEN AND RE-AVERAGE--

```
C          THIS PROGRAM USES THE AVERAGE WAVEFORMS AND THE
C STANDARD DEVIATION CALCULATED IN THE PREVIOUS PROGRAM TO
C SCREEN OUT DATA WHICH LIES OUTSIDE OF TWO STANDARD DEVIA-
C TIONS OF THE AVERAGE. IT RECOMPUTES THE AVERAGE  AND
C STANDARD DEVIATION WITH THE SCREENED DATA.
C
C
      DIMENSION DATA(3600),AVG(3600),KSTAR(12),KF(100,12),
     *KG(3600),DEV(3),STDEV(3600)
      REWIND 2
      REWIND 4
      NF=1
      READ(3) KF
      REWIND 3
      STD=2.
C
    5 NR=0
      READ(4) AVG,DEV
      DO 2 I=1,3600
      STDEV(I)=AVG(I)**2
    2 KG(I)=1
    1 NR=NR+1
      READ(2,ERR=1,END=50) DATA
      IF(KF(NR,NF).EQ.00) GO TO 1
C
      KN=0
      DO 3 I=1,3600
      J=I/1200+1
      DIV=KG(I)
      COM=AVG(I)/DIV
      TEST=ABS(COM-DATA(I))
      TEL=STD*DEV(J)
      IF(TEST.GT.TEL) GO TO 3
      STDEV(I)=STDEV(I)+DATA(I)**2
      AVG(I)=AVG(I)+DATA(I)
      KN=KN+1
      KG(I)=KG(I)+1
    3 CONTINUE
      KF(NR,NF)=KN/36
      GO TO 1
C
C
   50 DO 6 I=1,3600
      DIV=KG(I)
      STDEV(I)=(STDEV(I)-AVG(I)**2/DIV)/(DIV-1.)
      IF(STDEV(I).LT.0.0) WRITE(6,203) I,STDEV(I)
      STDEV(I)=SQRT(ABS(STDEV(I)))
    6 AVG(I)=AVG(I)/DIV
C
      DO 8 J=1,3
      DEV(J)=0.0
      SUM=0.
      DO 9 I=1,1200
      II=I+(J-1)*1200
      SUM=SUM+KG(II)
    9 DEV(J)=DEV(J)+STDEV(II)**2*KG(II)
    8 DEV(J)=SQRT(DEV(J)/SUM)
      WRITE(9) AVG,DEV
      WRITE(6,200) DEV
      WRITE(6,201) AVG
      WRITE(6,202) (KF(I,NF),I=1,NR)
      NF=NF+1
      IF(NF.LE.10) GO TO 5
C
```

```
      WRITE(13) KF
C
  200 FORMAT('1    DEVIATIONS ARE ',3E12.3)
  201 FORMAT(60(1X,10F12.4,/),/)
  202 FORMAT('0',10(10X,10I5,/))
  203 FORMAT('  STDEV SQUARED IS NEGATIVE',I5,E12.2)
      STOP
      END
```

3. STEP THREE --DELAY,OVERLAY AND ZERO--

```
C          THIS PROGRAM TAKES THE AVERAGED WAVEFORMS AND
C DELAYS THEM, REDUCING THE NUMBER OF POINTS FROM 1200 TO
C 600 IN EACH.  IT ALSO ZEROES THE BASE AND OVERLAYS A
C FALSE SIGNAL DUE TO AN ELECTROSTATIC INTERACTION.  THE
C RESULTS ARE STORED FOR THE NEXT STEP, WHICH IS THE FOURIER
C TRANSFORMATION.
C
C
      DIMENSION DA(1200,3),IND(3,10),SIG(600,3),DEV(3),AVG(3
     1          IPOINT(2,3,10)
      EQUIVALENCE (DA(1,1),SIG(1,1))
      DATA IPOINT/0,600,0,600,0,600,240,600,120,270,0,288,24
     *96,288,0,288,240,600,121,238,0,288,240,600,204,276,0,2
     *240,600,216,288,0,264,240,600,108,275,0,250,240,600,10
     *0,240,240,600,120,220,0,240,240,600,120,240,0,240/
      KF=0
      NF=0
      REWIND 4
      READ(5,100) ((IND(J,I),J=1,3),I=1,10)
C
  301 NF=NF+1
      READ(4,END=305) DA,DEV
      KF=KF+1
      IF(NF.EQ.1) GO TO 312
      A=URN(0)
      DO 311 I=100,240
      JI=130.*URN(1)+240
  311 DA(I,2)=DA(JI,2)
  312 CONTINUE
C
      DO 304 J=1,3
      KC=IND(J,KF)
      DO 302 I=1,600
  302 SIG(I,J)=DA(KC+I,J)
  304 CONTINUE
      DO 321 J=1,3
      AVG(J)=0.0
      IP1=IPOINT(1,J,NF)
      IP2=IPOINT(2,J,NF)
      DO 322 I=IP1,IP2
  322 AVG(J)=AVG(J)+SIG(I,J)
      DIV=IP2-IP1
  321 AVG(J)=AVG(J)/DIV
C
      DO 323 J=1,3
      DO 324 I=1,600
  324 SIG(I,J)=SIG(I,J)-AVG(J)
      WRITE(6,200) KF,J
      DO 303 I=1,589,12
  303 WRITE(6,202) (SIG(I+KM-1,J),KM=1,12)
  323 CONTINUE
C
      WRITE(8) SIG ,DEV
C
      GO TO 301
C
C
  305 STOP
  100 FORMAT(12I5)
```

```
  200 FORMAT('1       R.TRIPP    FILE ',I3,'  CHANNEL',I4)
  201 FORMAT(20A4)
  202 FORMAT(1X,12F10.4)
      END


          4.STEP FOUR  --TRANSFORM--

C         THIS PROGRAM DETERMINES THE SPECTRAL DECOMPOSITION
C OF THE WAVEFORMS AND THEIR STANDARD DEVIATIONS.  GAIN AND
C DIODE SENSITIVITY ARE CORRECTED FOR.
C
CCC                     INITIALIZE VALUES
C
      DIMENSION SIG(600,3),SPECT(600,3),T(600),FREQ(60),
     1          SHO(200),BIAS(3),GAIN(3),SENS(3),IP(3),
     2          SDEV(40,3),SREQ(60),DEV(3),INV(200),S(200)
      EQUIVALENCE (SIG,SPECT),(SHO,SDEV)
      COMMON SIG,SDEV,S,INV
      DATA PI,GAIN,NPNTS,NF,PERIOD/3.14159265,3*50.,600,0,
     1    0.00512/
      DO 300 I=1,NPNTS
  300 T(I)=I
      DO 301 I=1,40
      FREQ(I)=(I-1)/PERIOD
  301 SREQ(I)=SQRT(FREQ(I))
C
CC                    READ DATA FOR NEW DATA SET
C
   17 CONTINUE
      NF=NF+1
      READ(8,END=99) SIG,DEV
      READ(5,101) SENS
      WRITE(6,101) SENS
C
CCC                   CORRECT FOR AMPLIFIER GAIN
CCC                   AND DIODE SENSITIVITY
C
      DO 705 J=1,3
      FACT=GAIN(J)*SENS(J)
      DEV(J)=DEV(J)/FACT
      DO 303 I=1,NPNTS
  303 SIG(I,J)=SIG(I,J)/FACT
C
CCC                   DISPLAY WAVEFORM ON PRINTER
C
      DO 305 I=1,199
  305 SHO(I)=(SIG(3*I-2,J)+SIG(3*I,J)+SIG(3*I+2,J))/3.
      SHO(200)=SIG(600,J)
      WRITE(6,200)
  705 CALL PLOTP(T,SHO,200,0)
C
CCC       IF THIS IS THE FIRST DATA SET, DETERMINE CORRECT
CC    GAIN FOR REMAINDER OF DATA SETS.
C
      IF(NF.EQ.1) GO TO 313
C
CCC                   DETERMINE SPECTRUM AND STD. DEVIATION
C
      CALL SPCTRA
      DO 304 J=1,3
  304 SDEV(1,J)=SQRT(SDEV(1,J)**2+DEV(J)**2)
   18 WRITE(10)((SPECT(I,J),SDEV(I,J),J=1,3 ),FREQ(I),I=1,25
C
CCC                   DISPLAY RESULTS AND PASS THEM TO NEXT
CCC                   PROGRAM
C
      DO 307 J=1,3
      WRITE(6,200)
```

```
      DO 309 I=1,40
      SIG(I+40,J)=SIG(I,J)-SDEV(I,J)
      IF(SPECT(I+40,J).LT.0.0) SPECT(I+40,J)=0.0
      SIG(I+80,J)=SIG(I,J)+SDEV(I,J)
  309 CONTINUE
      DO 308 KJ=1,3
      KM=121-KJ*40
      CALL PLOTP(FREQ,SIG(KM,J),40,KJ)
  308 CONTINUE
  307 CONTINUE
C
C
      I=0
      DO 302 K=1,27
      I=I+1
      WRITE(6,210) K,(SPECT(K,J),SDEV(K,J),J=1,3),FREQ(K),SR
      RATIO=SPECT(K,3)/SPECT(K,2)
      SPECT(I,2)=ALOG(SPECT(K,2))
      SPECT(I,3)=RATIO
      SPECT(I,1)=ALOG(RATIO)
  302 CONTINUE
C
C
      WRITE(6,200)
      CALL PLOTP(FREQ,SPECT(1,3),27,0)
      CALL PLOTP(SREQ,SPECT(1,1),27,0)
      GO TO 17
C
C                    CALIBRATE GAIN
C
  313 CALL RHARM(SPECT(1,2),8,INV,S,IER)
      SPECT(1,2)=      SQRT(SPECT(53,2)**2+SPECT(54,2)**2)
      GAIN(2)=GAIN(2)*SPECT(1,2)
      CALL RHARM(SPECT(1,3),8,INV,S,IER)
      SPECT(1,3)=      SQRT(SPECT(53,3)**2+SPECT(54,3)**2)
      GAIN(3)=GAIN(3)*SPECT(1,3)
      WRITE(6,101) GAIN,SPECT(1,2),SPECT(1,3)
      GO TO 17
C
C
C                              FORMAT STATEMENTS
  100 FORMAT(20A4)
  101 FORMAT(3F10.5)
  200 FORMAT(1H1)
  202 FORMAT(1H1,/,'     TIME AND SIGNAL  ',/,50(12F10.4,/))
  203 FORMAT(1H1,/,T10,'SPECTRAL ANALYSIS OF SIGNAL FOR ',
     1'DIODE ',I2,/,T6,'INDEX  FREQUENCY    COSINE        ',
     2'SINE     AMPLITUDE   PHASE')
  204 FORMAT(I10,1P3E11.3,0P2F11.4)
  206 FORMAT(' ','          UVL=',E10.2)
  207 FORMAT('     FILE ',I4)
  210 FORMAT(I5,8E11.3,I5)
  211 FORMAT(20A4)
  500 FORMAT(1H ,T10,'LESS THAN TEST')
   99 STOP
      END
C
C
C     SUBROUTINE SPCTRA
C         THIS SUBROUTINE DETERMINES THE FOURIER TRANSFORMS
C OF THE WAVEFORMS FOR FIVE START POINTS.  IT THEN AVERAGES
C THEM AND CALCULATES THE STANDARD DEVIATION OF EACH ONE.
C
C
      SUBROUTINE SPCTRA
      IMPLICIT COMPLEX*8(Q)
      DIMENSION  SPEC(516,3),S(200),INV(200),M(3),A(2,258,3)
     1          SIG(600,3),SDEV(40,3),AVG(40,3)
      COMMON SIG,SDEV,S,INV
      EQUIVALENCE  (SPEC,A)
```

```
      DO 201 I=1,40
      DO 202 J=1,3
      AVG(I,J)=0.0
  202 SDEV(I,J)=0.0
  201 CONTINUE
C
C
      DO 706 KT=1,5
      NL=10*(KT-1)
      DO 705 J=1,3
      DO 707 I=1,512
      SPEC(I,J)=SIG(NL+I,J)
  707 CONTINUE
      CALL RHARM(SPEC(1,J),8,INV,S,IER)
      IF(IER.NE.0) WRITE(6,100) IER
  705 CONTINUE
C
C
      DO 302 J=1,3
      DO 301 I=1,40
      RSPEC=A(1,I,J)**2+A(2,I,J)**2
      SDEV(I,J)=SDEV(I,J)+RSPEC
  301 AVG(I,J)=AVG(I,J)+SQRT(RSPEC)
  302 CONTINUE
  706 CONTINUE
C
C
      DO 304 J=1,3
      DO 303 I=1,40
      SDEV(I,J)= ABS((SDEV(I,J)-AVG(I,J)**2*.2))
      SDEV(I,J)=SQRT(SDEV(I,J))*.25
  303 SIG(I,J)=AVG(I,J)*.2
  304 CONTINUE
      RETURN
  100 FORMAT('    HARM ERROR    IERRT=',I3)
      END
```

5. STEP FIVE --TRANSFER FUNCTIONS--

```
C          THIS PROGRAM TAKES THE FIRST 25 COMPONENTS OF THE
C SPECTRAL DECOMPOSITION OF THE WAVEFORMS AND USES THEM TO
C OBTAIN THE ACOUSTIC TRANSFER FUNCTION.  IT ALSO DETERMINES
C THE SOURCE TRANSFER FUNCTION AND DISPLAYS THE DATA ALONG
C WITH A CURVE REPRESENTING THE PREDICTED FORM , WHICH WAS
C FITTED TO PASS THROUGH ONE POINT.  THE STANDARD DEVIATIONS
C OF THE RESULTS ARE ALSO CALCULATED.
C
      IMPLICIT REAL*8 (D),COMPLEX*8 (Q)
      REAL*8 TITLE(10)/7*' ','TRIPP   ',2*' '/
      DIMENSION DX(25),DY(25),DF(25),DW(25),DELY(25),
     1          DB(20),DSB(20),X(3),SPECT(25,3),FREQ(25),
     2          XX(2),YY(2),SDEV(25,3),Z(25,3),UL(2),
     3          SREQ(80),YZ(80),USRCE(25)
C
      DATA DW,X/25*1.D0,0.0,98.7,251.3/,
     1     XX,YY/0.0,4500.,10.,0.0/
      K=25
      NF=0
   10 CONTINUE
      NF=NF+1
      READ(10,END=99) ((SPECT(I,J),SDEV(I,J),J=1,3),
     1                 FREQ(I),I=1,25)
      DO 300 I=1,25
  300 USRCE(I)=SPECT(I,3)/SPECT(I,2)
      WRITE(6,203) (USRCE(I),FREQ(I),I=1,25)
C
C                  CONVERT TO DOUBLE PRECISION
C
      L=0
      DSUM=0.0
```

```
      DO 301 I=2,K
      FSPQ=(SDEV(I,2)/SPECT(I,2))**2
     1    +(SDEV(I,3)/SPECT(I,3))**2
      L=L+1
      DY(L)=ALOG(USRCE(I))
      DW(L)=1.D0/FSPQ
      DSUM=DSUM+DW(L)
      DX(L)=SQRT(FREQ(I))
  301 CONTINUE
      IF(L.LT.4) GO TO 10
      DL=L*50
      DO 311 I=1,L
  311 DW(I)=DW(I)*DL/DSUM
C
C                     DETERMINE ALPHA
C
      CALL LSQPL2(L,1,DX,DY,DW,DF,DELY,DB,DSB,TITLE)
      ALPHA=-SNGL(DB(2))/(X(3)-X(2))
      UALPHA=SNGL(DSB(2))/(X(3)-X(2))
      WRITE(6,205) ALPHA,UALPHA
C
C                     DISPLAY LEAST SQUARES FIT
C                     DISPLAY TUBE TRANSFER FUNCTION
C
      ZINC=FREQ(K)/79.
      FA=DB(2)
      YZ(1)=DB(1)
      YZ(1)=EXP(YZ(1))
      SREQ(1)=0.
      DO 304 I=2,80
      SREQ(I)=(I-1)*ZINC
  304 YZ(I)=YZ(1)*EXP(FA*SQRT(SREQ(I)))
C
      CALL PLOTP(SREQ,YZ,80,1)
      CALL PLOTP(FREQ,USRCE,25,3)
      GO TO (1),10,10,10,10,11,10,11,10) ,NF
   11 CONTINUE
C                     DETERMINE SOURCE AND SOURCE UNCERTAINTY
C
      UL(1)=0.
      UL(2)=0.
      WRITE(6,204)
      A1=251.3/152.6
      A2=-98.7/152.6
      DO 303 I=1,K
      Z(I,1)=SPECT(I,2)**A1*SPECT(I,3)**A2
      USRCE(I)=(A1*SDEV(I,2)/SPECT(I,2))**2
     1         +(A2*SDEV(I,3)/SPECT(I,3))**2
      USRCE(I)=Z(I,1)*SQRT(USRCE(I))
      Z(I,2)=Z(I,1)+USRCE(I)
      Z(I,3)=Z(I,1)-USRCE(I)
      UL(2)=AMAX1(Z(I,2),UL(2))
      WRITE(6,201) I,Z(I,1),USRCE(I),FREQ(I)
  303 CONTINUE
C
C                     DISPLAY SOURCE SPECTRA
C
      WRITE(6,202)
      CALL PLOTP(XX,UL,2,1)
      CALL PLOTP(FREQ,Z(1,1),K,2)
      CALL PLOTP(FREQ,Z(1,2),K,2)
      CALL PLOTP(FREQ,Z(1,3),K,3)
C
C                     DETERMINE TRANSFER FUNCTION AND
C                      UNCERTAINTY
C
      YY(1)=0.0
      DO 302 I=1,K
      TZ=Z(I,1)
      Z(I,1)=Z(I,1)/SPECT(I,1)
      SDEV(I,1)=Z(I,1)*SQRT((USRCE(I)/TZ)**2
     1                      +(SDEV(I,1)/SPECT(I,1))**2)
```

```
      Z(I,2)=Z(I,1)+SDEV(I,1)
      Z(I,3)=Z(I,1)-SDEV(I,1)
      WRITE(6,201) I,Z(I,1),SDEV(I,1),FREQ(I)
      YY(1)=AMAX1(YY(1),Z(I,1))
  302 CONTINUE
      YY(1)=YY(1)*1.2
C
CC                    DISPLAY TRANSFER FUNCTION
C
      WRITE(6,200)
      CALL PLOTP(XX,YY,2,1)
      CALL PLOTP(FREQ,Z(1,1),K,2)
      CALL PLOTP(FREQ,Z(1,2),K,2)
      CALL PLOTP(FREQ,Z(1,3),K,3)
      YS=0.75E-04
      CALL DRAW(K,FREQ,Z(1,1),1,1,TITLE,TITLE,1000.,YS,0,0,
     1          2,2,5,6,0,LAST)
      CALL DRAW(K,FREQ,Z(1,2),2,2,TITLE,TITLE,1000.,YS,0,0,
     1          2,2,5,4,0,LAST)
      CALL DRAW(K,FREQ,Z(1,3),2,2,TITLE,TITLE,1000.,YS,0,0,
     1          2,2,5,4,0,LAST)
C
CC                     DISPLAY PREDICTED CURVE FITTED TO DATA
C
      READ(5,102) AA
  102 FORMAT(F10.5)
      FACT=SIN(AA*1.0134E-04*FREQ(14))/FREQ(14)
      FACT2=Z(14,1)/FACT
      SREQ(1)=1.
      DO 306 I=1,80
      FACT=SIN(AA*1.0134E-04*SREQ( I))/SREQ( I)
  306 YZ(I)=FACT*FACT2
      CALL DRAW(80,SREQ,YZ,2,0,TITLE,TITLE,1000.,YS,0,0,
     1          2,2,5,4,0,LAST)
      DO 305 I=1,K
      SREQ(1)=FREQ(I)
      SREQ(2)=FREQ(I)
      SDEV(2,1)=Z(I,3)
      SDEV(1,1)=Z(I,2)
      KK=I/K+2
  305 CALL DRAW(2,SREQ(1),SDEV,KK,0,TITLE,TITLE,1000.,YS,0,
     1          0,2,2,5,4,0,LAST)
      GO TO 10
   99 STOP
  100 FORMAT(20A4)
  101 FORMAT(I5)
  200 FORMAT('1      TRANSFER FUNCTION OF SOURCE')
  201 FORMAT(10X,I3,3E12.3)
  202 FORMAT('1     SOURCE SPECTRA')
  203 FORMAT('0              RATIO          FREQ',
     1       /,25(10X,2F12.5,/))
  204 FORMAT('0',T15,'SOURCE          FREQ')
  205 FORMAT('0','       ALPHA IS',1P1E10.2,' +/-',E10.2,/)
      END
```

```
      II. INGARD-SCHULZ ANALYSIS

C
C           THE FIRST PART OF THE PROGRAM INITIALIZES VALUES.
C SYMBOLS FOR THE CONSTANTS OF THE GAS ARE:
C                  CD   MOLECULAR DIAMETER
C                  CMN  MASS OF ONE MOLECULE
C                  CG   RATIO OF SPECIFIC HEATS
C           VALUES OF THE INTEGRALS USED IN EVALUATING THE
C ELECTRON-NEUTRAL COLLISION FREQUENCY AND THE AVERAGE CROSS
C SECTION ARE CONTAINED AS A TABLE OF ENTRIES AS Y1 AND Y2
C RESPECTIVELY.  EN IS THE VALUE OF ELECTRON TEMPERATURE
C USED AS ENTRY INTO THE TABLE.  FOR THE COMPUTATIONS, THE
C MKSA SYSTEM OF UNITS ARE USED EXCEPT MASSES ARE IN GRAMS
C AND LENGTHS IN CENTIMETERS.
C
      REAL*4 X(5),XI(2),STARPT(5),LOWLIM(5),UPLIM(5),XMN(5)/
     *NAME(6)
      DIMENSION XX(100),YY(100),EE(40),SIG(40)
      DIMENSION PO(5),DS(5)
      COMMON /INNER/C(20),EN(100),Y1(100),Y2(100),ARG(10),VA
      COMMON /BLOC1/OUT(20)/BLOC2/MO
      PI=3.14159265
      CK=1.380622E-16
      CME=9.109558E-28
      CA=.52917715E-8
      CQE=1.6021917E-19
      CE=8.8542E-21
C
C                    EVALUATION OF CONSTANTS
C
      READ(5,101) CD,CMN,CG,CR,NE,NAME
      DO 301 I=1,20
      OUT(I)=0.0
  301 C(I)=0.0
      C(1)=SQRT(CG*CK/CMN)
      C(2)=1./(1.4142*PI*CD**2)
      C(3)=PI*.5*CA**2
      C(7)=CME/CMN
      C(9)=2.*CK/CME/PI
      C(4)=(CG-1)*C(7)**2*C(9)**1.5
      C(5)=SQRT(8./PI/CG)
      C(6)=2.*C(3)*SQRT(C(9))
      C(8)=CG
      C(10)=CR
      C(11)=CQE/SQRT(CME*CE)
      C(12)=CQE**2/4./PI/CE/CK
      C(13)=SQRT(CK/CME)
      C(14)=SQRT(1.667*CK/CME)
      C(15)=12.*PI
      WRITE(6,201) C
C
C                    ESTABLISH INTEGRAL TABLE
C
      READ(5,104) (EN(I),Y1(I),Y2(I),I=1,100)
C
C           AFTER INITIALIZATION, THE MAIN PROGRAM CONTROLS
C ACCESS TO THE SUBROUTINE 'INGARD'.  THE SUBROUTINE
C EVALUATES THE DISPERSION RELATION OF INGARD AND SCHULZ.
C THE ARRAY 'OUT' CONTAINS I
C THE ARRAY 'OUT' CONTAINS VALUES OF INTEREST CALCULATED IN
C THE EVALUATION. THE CONTROL VARIABLE 'KCC' IS USED TO GIVE
C A LARGE QUANTITY OF INFORMATION IN A SINGLE CALL TO INGARD
C A VALUE OF KCC=1 CAUSES SEVERAL NAMELISTS TO BE PRINTED,
C GIVING THE VALUES OF ALL INTERMEDIATE QUANTITIES.  FOR ANY
C OTHER VALUE, THE SECOND PART IS USED TO CALCULATE THE EXPE
C ATTENUATION FACTOR FOR A SET OF PARAMETERS AND DETERMINE
C THE UNCERTAINTY OF THE RESULT.
C
C
      KCC=2
      J=3
```

```
      READ(5,103) STARPT
      CALL INGARD (STARPT)
      WRITE(6,209) OUT(19)
C
C                    DETERMINE ATTENUATION CONSTANT FOR
C                    COMPARISON WITH EXPERIMENT
C
      C(10)=2.5
      LR=1
  800 READ(5,103,END=999) STARPT
      READ(5,103) DS
      KCC=1
      DO 310 LQ=1,2
      IF(LQ.GT.1) STARPT(1)=600.
      WRITE(6,208) STARPT ,DS
      DO 304 MO=15,17
      CALL INGARD(STARPT)
      KCC=2
      TO=OUT(MO)
      DO 302 L=1,5
      TX=STARPT(L)
      STARPT(L)=TX*1.1
      CALL INGARD(STARPT)
      PO(L)=(OUT(MO)-TO)/(.1*TX)
  302 STARPT(L)=TX
      VAR=0.0
      DO 303 L=1,5
  303 VAR=VAR+(PO(L)*DS(L))**2
      VAR=SQRT(VAR)
      WRITE(6,206) MO,TO,VAR,PO
  304 CONTINUE
  310 CONTINUE
      IF(LR.GT.1) C(10)=2.
      LR=LR+1
      GO TO 800
C
C
  101 FORMAT(4E10.0,I2,6A1)
  102 FORMAT(2F10.0)
  103 FORMAT(5E10.0)
  104 FORMAT(3E16.7)
  105 FORMAT(3I5)
  201 FORMAT(1H ,/,4(1P5E12.3,/))
  202 FORMAT(1H1)
  203 FORMAT(1H1,/T10,'MINIMUM FOR OUT(',I2,') IS ',1PE9.1,
     *3X,' AT ',5E10.1)
  204 FORMAT(1H0,T10,'START POINT WAS ',1P5E10.1)
  205 FORMAT(1H0,T10,'OUTPUT VALUES ARE:',/,4(1P5E12.3,/))
  206 FORMAT(' OUT(',I2,') IS ',E12.3,'WITH STD DEV',E12.3,
     1       /,'     PARTIALS ARE ',5E12.3)
  208 FORMAT(1H ,1P5E15.3,/)
  209 FORMAT('     SOURCE TERM  ',1P1E12.3)
  214 FORMAT(1H1,T30,'PLOT FOR ',6A1)
C
  999 STOP
      END


C     SUBROUTINE INGARD(X)
C
C
C          THIS SUBROUTINE SOLVES FOR THE REAL AND IMAGINARY
C     COMPONENTS OF THE PROPAGATION CONSTANT 'K' OF AN
C     ACOUSTIC WAVE TRAVELING IN A CIRCULAR TUBE THROUGH AN
C     IONIZED GAS, ACCORDING TO THE EQUATIONS DEVELOPED BY
C     INGARD AND SCHULZ.
C
C               VARIABLES AND THEIR SYMBOLS ARE:
C
C          ANGULAR FREQUENCY          X(1)
C          NEUTRAL DENSITY            X(2)
```

```
C           ELECTRON DENSITY          X(3)
C           NEUTRAL TEMPERATURE       X(4)
C           ELECTRON TEMPERATURE      X(5)
C
C       VALUES OF CONSTANTS ARE COMPUTED IN THE MAIN
C     PROGRAM AND PASSED IN COMMON. LIKEWISE THE PRODUCTS OF
C     THE INTEGRATION SUBROUTINE ARE PASSED FROM THE MAIN
C     PROGRAM IN COMMON.  ALSO THE RESULTS OF THIS SUBROUTINE
C     ARE PASSED BACK TO THE CALLING PROGRAM IN COMMON. THEY
C     ARE STORED IN THE ARRAY 'OUT'.  THE INDEX NUMBERS OF
C     THIS ARRAY AND THE QUANTITIES STORED THERE ARE:
C
C           1     REAL PART OF N-SQUARED
C           2     IMAGINARY PART OF N-SQUARED
C           3     REAL PART OF PROPAGATION CONSTANT
C           4     IMAGINARY PART OF PROPAGATION CONSTANT
C           5     MAGNITUDE OF ION VELOCITY
C           6     PHASE OF ION VELOCITY
C           7     MAGNITUDE OF ELECTRON VELOCITY
C           8     PHASE OF ELECTRON VELOCITY
C           9     RATIO OF OUT(4) TO THAT WITHOUT IONIZATION
C          10     IMAGINARY COMPONENT OF 'K' WITHOUT IONIZ.
C          11     REAL PART OF N-SQUARE                (APRROX.)
C          12     IMAGINARY PART OF N-SQUARED          (APPROX.)
C          13     REAL PART OF PROPAGATION CONSTANT    (APPROX.)
C          14     IMAGINARY PART OF PROP. CONSTANT     (APPROX.)
C          15     ATTENUATION CONSTANT WITH IONIZATION
C          16     ATTENUATION CONSTANT WITHOUT IONIZATION
C          17     CHANGE IN ATTENUATION DUE TO IONIZATION
C          19     ACOUSTIC SOURCE STRENGTH
C


      SUBROUTINE INGARD(X)
      IMPLICIT REAL*8 (D)
      IMPLICIT COMPLEX*8 (Q)
      REAL*4 X(5),I1,I2,LOSS,D,DI
      INTEGER*4 KLIC/0000/
      EQUIVALENCE (QY1,RQY1)
      COMMON /INNER/C(20),EN(100),Y1(100),Y2(100),ARG(10),
     *VAL(10),KCC,J
      COMMON /BLOC1/OUT(20)
C
      NAMELIST /LISTA/CN,CL,BULK,WALL,LOSS
      NAMELIST /LISTB/SIGMA,TAU,WIN,WNI,WEN,WNE,GN,I1,I2
      NAMELIST /LISTC/GN,D,DI,AA,B1,B2,B
      NAMELIST /LISTD/WE,WI,CCP,CLII,CLI,WEI,WIE,CE,TAUI
      NAMELIST /LISTE/QA,QB,QC,QD,QE,QF,QG,QH,QI
      NAMELIST /LISTF/QY1,QY2,QY3,QY
      NAMELIST /LISTG/QVI,QVE
      NAMELIST /LISTH/RM,RD,THETA
C
C
      CN=C(1)*SQRT(X(4))
      CL=C(2)/X(2)
      BULK=1.54919*CL/CN*X(1)**2
      WALL=2.074443*SQRT(X(1)*CL*CN)/C(10)
      LOSS=BULK+WALL
      IF(KCC.EQ.1) WRITE(6,LISTA)
C
C
C         ENTER TABLE OF ENTRIES WITH VALUE OF ELECTRON TEMP
C     AND OBTAIN VALUE OF Y2. USE TO CALCULATE TAU.
C
C
      CALL ATSM(X(5),EN,Y2,100,1,ARG,VAL,5)
      CALL ALI(X(5),ARG,VAL,I2,5,.1E-2,IER)
      SIGMA=C(3)*I2
      TAU=C(4)*X(5)**1.5*X(3)*SIGMA/CN**2
C
C
C           ENTER TABLE OF ENTRIES WITH VALUE OF ELECTRON TEMP
```

```
C     AND OBTAIN VALUE OF Y1. USE TO CALCULATE  WEN
      CALL ATSM(X(5),EN,Y1,100,1,ARG,VAL,5)
      CALL ALI(X(5),ARG,VAL,I1,5,.1E-2,IER)
      WEN=C(6)*X(2)*SQRT(X(5))*I1
      WNE=X(3)/X(2)*C(7)*WEN
      WIN=C(5)*CN/CL
      WNI=WIN*X(3)/X(2)
      GN=WNE+WNI
      IF(KCC.EQ.1) WRITE(6,LISTB)
C
C
      IF(J.EQ.2) GO TO 401
C
C
      WE=C(11)*SQRT(X(3))
      WI=WE*SQRT(C(7))
C
C
      RM=C(12)/X(4)
      RD=C(13)/WE*SQRT(X(5))
      THETA=RD/RM
      IF(THETA.GE.1.) GO TO 500
      IF(KLIC.LE.2) WRITE(6,LISTH)
      THETA=1.1
      KLIC=KLIC+1
  500 CONTINUE
      IF(KCC.EQ.1) WRITE(6,LISTH)
C
C
      CLII=1./(X(3)*RM**2*ALOG(THETA))
      CLI=1./(1./CLII+1./CL)
      IF(CLI.LE.0.0) WRITE(6,LISTD)
      TAUI=1.5492*CLI/CN*X(1)**2+2.07444*SQRT(X(1)*CLI*CN)
     */C(10)
      CCP=C(15)*RD**3*X(3)
      WEI=3.62E-12*X(3)*ALOG(CCP)/X(5)**1.5
      WIE=C(7)*WEI
      CE=C(14)*SQRT(X(5))
      IF(KCC.EQ.1) WRITE(6,LISTD)
C
C
      QQ=(0.,1.)
      QA=1.+QQ*(LOSS+GN)/X(1)
      QB=-QQ*WNI/X(1)
      QC=(TAU-QQ*WNE)/X(1)
      QD=-QQ*WIN/X(1)
      QE=-(WI/X(1))**2+QQ*(TAUI+WIN+WIE)/X(1)
      QF=(WI/X(1))**2-QQ*WIE/X(1)
      QG=-QQ*WEN/X(1)
      QH=(WE/X(1))**2-QQ*WEI/X(1)
      QI=-(WE/X(1))**2+1./C(8)*(CE/CN)**2+QQ*(WEN+WEI)/X(1)
      IF(KCC.EQ.1) WRITE(6,LISTE)
C
C
      QY1=QE*QI-QH*QF
      RQY1=-((WI*CE/CN)**2*0.6+(TAUI+WIN)*(WEN+WEI)-WIE*WEN)
     */X(1)**2
      QY2=QC*(QD*QH-QE*QG)
      QY3=QB*(QG*QF-QD*QI)
      QY=QA+(QY2+QY3)/QY1
      IF(KCC.EQ.1) WRITE(6,LISTF)
C
C
      OUT(1)=REAL(QY)
      OUT(2)=AIMAG(QY)
      QS1=CSQRT(QY)
      OUT(3)=REAL(QS1)*X(1)/CN
      OUT(4)=AIMAG(QS1)*X(1)/CN
C
C
      IF(J.EQ.1) GO TO 999
C
```

```
C
C
  401 CONTINUE
      D=X(1)*X(3)*X(5)/C(8)/X(2)/X(4)/GN
      DI=1./(1.+D*D)
      AA=(GN+TAU)*D*DI/X(1)
      B1=GN*D*D*DI
      B2=TAU*DI
      B=(LOSS+B1-B2)/X(1)
      IF(KCC.EQ.1) WRITE(6,LISTC)
      OUT(11)=1.-AA
      OUT(12)=B
      QX=CMPLX(OUT(11),OUT(12))
      QS1=CSQRT(QX)
      OUT(13)=REAL(QS1)*X(1)/CN
      OUT(14)=AIMAG(QS1)*X(1)/CN
C
C
      IF(J.NE.3) GO TO 999
C
C
      QVI=-(QD*QI-QG*QF)/QY1
      OUT(5)=CABS(QVI)
      T1=REAL(QVI)
      T2=AIMAG(QVI)
      OUT(6)=ATAN2(T2,T1)
C
      QVE=-(QE*QG-QD*QH)/QY1
      OUT(7)=CABS(QVE)
      IF(KCC.EQ.1) WRITE(6,LISTG)
      T1=REAL(QVE)
      T2=AIMAG(QVE)
      OUT(8)=ATAN2(T2,T1)
C
C
      F1=1.0328*CL/CN*X(1)**2+1.24467*SQRT(X(1)*CL*CN)/C(10)
      F2=1.291*CL/CN*X(1)**2+2.0744*SQRT(X(1)*CL*CN)/C(10)
      QN1=1.+QQ*F1/X(1)
      QN2=1.-.4*QQ*F2/X(1)/(1.+QQ*F2/X(1))
      QN=QN1/QN2
      QS1=CSQRT(QN)
      OUT(10)=AIMAG(QS1)*X(1)/CN
C
C
C
      DOUT=OUT(4)/OUT(10)
      DOUT2=DOUT-1.D0
      OUT(9)=DOUT2
      OUT(15)=OUT(4)/SQRT(X(1)/6.283183)
      OUT(16)=OUT(10)/SQRT(X(1)/6.283183)
      OUT(17)=OUT(4)-OUT(10)
      OUT(19)=CN**2*TAU
C
C
  999 RETURN
      END
```

BIBLIOGRAPHY

1. Partlow, James G., Measurement of Acoustic Pressures Associated with Moving Striations in a Neon Glow Discharge, M.S. Thesis, Naval Postgraduate School Monterey, 1963.

2. Carretta, A.A. Jr., and Moore, W.N., Acoustical Effects in a Neon Glow Discharge, M.S. Thesis, Naval Postgraduate School, Monterey, 1965.

3. Wilson, O.B. Jr., Observation of Acoustic Waves Generated in a Neon Glow Discharge, paper presented at meeting of Acoustical Society of America, Session 6H6, Boston, 3 June 1966.

4. Crandall, J.L., Jr., Acoustical Perturbation of a Neon Glow Discharge, Ph.D. Thesis, Naval Postgraduate School, Monterey, 1967.

5. Melville, R.D.S. Jr., Acoustic Interaction with the Positive Column of a Neon Glow Discharge, M.S. Thesis, Naval Postgraduate School, Monterey, 1967.

6. Ingard, U., "Acoustic Wave Generation and Amplification in a Plasma," Phys. Rev., v. 145, 41 (1966).

7. Ingard, U., and Schulz, M., "Acoustic Wave Mode in a Weakly Ionized Gas," Phys. Rev., v. 158, 106 (1967).

8. Yatsui, K., Kobayashi, T., and Inuishi, Y., "Ultrasonic Wave Amplification in Gaseous Plasma," Tech. Reports Osaka U., v. 18, No. 812 (1968).

9. Yatsui, K., Kobayashi, T., and Inuishi, Y., "Ultrasonic Wave Amplification in Gaseous Plasmas," J. Phys. Soc. Japan, v. 24, 1186 (1968).

10. Schulz, H.M. III, Interactions of Electrons and Acoustic Waves in a Plasma, Ph.D. Thesis, Massachusetts Institute of Technology, Cambridge, 1967.

11. Watanabe, M.S. and Oleson, N.L., "Traveling Density Waves in Positive Columns," Phys. Rev., v. 99, 1701 (1955).

12. Wojaczeck, Karl, "Schall im Niederdruckplasma", Beitr. Plasmaphys., v. 3, 127 (1961).

13. Strickler, S.D., and Stewart, A.B., "Radial and Azimuthal Standing Sound Waves in a Glow Discharge," Phys. Rev. Ltrs., v. 11, 527 (1963).

14. Riley, J.R., and Hall, D.S., "Neutral Particle Density Modulation in the Positive Colume of a Mercury Discharge," Proceedings, VII International Conf. on Ionization Phen. in Gases. Panel 3.1.8.

15. Schulz, M. and Ingard, U., "Acoustic Kink Instability in an Argon Discharge," Phys. Fluids, v. 10, 1031 (1967).

16. Fitaire, M. and Mantei, T., "Acoustic Wave Generation by Temperature Modulation of a Plasma," Phys. Rev. Ltrs., v. 29A, 84 (1969).

17. Turner, R., Hochberg, A.K. and Poehler, T.O., "Multiple Pulse Emission From a HCN Laser," Appl. Phys. Ltrs., v. 12, 104 (1968).

18. Born, G.K., "Acoustic Perturbations in Pulsed Gas Lasers," J. Appl. Phys., v. 39, 4479 (1968).

19. Hayess, Erhard, "Die Dampfung von Schallwellen in der Entladungsaüle des Niederdruckplasmas," Beitr. Plasmaphys., v. 4, 211 (1964).

20. Hayess, Erhard, "Schallimpulse im Niederdruckplasma, I. Erzeugung und Nachweis der Schallimpulse," Beitr. Plasmaphys., v. 6, 377 (1966).

21. Nygaard, K.J. and Meltz, G., "Sound Production in Glow Discharges", Proceedings, VIII Int. Conf. on Phenomena in Ionized Gases, Vienna (1967).

22. Nygaard, K.J. and Meltz, G., "Generation and Detection of Acoustic Waves in Pulsed Electrical Discharges," J. Acoust. Soc. Am., v. 44, 1566 (1968).

23. Goldstein, L. Roux, M.R. and Dayton, J.A. Jr., "Production of Acoustic Waves by R.F. Breakdown in Low Pressure Gases," Proceedings, VI Inter. Conf. on Ionization Phenomena In Gases, v. III, 115 (1963).

24. Berlande, J., Goldan, P.D. and Goldstein, L.,"Formation and Propagation of a Pressure Wave in a Weakly Ionized Gas," Appl. Phys. Ltrs., v. 5, 51 (1964).

25. Born, G.K. and Buser, R.G.,"Determination of the Gas Temperature in the Afterglow of Pulsed Discharges by Microwave Probing of Standing Acoustic Waves," J. Appl. Phys., v. 37, 4918 (1966).

26. Macon, J.L., Generation and Amplification of Longitudinal Waves in a Plasma, M.S. Thesis, Massachusetts Institute of Technology, Cambridge, (1966).

27. Tanenbaum, B.S., "Wave Propagation in a Partly Ionized Gas," Phys. Fluids, v. 5, 1226 (1962).

28. Sessler, G.M., "Propagation of Longitudinal Waves in a Weakly Ionized Gas," Phys. Fluids, v. 7, 90 (1964).

29. Veselovskiy, I.I., "Sound Propagation in Partly Ionized Plasma," Geomagn, and Aeronomy 7, 1, 35-42 (1967).

30. Ishii, T., and Inuishi, Y., "Amplification of Neutral Waves in Gaseous Plasmas," Jap. J. Appl. Phys., v. 8, 1531 (1969).

31. Aubrecht, L., "Theoretical Study of the Interaction of Acoustic Waves with a Plasma," Phys. Ltrs.,v. 27A, 526 (1968).

32. Aubrecht, L., "General Solution of a System of Equations for Acoustic Wave Propagation in a Partially Ionized Gas in an External Electric Field", Czech. J. Phys., B19, 1322 (1969).

33. Aubrecht, L., "Low Frequency Waves in a Positive Column of Discharge," Czech. J. Phys., B20, 12 (1970).

34. Browne, E.T., Introduction to the Theory of Determinants and Matrices, Univ. of N.C. Press., 1958.

35. Morse, P. and Ingard, U., Theoretical Acoustics, McGraw Hill, 1968.

36. Present, R.D., Kinetic Theory of Gases, McGraw Hill, 1958.

39. McDaniel, E.W., Collision Phenomena in Ionized Gases, McGraw Hill, 1964.

40. Von Engel, A., Ionized Gases, 2 ed., Oxford University Press, 1968.

41. Tanenbaum, B.S., Plasma Physics, 348, McGraw Hill, 1967.

42. Wu, Ta-you, Kinetic Equations of Gases and Plasmas, Addison-Wesley Pub. Co., 1966.

43. Cooper, A.W.M., Moving Striations in Inert Gas Glow Discharges, Ph.D. Thesis, Queens University, Belfast, 1961.

44. Brown, S., Basic Data of Plasma Physics, (MIT - Wiley 1959).

45. Taylor, B.N., Parker, W.H., and Langenberg, D.N.,"Determination of e/h, using Macroscopic Quantum Phase Coherence in Superconductors," Rev. Mod. Phys., v. 41, 375 (1969).

46. Cook, G.A., ed., Argon, Helium and the Rare Gases, v. 1., Interscience Publishers, 1961.

47. Kinsler, L.E., and Frey, A.R., Fundamentals of Acoustics, 2 ed., 226, John Wiley and Sons, 1962.

48. Bracewell, R.N., The Fourier Transform and Its Applications, McGraw Hill, 1965.

49. Hayess, E., Venzke, P. and Wojoczek, K.,"Die Neutragas-temperatur in der Argon-Mitteldruckentladung," Beitr Plasmaphys., v.7, 461 (1967).

50. Hayess, Erhard, "Schallimpulse im Niederdruckplasma II. Die Schallausbreitung," Beitr Plasmaphys., v. 7, 327 (1967).

51. Venzke, D., Hayess, E. and Wojoczek, K, "Similarity Relations for Discharge Columns in Noble Gases at Medium Pressures," Beitr. Plasmaphys, v. 6, (1966).

52. Chalupnik, J.D., Rule, E., and Suellentrop, F.J.,"Pressure Response of Condenser Microphones at Low Ambient Pressures," J. Acoust. Soc. Am., v. 33, p 177 (1961).

53. Dayton, J.A., Verdeyen, J.T., and Virobik, P.F.,"Method for Detecting Weak Sound Waves in a Low Pressure Gas," Rev. Sci. Ins., v. 34, 1451 (1963).

54. Geppert, D.V., Basic Electron Tubes, p. 81, McGraw Hill, 1951.

55. Cobine, J.D., Gaseous Conductors, p. 128, McGraw Hill, 1941.

56. Rosebury, F., Handbook of Electron Tube and Vacuum Techniques, Addison Wesley, 1965.

DOCUMENT CONTROL DATA - R & D

(Security classification of title, body of abstract and indexing annotation must be entered when the overall report is classified)

1 ORIGINATING ACTIVITY (Corporate author)
Naval Postgraduate School
Monterey, California 93940

2a. REPORT SECURITY CLASSIFICATION
Unclassified

2b. GROUP

3 REPORT TITLE
Creation and Modification of Acoustic Signals by Discharge Plasma

4 DESCRIPTIVE NOTES (Type of report and inclusive dates)
Ph.D. Thesis, June 1971

5. AUTHOR(S) (First name, middle initial, last name)
Richard Willis Tripp, Jr.

6 REPORT DATE
June 1971

7a. TOTAL NO. OF PAGES
170

7b. NO. OF REFS
56

8a. CONTRACT OR GRANT NO.

b. PROJECT NO.

c.

d.

9a. ORIGINATOR'S REPORT NUMBER(S)

9b. OTHER REPORT NO(S) (Any other numbers that may be assigned this report)

10. DISTRIBUTION STATEMENT
Approved for public release; distribution unlimited.

11. SUPPLEMENTARY NOTES

12. SPONSORING MILITARY ACTIVITY
Naval Postgraduate School
Monterey, California 93940

13. ABSTRACT

Sound production and modification in an Argon discharge plasma was investigated theoretically and experimentally. Sound production by ions in the cathode region was shown to be feasible and consistent with earlier experimental results. A numerical analysis of the theoretical dispersion relation of Ingard and Schulz showed that plasma amplification effects will not compensate for acoustic losses. The theory of the mobility-limited thermionic diode operated as a microphone was expanded. Such microphones were used in an experimental investigation of sound production and modification by a discharge plasma. Possible plasma effects on sound propagation were observed. The characteristics of sound production by the plasma were found to be in reasonable agreement with theory. A departure from theory at low frequencies was interpreted as arising from the effects of particle diffusion, an effect not previously observed in acoustics.

KEY WORDS	LINK A		LINK B		LINK C	
	ROLE	WT	ROLE	WT	ROLE	WT
Acoustic interaction						
Plasma acoustics						
Acoustic						
Plasma						
Diode microphone						
Microphone						

Thesis
T799
c.1
Tripp
128452
Creation and modification of acoustic signals by discharge plasma.